REPUBLIC OF TURKEY

GAZİANTEP UNIVERSITY

GRADUATE SCHOOL OF NATURAL & APPLIED SCIENCES

INVESTIGATION OF SPECTRAL RADIANCE RESPONSIVITY FOR OPTICAL SYSTEMS

Ph.D. THESIS

IN

ENGINEERING PHYSICS

BY

MUSTAFA KILIN

DECEMBER 2020

DECEMBER 2020

Ph.D. in Engineering Physics

MUSTAFA KILIN

INVESTIGATION OF SPECTRAL RADIANCE RESPONSIVITY FOR OPTICAL SYSTEMS

Ph.D. Thesis
in
Engineering Physics
Gaziantep University

Supervisor
Prof. Dr. Hayriye TÜTÜNCÜLER

Co-Supervisor
Assoc. Prof. Dr. Özcan BAZKIR

by
Mustafa KILIN
December 2020

©2020[Mustafa KILIN]

REPUBLIC OF TURKEY
GAZİANTEP UNIVERSITY
GRADUATE SCHOOL OF NATURAL & APPLIED SCIENCES
ENGINEERING PHYSICS

Name of the Thesis : Investigation of Spectral Radiance Responsivity for Optical Systems

Name of the Student : Mustafa KILIN

Exam Date : 03.12.2020

Approval of the Graduate School of Natural and Applied Sciences

Assoc. Prof. Dr. Mehmet İshak YÜCE
Director

I certify that this thesis satisfies all the requirements as a thesis for the degree of Doctor of Philosophy.

Prof. Dr. Ramazan KOÇ
Head of Department

This is to certify that we have read this thesis and that in our consensus opinion it is fully adequate, in scope and quality, as a thesis for the degree of Doctor of Philosophy.

Assoc. Prof. Dr. Özcan BAZKIR
Co-Supervisor

Prof. Dr. Hayriye TÜTÜNCÜLER
Supervisor

Examining Committee Members:	Signature
Prof. Dr. Ramazan KOÇ	…………………..
Prof. Dr. Gültekin ÇELİK	…………………..
Prof. Dr. Hayriye TÜTÜNCÜLER	…………………..
Prof. Dr. M. Fatih HASOĞLU	…………………..
Prof. Dr. Ahmet BİNGÜL	…………………..

I hereby declare that all information in this document has been obtained and presented in accordance with academic rules and ethical conduct. I also declare that, as required by these rules and conduct, I have fully cited and referenced all material and results that are not original to this work.

Mustafa KILIN

ABSTRACT

INVESTIGATION OF SPECTRAL RADIANCE RESPONSIVITY FOR OPTICAL SYSTEMS

KILIN, Mustafa
Ph.D. in Engineering Physics
Supervisor: Prof. Dr. Hayriye TÜTÜNCÜLER
Co-Supervisor: Assoc. Prof. Dr. Özcan BAZKIR
December 2020
117 pages

The aim of this thesis is establishment and determination of radiance responsivity to be used in calibrations of polychromatic radiation sources. In realizing the radiance, Ar-Ion (457, 477,488 and 514 nm), He-Ne (543, 594, 604, 612 and 632.8 nm) and Nd:YAG (532 nm,1064 nm) lasers and an integrating sphere with 15 cm diameter are used to get radiation sources having Lambertian distributions. Then silicon photodiode based trap detector which is treaceble to the liquid helium cooled laser based cryogenic radiometer is used to measure the photocurrent corresponding to each wavelength and thereby to obtain radiance. The measurement system used to have spectral current response of this laser based radiance is a double grating monochromator with 2 x 300 mm focal length and triple gratings in its each turrets. The gratings used for these measurements have 2400 g/mm and 1200 g/mm grove densities and blazed to 250 nm and 500 nm respectively. The laser beams emerged from the integrating sphere after the radiance evaluation directed on monochromator and from its exit slit the photocurrent responses record at each laser wavelengths. From the radiance realized at laser wavelengths and the photocurrent, values recorded at the exit slit of monochromator, transfer function (radiance responsivity) of the optical system is obtained. This radiance responsivity together with monochromator system is used to derive the spectral radiance of polychromatic radiation sources with low uncertainty. Moreover, in this work the uncertainty scale is determined using both classical and Monte Carlo methods.

Key Words: Radiometry, Spectral Radiance, Radiance Responsivity, Monte Carlo Method.

ÖZET

OPTİK SİSTEMLER İÇİN TAYFSAL IŞIMA DUYARLILIĞININ ARAŞTIRILMASI

KILIN, Mustafa
Doktora Tezi, Fizik Mühendisliği
Danışman: Prof. Dr. Hayriye TÜTÜNCÜLER
İkinci Danışman: Doç. Dr. Özcan BAZKIR
Aralık 2020
117 sayfa

Bu tezin amacı, polikromatik radyasyon kaynaklarının kalibrasyonların da kullanılacak ışıma duyarlılığının oluşturulması ve belirlenmesidir. Işımayı gerçekleştirirken, Ar-Ion (457, 477,488 ve 514 nm), He-Ne (543, 594, 604, 612 ve 632.8 nm) ve Nd: YAG (532 nm, 1064 nm) lazerler ve 0.15m'lik bir toplama küresi Lambertian dağılımına sahip ışıma kaynakları elde etmek için kullanılır. Daha sonra sıvı helyum soğutmalı lazer tabanlı kriyojenik radyometreye karşı izlenebilir olan silikon fotodiyot tuzak detektörü, her bir dalga boyuna karşılık gelen fotoakımı ölçmek ve böylece ışıma elde etmek için kullanılır. Bu lazer tabanlı ışımanın tayfsal akım yanıtına sahip olmak için kullanılan ölçüm sistemi, her kasasında 2 x 300 mm odak uzunluğuna ve üçlü ızgaralara sahip çift ızgaralı bir monokromatördür. Bu ölçümler için kullanılan ızgaralar 2400 g / mm ve 1200 g / mm oluk yoğunluğuna sahip olup sırasıyla 250 nm ve 500 nm olarak etkili dalga boyuna ayarlanır. Toplama küresinden çıkan lazer ışımaları, radyans olarak monokromatöre yönlendirilir ve onun çıkışında her bir dalga boyu için fotoakım olarak kayıt edilir. Lazer dalga boylarında gerçekleşen ışıma ve fotoakımdan, monokromatörün (ışıma duyarlılığı) çıkış yarığında kaydedilen değerler ile optik sistemin transfer fonksiyonu elde edilir. Monokromatör sistemi ile birlikte bu ışıma tepkisi, düşük belirsizlikle polikromatik radyasyon kaynaklarının spektral parlaklığını türetmek için kullanılır. Ayrıca bu çalışmada belirsizlik ölçeği hem klasik hem de Monte Carlo yöntemleri kullanılarak belirlenir.

Anahtar Kelimeler: Radyometri, Tayfsal Radyans, Radyans Duyarlılığı, Monte Carlo Method.

''Dedicated to my wife and my daughter''

ACKNOWLEDGEMENTS

Foremost, I would like to express my sincere gratitude to my advisor Prof. Dr. Hayriye TÜTÜNCÜLER for the continuous support of my Ph. D. Besides, I would like to thank for whole atomic and molecular physics group members’ for their support and help at first to Prof. Dr. Ramazan KOÇ which is the head of the department of this group.

I would like to thank a TUBITAK-UME optic laboratory employee, who helps me for my experimental study, mainly as the laboratory manager and my co-supervisor Assoc. Dr. Özcan BAZKIR's invaluable guidance and optimistic attitude is crucial to the completion of my Ph.D. In addition, I would like to express my endless thanks to Dr. Seval MERİÇ for her support, interest and assistance as a big sister.

For their friendship and help, Prof. Dr. Ahmet BİNGÜL and Dr. Uygar ŞAŞMAZ, I would like to express my sincere thanks.

Meanwhile, I want to say thank to my research colleagues in the department for their friendship and pleasant coffee break conservations.

Once for all, I would like to express my appreciation to my wife Eylem KILIN, and my daughter Berna KILIN, for their supports and patience in this exhausting Ph.D. process. I am grateful also to my dear mother, father, sisters and brothers in law who taught me the value of knowledge, for their unconditional supports.

TABLE OF CONTENTS

Page

LIST OF TABLES

LIST OF FIGURES

Page

LIST OF SYMBOLS

Q	Radiant Energy
Φ	Radiation Flux
I	Radiation Intensity
E	Irradiance
L	Radiance
$\mathbf{Q_v}$	Luminous Energy
$\mathbf{\Phi_v}$	Luminous Flux
$\mathbf{I_v}$	Luminous Intensity
$\mathbf{E_v}$	Illuminance
$\mathbf{L_v}$	Luminance
$\mathbf{K_m}$	Spectral Luminous Efficacy
V(λ)	spectral luminous efficiency
J	Joule
W	Watt
lm	Lumen
sr	Steradian
cd	Candela
lx	Lux
$\mathbf{\Phi_0}$	Incidence Radiation lux
$\mathbf{R_M}$	Spectral Radiance Responsivity of the Measurement System
w	Exit Slit Width
G'	Grating Blaze Wavelength
g	Grating Groove number
f	Focal Length

k	Sigma
$\mathbf{CorFac_{WS}}$	Correction Factor of the Wavelength Shift
$\mathbf{CorFac_{BW}}$	Monochromator Bandwidth
$\mathbf{u_c}$	Standard Uncertainty
$\mathbf{u_c^2}$	Variance
ρ	Reflectance
T	Temperature
$\mathbf{T_0}$	Reference Temperature
G	Thermal Conductor
i	Current
R	Responsivity
η	Quantum Efficiency
h	Plank constant
ν	Frequency
q	Electron charge
λ	Wavelength
$\mathbf{E_g}$	Forbidden Energy
$\mathbf{R_s^*}$	Spectral Power Responsivity of the Trap Detector
C	Geometric Constant of the Radiance Equation

LIST OF ABBREVIATIONS

BIPM	International Bureau of Weights and Measures
NMI	National Metrology Institute
NIST	National Institute of Standard and Technology
NPL	National Physics Laboratory
UME	Ulusal Metrology Enstitüsü
ESCR	Electrical Substitution Cryogenic Radiometer
UV	Ultraviolet
Vis	Visible
IR	Infrared
Ar-Ion	Argon ion
He-Ne	Helium Neon
Nd-Yag	Neodymium-Doped Yttrium Aluminum Garnet
CIE	International Commission on Illumination
SI	International System of Units
CIPM	International Committee on Weights and Measures
Si	Silicone
Ge	Germanium
InGaAs	Indium Gallium Arsenide
FOV	Field of View
SNR	Signal Noise Ratio
BaSO4	Bariumsilfate
PTFE	Polytrafluoreethylene
SSW	Spectral Slit Width
SB	Spectral Band
Hg	Mercury

Ar	Argon
SBW	Spectral Band Width
Au	Gold
NEP	Noise Equivalent Power
FWHM	Full Width Half Maximum

CHAPTER 1

INTRODUCTION

Metrology is defined as the science of measurement, by including both experimental and theoretical determinations at any level of uncertainty for field of science and technology. In recent years, the demand for science and technology is increasing to develop new technologies. The most obvious common feature of these systems is sensitive optical measurement capability. These precision measurement capabilities promote the importance of the optical metrology. New industrial areas with contribution of the optical metrology reveal more efficient and realizable products. The development of new technologies is directly dependent on new traceability with low uncertainty [1].

The electromagnetic spectrum includes wavelength of electromagnetic radiation ranging from short wavelength gamma rays to long wavelength radio waves as shown in Figure 1.1. In order to measure and control this radiation many requirements have to be taken into account. One of the main working areas of the metrology developed and realized by the National Metrology Institutes (NMIs) of the countries is optical radiation measurements. Optical radiation measurement has main two concepts that are the radiometry, which measures the electromagnetic radiation as physical quantities such as power of light [2], and photometry that measures the electromagnetic radiation as the response of the human eyes [3].

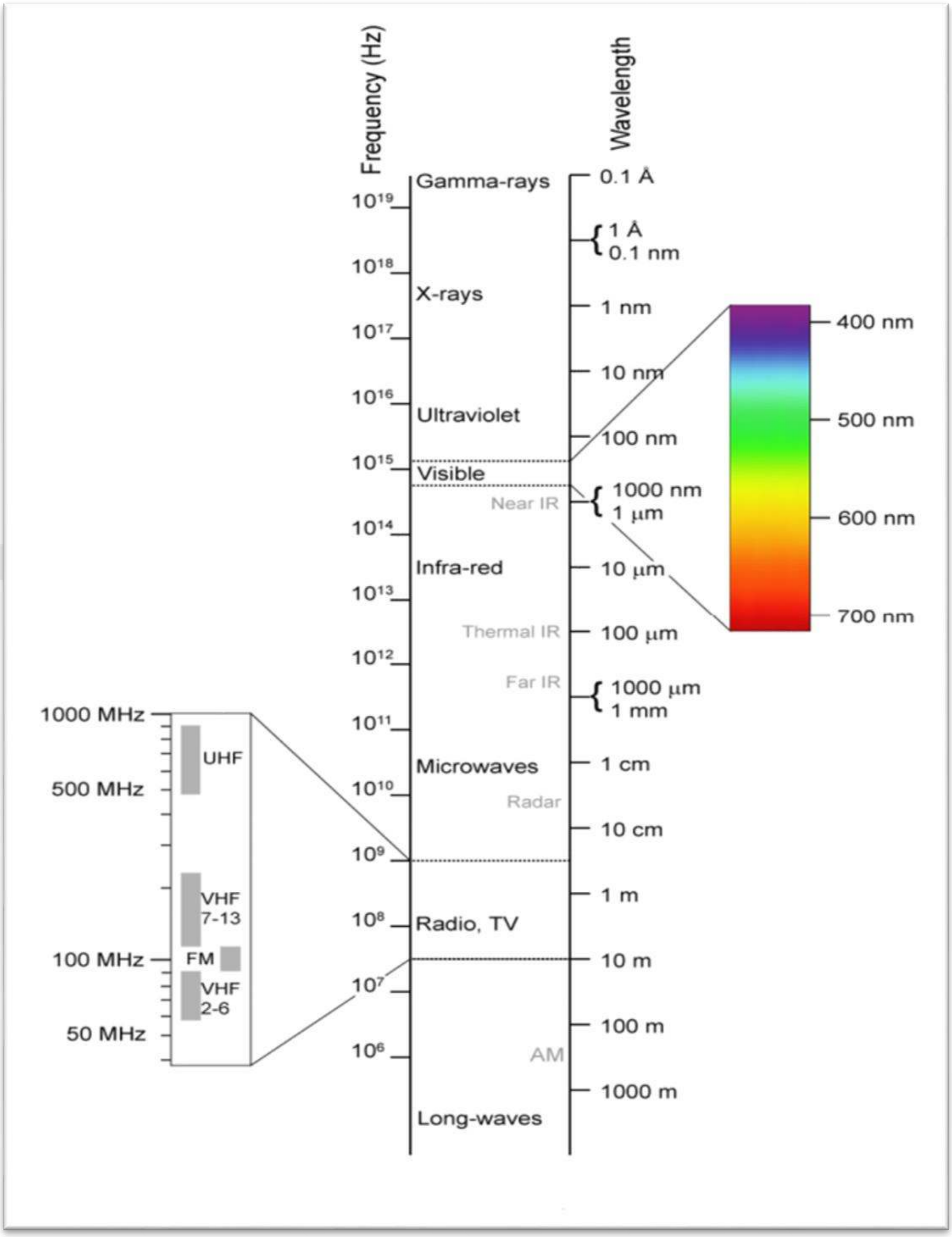

Figure 1.1 Electromagnetic spectrum.

1.1 Historical Development about Spectral Radiance Measurements

Many applications are improved to obtain primary scale of the NMIs with lower uncertainty in the both radiometry and photometry measurements. In this sense, there are three main optical measurement components, which are radiation sources, radiation detectors and opto-mechanics parts. In the past years, in order to achieve optical control of this equipment many experiments were done by NMIs [1].

Measurement traceability chains are realized by using uniform source [4] which described a laser-based calibration facility for irradiance and radiance measuring instruments and detector based methods [5] described the realization of the National Institute of Standard and Technology (NIST) detector-based spectral irradiance scale.

Source based traceability measurement chains was started to investigate with the first time describing of the black body radiation by G. Kirchhoff in 1860 [6]. After that the describing this principle until today, source based measurement systems was used for the realizations of the spectral radiance and irradiance scales by determining the accurate temperature. The source based measurement system was obtained comparatively with Black Body Radiator system that determines the accurate temperature [7-11]. The first laser radiometric measurement system was developed in 1984 by Scheafer and Eckerle in the NIST, since the radiance and irradiance responsivity values could not be measured directly due to the low flux created by a polychromatic lamp at the output of the monochromator [12]. In 1986, the irradiance measurement system based on black body radiation was compared with the silicon photo diode based laser calibration system that can be traced according to the cryogenic radiometer [13]. Other one is that the detector based measurement chain was formed as the traceable to radiometry that is called low temperature radiometry operating with electrical substitution principle at the liquid helium temperature (4.2 K) [14-16]. This method was investigated alternatively to source based method and in this method, detector and monochromator systems used in the radiance measurements were calibrated against for low temperature radiometry [17, 18]. In contrast with source-based system, its uncertainty value is very low but, because the ratio of the signal over noise is very low, the increase of uncertainty occurs in the resolution where measurements are made. For that reason, that in the recent years instead of the polychromatic light source in order to determine of the radiation scale and definition of the monochromator transfer function was developed in the all metrology laboratory laser radiation source, which is narrow band, more stable and stronger was started to use [5, 19-21].

In this sense silicon, photodiode self-calibration technique was developed by NIST [22, 23]. This technique offers a more modern approach in terms of accuracy and simplicity compared with thermally and electrically operating radiometric systems. The uncertainty of the optic power was realized by using electrical substitution radiometers methods with liquid helium at low temperatures by NPL (National Physics Laboratory) [14]. This method is based on the comparison of the temperature generated by the optical radiation in the interfering cavity with the temperature increase generated electrically [24]. These measurements made at low temperature are adopted by NMIs as their primary standard [25, 26]. In addition, the metrology laboratory of Turkey UME (Ulusal Metroloji Enstitüsü) was attended this group [27].

After this primary standard was defined as electrical substitution cryogenic radiometer system (ESCR), the responsivity standard of the photodiodes was changed considerably and was started to use in the specific number and configuration. This detector configuration is based on original design by E.F. Zalewski [28] and it is called as trap detector. While in the NMIs laboratories the reflection type trap detectors used as transfer standard display the stable distribution in the visible (VIS) wave length range, in the ultraviolet (UV) wave length range it approach the unstable and in the infrared (IR) wave length region it is limited distribution [29-31]. Used optical range has high accuracy the realization of the optical power, spectral responsivity and spectral irradiance responsivity [32].

1.2 Thesis Outline

The motivation of this work is establishment and determination of the radiance responsivity to be used in calibrations of polychromatic radiation sources with low uncertainty in TUBITAK-UME (National Metrology Institute). In realizing the radiance, Ar-Ion, He-Ne and Nd-Yag lasers and an integrating sphere with 0.15 m diameter are used to get radiation sources having Lambertian distributions. Then silicon photodiode based reflection type trap detector, which is traceable to the liquid helium cooled laser based cryogenic radiometer, is used to measure the photocurrent corresponding to each wavelength and thereby to obtain radiance. The system, which measures spectral current response of this laser-based radiance, is a double grating monochromator with 2 x 0.3 m focal length and triple gratings in its each turret. Primarily the radiance of the laser beam emerged from the integrating sphere is calculated and then the radiance responsivity of the system is obtained by measuring the photocurrent responded from exit slit of the monochromator at each laser wavelengths. At last, the spectral radiance values of the polychromatic lamps are obtained using this radiance responsivity of the system. Consequently, it is aimed to provide the derivation and traceability of the other radiometric and photometric quantities with low uncertainty from the fundamental radiometric radiance unit. Measurement results obtained in extended measurement uncertainty scale are determined using both classical and Monte Carlo methods.

The spectral radiance responsivity is obtained with low uncertainty compared to source based and detector based measurement systems [32]. Moreover, measurement techniques formed the base for radiance measurement systems are used for applications like space, defense etc. The absolute radiance responsivity measurements are realized by transferring from tunable laser system had Lambertian distribution obtained by using integrated sphere and spectral power responsivity of the reflection-type trap detector that is characterized against the ESCR to spectroradiometric system [28, 33-35]. The traceability of the spectral radiance measurements of the radiation of the unknown sources is obtained by using these measurements results in the high resolution. This measurement system formed with laser-based system is an accurate way to reduction of the uncertainty compared to the traditional methods [30, 31].

The traceability chain obtained by using laser, integrating sphere, trap detector, telescope and spectrometer provides the possibility of removing external dependence on behalf of our country for optical measurements of unknown radiation irradiators or surfaces. In terms of traceability, reproducibility, and repeatability, a reference standard can be used for measurements in the all-optical region, measurement system.

In this research firstly, monochromator used for the radiance measurement is calibrated in terms of wavelength accuracy [33]. Secondly, reflection type Si based trap detector, used in the NMIs laboratory as radiometric transfer standards [24, 29] is characterized in terms of homogeneity, polarization dependence, nonlinearity, quantum efficiency and responsivity comparatively by using reflection type Si based trap detector, which is characterized before against electrical substitution cryogenic radiometry (ESCR) system in the TÜBİTAK-UME optic laboratory [12, 23]. Thirdly, by using integrated sphere and laser Lambertian distributed radiance beam is determined. The integrating sphere is a nearly Lambertian source that has same radiance over its entire surface area and in all direction, and it is better suited in general for radiance and irradiance measurement [4]. In the specific laser wavelength region, radiance values of the created laser beam integrating sphere is obtained by using He-Ne tunable (543, 594, 604, 612 and 632.8nm), Argon-Ion (457, 477, 488 and 514nm) and Nd-Yag (1064nm) lasers. Finally, using monochromator, detector and polychromatic light spectral radiance is measured. By using the obtained radiance values, the transfer function of the monochromator is achieved and the radiation values of an unknown source are accomplished with standard uncertainty measurements both classical approach and Monte Carlo approach. Radiance is the basic unit in the optical region measurements and this unit easily is transferred to other unit. For this reason, measurement of radiance is very important for the radiometric and photometric measurements.

In Chapter 1, historical development and purpose of this study are briefly discussed. In Chapter 2, definition about optical radiometric and photometric terms, radiometric measurement methods are given. In Chapter 3, all optical, optoelectronic and opto-mechanical devices used in laboratory measurements are briefly introduced and the part where they are used is emphasized. In addition, a theoretical model is created for the calculations made after the spectral radiance measurement. In Chapter 4, the discussion of the experimental measurement of the spectral radiance measurement system, correction factors and calibration are made by using some mathematical model. Uncertainty calculation both classical and Monte Carlo method are tested for spectral radiance measurement in Chapter 5. In Chapter 6, generally, spectral radiance transfer function of the measurement setup and results of the unknown radiation source or surface are defined. Finally, in the conclusion part, the contribution of this study to literature, science and technology, especially to the field of metrological measurement is explained.

CHAPTER 2
THEORY OF THE OPTICAL RADIOMETRY

In optical measurement studies, a certain part of the electromagnetic spectrum is examined. The optical part in the spectrum is the part defined as the region between 200 nm and 2500 nm, which is defined as UV-VIS and IR. The science that deals only with the visible region is photometric, and the science that deals with other parts including the visible region is radiometry.

The branch of science that tries to define the energy distribution of electromagnetic radiation by using the relations between the radiation source, optical environment and detector is called radiometry or photometry. The only real difference between radiometry and photometry is that radiometry includes the entire optical radiation spectrum, while photometry is limited to the visible spectrum as defined by the response of the eye [36].

2.1 Introduction

Radiometry and photometry deal with the quantities that can be easily converted into each other in the optical region. Although their metric theories are similar, they differ completely in terms of method and devices used. Although the geometric descriptions are the same as shown in Table 2.1, the unit analyzes are completely different.

Radiometry evaluates the irradiations in the UV, VIS and IR regions of the electromagnetic spectrum by using geometric descriptions on the energy scale. In photometry, the measurements deal with the same problem, while the electromagnetic spectrum deals only with the part of the visible region, and the measuring devices used to detect radiation are made to the human observer in the most appropriate way.

Table 2.1 Radiometric and photometric quantities, their symbols and units.

Radiometric Quantity	Symbol	Unit
Radiation Energy	Q	J
Radiation Flux (Power)	Φ	W
Radiation Intensity	I	W / sr
Irradiance and Exitance	E	W / m^2
Radiance	L	W / (m^2 sr)
Photometric Quantity	**Symbol**	**Unit**
Luminous Energy	Q_v	lm s
Luminous Flux	Φ_v	lm
Luminous Intensity	I_v	lm / sr = (cd)
Illuminance	E_v	lm / m^2 = (lx)
Luminance	L_v	lm / (m^2 sr) = (cd/m^2)

Note: J=joule, W=Watt, lm=lumen, lx=lux, m=meter, sr=steradian, s=second, cd=candela.

In terms of both application and terminology, photometry is easier but more difficult to understand in practice due to the limited spectrum of interest. Radiometry, on the other hand, is conceptually somewhat simpler, but is far more difficult to actually [36]. There is a relationship between radiometric and photometric quantities described as [37].

$$X_v = K_m \int_{360\ \mathrm{nm}}^{830\ \mathrm{nm}} X_{e,\lambda} V(\lambda) d\lambda \qquad (2.1)$$

where a photometric quantities X_v is related to the corresponding radiometric quantity $X_{e,\lambda}$. The constant, K_m=683 lm/W, relates the photometric and radiometric quantities and is called the maximum spectral luminous efficacy of radiation. V(λ) is the relative spectral sensitivity of the average human eye and is called spectral luminous efficiency for photopic vision. It is defined in the domain from 360 to 830 nm, and is normalized to unity at its peak, 555 nm and is given Figure 2.1 [38].

In addition to short definition of the both radiometry and photometry quantities are given following sections and their quantities and symbols are given in Table 2.1.

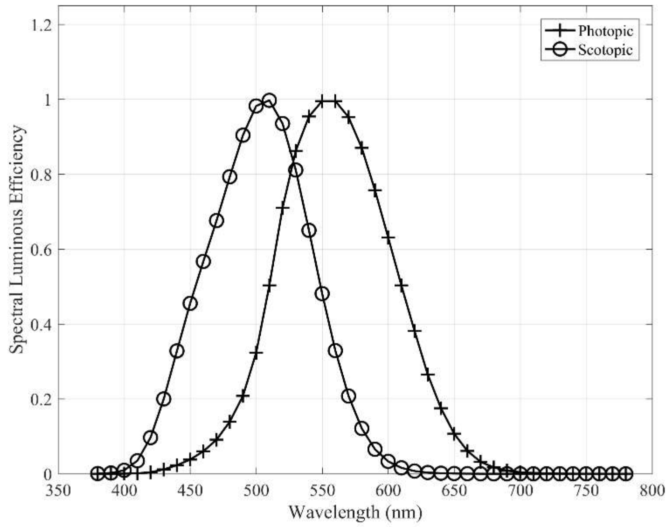

Figure 2.1 Spectral luminous efficiency for photopic and scotopic vision [39]

2.2 Radiometric and Photometric Terms

Radiation from a source or surface passes through an optical medium, leaving an effect on the respective detector. This effect has different geometrical results for each different measurement. For these reasons, radiometric and photometric measurement methods give accurate results when geometric calculations are defined. Both radiometric and photometric terms are described in detail in the following subsections.

2.2.1 Radiation Flux (Power)

The radiation emitted from a radiation source with Q energy per unit time is called radiation flux and it is described as Φ in the Figure 2.2. In the radiometry unit of the radiation flux is Watt=Joule/second.

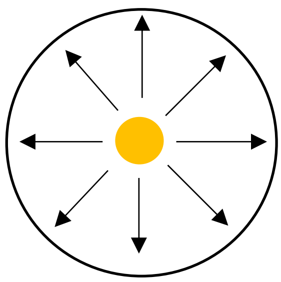

Figure 2.2 Radiation flux

In the photometry, it is known as luminous flux Φ_v and it is lumen (lm) unit and is given by [40].

$$\Phi = \frac{dQ}{dt} \tag{2.2}$$

2.2.2 Radiation Intensity

The intensity generated by the radiation flux emitted from a source in a certain direction is called the radiation intensity as shown in the Figure 2.3. In the radiometry, it is defined as watt per unit steradian. Also in the photometry, it is called candela, which is equal to lumen per unit steradian. Candela is one of the seven SI (International System of Units) units, and defined as luminous intensity and is originally described as candela power. In the 1920s, the luminous intensity unit was accepted as an international candle by the International Commission on Illumination (CIE). In 1979, a new definition of candelas was made by CIPM (the International Committee on Weights and Measures) [40-42].

The luminous intensity, in a given direction, of a source that emits monochromatic radiation of frequency 540 x 10^{12} hertz and that has a radiant intensity in that direction of (1/683) watt per steradian [40].

The radiation generated at the defined frequency corresponds to approximately 555 nm, which is the peak for photopic vision as shown in Figure 2.1, and is the point that the human eye can best detect.

The luminous intensity value for a monochromatic radiation is known to calculate by the formula described in Eqn. (2.1), where conversion between W / sr and lm / sr (cd) is possible. Eqn. (2.1) is used not only for radiation intensity but also for converting between other radiometric and photometric units, but the spectral luminous efficiency for photopic and scotopic vision values in Figure 2.1 must be used correctly for the respective wavelength.

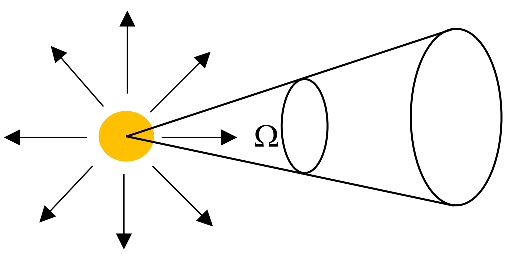

Figure 2.3 Radiation intensity

Radiation intensity is expressed as

$$I = \frac{d\Phi}{d\Omega} \tag{2.3}$$

where Φ is radiant flux or power defined the radiant energy per unit time. Solid angle Ω is a measure of the amount of the field of view from some particular point that a given object covers.

2.2.3 Irradiance and Exitance

Radiometric quantity defined as the luminous flux measured on a surface or measured from a certain area of a surface is called irradiance E or radiant exitance M. Irradiance is power per unit area incident from all directions in a hemisphere onto a surface that coincides with the base of that hemisphere. A similar quantity is radiant exitance, which is power per unit area leaving a surface into a hemisphere whose base is that surface [36].

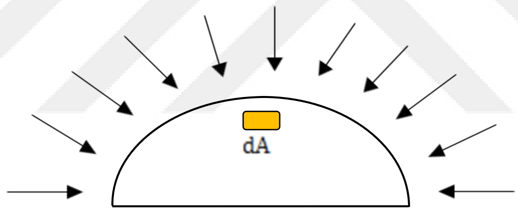

Figure 2.4 Irradiance of a small area of a surface

The irradiance or exitance unit described in Figure 2.4 is defined as the derivative of the radiation flux (power) per unit area and it is in watts/m^2 and is given Eqn. (2.4). Its photometric equivalent illuminance is defined with E_v and is defined in unit lumen/m^2 or lux.

$$E = \frac{d\Phi}{dA} \tag{2.4}$$

According to the inverse square law, the irradiance of a point source is inversely proportional to the square of the distance from that source because the same area receives less flux [32].

2.2.4 Radiance

In the radiometry, primary quantity is the radiance L used in many spectral radiometric measurements also, its photometric equivalent is the luminance L_v. This quantity is defined as the intensity of radiation produced by any amount of radiation generated in any direction from the unit projection field of surface to the unit solid angle as shown in Figure 2.5. It is expressed in the form of

$$L = \frac{d^2\Phi}{d\Omega dA\cos\theta} \tag{2.5}$$

where Φ is the radiation flux, Ω is the solid angle and detector area A.

Although some radiometric measurements are also considered as power-priority quantities, some radiometric measurements are considered most important quantity that is radiation of the light source (Radiance) and radiation amount falling on the surface (Irradiance) and conversion to other radiometric / photometric units.

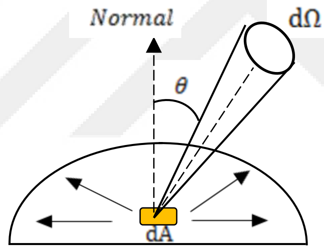

Figure 2.5 Radiance of an extended source

In the radiometry, radiance is defined unit of W/m^2 sr and its photometric equivalent luminance is defined lm/m^2 sr = cd/m^2

2.2.5 Lambertian Source

Radiation from a radiation source or a surface is defined as a source with a Lambert distribution if it exhibits the same radiation intensity in all directions. If radiation from a source or reflective surface is independent of the point of view, that radiation is called a perfect dispersing or Lambertian scattering radiation. Integrating spheres or practical black body rays are systems with approximately Lambertian distribution. As shown in Figure 2.6, the surface reflection with a Lambertian surface is independent of the intensity value of the direction viewed that is dependent on the cosine compound. This is called the Lambert Cosine law [40].

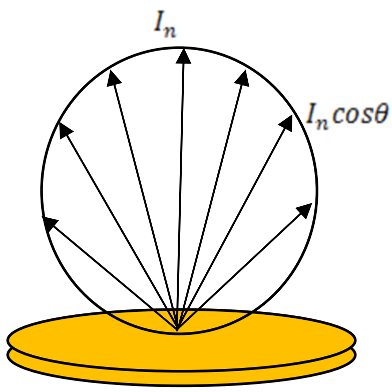

Figure 2.6 Perfect diffuser as a Lambertian source

2.3 Primary Radiometric Methods and Traceability Chain

The measurements systems in the optic radiometry consist of three main components. These are radiation source, detector and various optical and opto-mechanical materials that make up the environment in which they are transferred. The measurement traceability chain for control of the optical performance of these components can be realized in two different ways like source and detector based standard.

Source-based measuring chains working with black body radiation principle, so called "Black Body Radiator" is formed as traceable to the high-precision systems [16, 43]. The detector based measuring chain is formed as traceable to the low temperature radiometry that operates on the principle of electrical substitution of the response of the detectors to optical power at the liquid helium temperature (4.2 K) [14-16, 44].

One of the methods developed to realize the radiation scale is to obtain the radiation of the light source compared with the Black Body Radiator system. These radiation measurements performed at a specific temperature by extending with physical modeling the spectral radiation data is obtained [45-47]. Another measurement method developed as an alternative to this measurement method; is a method obtained spectral radiation data using a sensor and monochromator system to be used in radiation measurements calibrated against low temperature radiometer operating at fluid helium temperature (4.2 K) [14,17]. The second one has a lower uncertainty than the first one but in the resolution required for radiation measurements signal over noise ratio of the monochromator causes high uncertainty of transfer function of it. A method developed to solve this problem, which is used in metrology laboratory in recent years is the use of laser radiation source instead of polychromatic radiation source. It has helped to obtain the radiation scale and to determine the monochromator transfer function in low uncertainty.

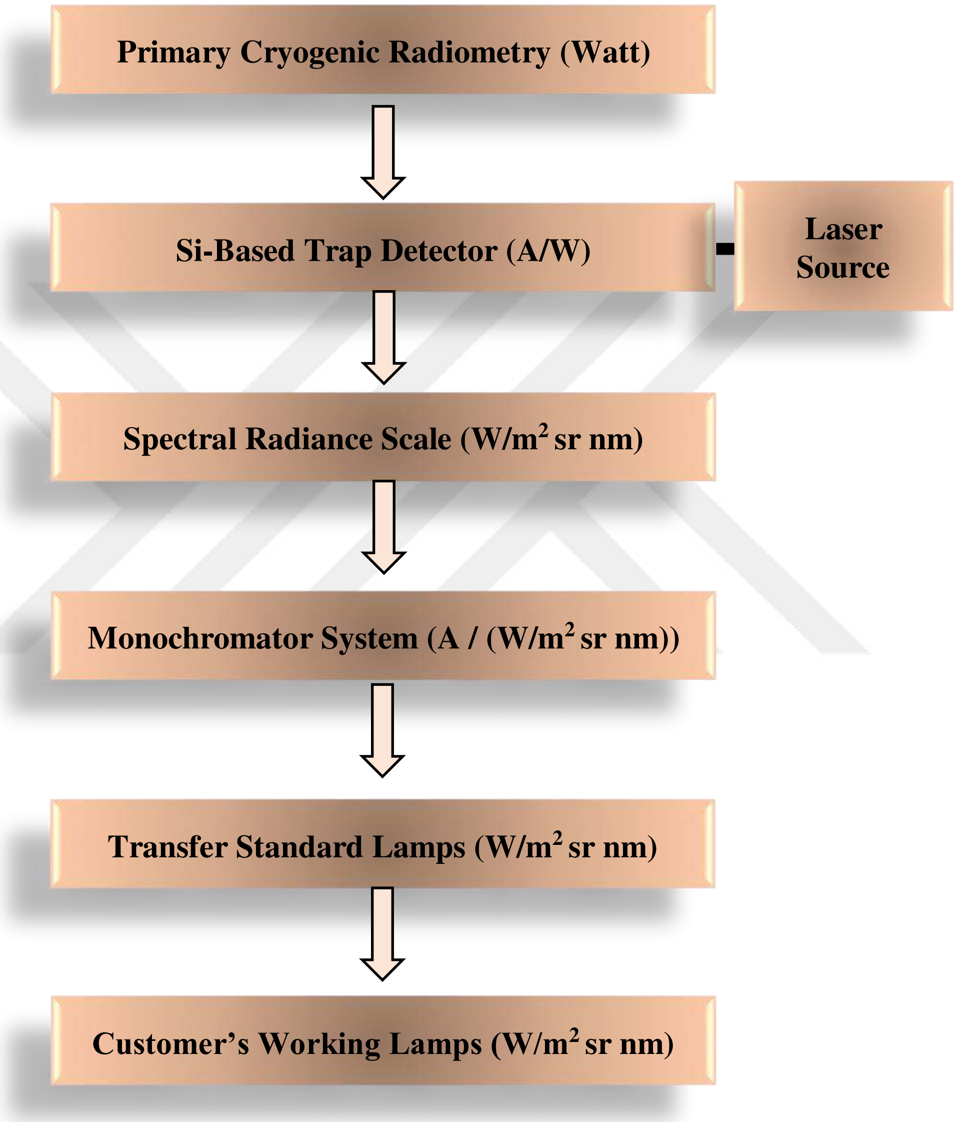

Figure 2.7 Spectral radiance scale with detector based by using laser source standard for current calibration chain at TUBITAK-UME optic laboratory.

By using laser radiation, source the above-mentioned problems can be greatly reduced, as more stable, narrow-band and high-powered beam can be obtained than polychromatic radiation source [4, 20, 21, 35]. Laser radiation sources become in the traceability chain as a reference standard. However, the wavelength and power calibrations of laser beams should be performed and monitored at regular intervals.

Figure 2.7 describes the traceability chain according to the results obtained for the radiance measurement planned in this study in the national metrology laboratory of TUBITAK-UME. According to this traceability chain, after determination of power of the laser radiation by using cryogenic radiometry, this power is transferred to detector. This method is defined as detector-based method and with improvement of the detector technology it has start to use as absolute radiometry.

2.3.1 Absolute Optical Radiation Detectors

Many of the developments in optical radiometric measurements are considered the results of developments in the field of Absolute Radiometers. From the perspective of traceability of the SI unit system, it can be seen that results obtained from the development of detector and detector responsivity measurements contribute to the development of this area.

There are two basic concepts used in the Absolute Radiometry, the use of electrical substitution (thermal) and that of quantum physics (photon). In both cases, the basic can be divided into conceptual subdivisions, but in their general application, it is largely general and similar. Detector-based measurement techniques have opened up new measurement fields over the past 20-30 years [40].

After 1979, the redefinition of candela became a turning point in optic radiometry and photometry. Thanks to newly defined detector technologies, it is easily passed from source-based measurements to detector-based measurements by re-formulating the candela [48].

With the use of solid-state devices and the development of semiconductor technology, the uses of silicon photodiodes as sensors have become advantages. They can directly deliver an electrical signal, usually current, which can be proportional to the input optical signal over many orders of magnitude. In addition, in terms of electronic characteristics, they provide high quality and cheap sensor systems for many optical radiation measurements [11, 46, 47].

With the effective uses of silicon devices, more advanced electrical substitution radiometers are developed. These radiometers are cryogenic devices operating at fluid helium temperature with low uncertainty [49]. Electrical Substitution Radiometers (ESRs) consists of a receiver that collects optical power, which is subject to temperature rise. This system generates electrical power against the temperature increase produced by optic power and provides an equal balance to the temperature increase or operates by trying to keep the system at a constant temperature. In the system, optic and electrical power is in equilibrium state. ESRs devices are often referred to as absolute detectors, because they determine the radiant flux incident upon them by direct reference to physical laws and do not depend upon another optical power-measuring device for their calibration. [50, 51]

The assumption of the equivalence of electrical power and optical power heating of a system is confirmed by the careful characterization of the radiometer. Similarly, in the case of silicon, semiconductor physics information is thought to be sufficient to describe the internal quantum efficiency and therefore the device's response to optical radiation. The measurement of high power and pulsed lasers raises difficult technical problems that lead to the development of special detectors, including those that are electrically calibrated. National laboratories check the accuracy of absolute optical power measuring devices through a series of international comparisons and other activities designed to establish equivalence of techniques. While a device such as silicon photodiode can be considered an absolute detector under the specified conditions, the actual fulfillment of the task may require considerable expertise and attention to certain procedures. Checking the procedures and practices used to perform absolute optical power measurement with a particular detector system is the main driving force for comparisons conducted by national laboratories. [52, 53].

Silicon detectors used for absolute radiometry and trap detectors designed to use these detectors more effectively should be clearly defined. The topic of the absolute optical radiation detectors express in subsection because trap detectors designed to reduce reflection losses of the single element silicone photodiode are used by National Metrology Institutes as absolute optical radiation detectors.

2.3.1.1 Silicon Photodiodes

When the theory of silicon photo diodes is examined, it is seen that they are ideal materials for optic region (from near infrared into the soft x-ray region). The electron hole pair formed in the junction region of the silicon photodiode after capturing the photon must exceed the energy band range at about 1.12 eV. This range corresponds to approximately 1200nm at wavelength. The absorbed photon form a current value on the silicon photo diode. When silicon photodiodes are examined, the electrical signal that occurs against optic power reveals an important feature. This is called the detector's responsivity value and is described in A / W unit. This value is described in wavelength and is defined as spectral power responsivity. In many cases, photo diodes are determined by current and voltage matching, and this is achieved by high quality voltmeters and amplifiers. Quality photodiodes generally have stable, uniform and sensitive features [48].

In 1980, Geist and Zalewski showed that the responsivity of silicon photo diodes could be determined with the self-calibration technique. This technique is calculated using the detector's internal quantum efficiency and reflectance. In this procedure, the internal quantum efficiency of silicon between 500 nm and 950 nm wavelengths is very close to unity. In addition, reflectance values can be calculated with ordinary optic techniques. The internal quantum efficiency is the ratio of the number of electron hole pairs created per absorbed photon. By accounting for the reflected light that is not absorbed, the number of photons incident on the silicon detector can be determined by measuring the electrical current produced. In this technique, the reflectance values of silicon detectors vary according to some physical properties. For example, its surface changes, because of additional oxidation, contamination, or even humidity changes in ordinary laboratory atmospheres can affect the reflectance of the photodiodes [22]. For this reason, the multi-detector idea predicted by Zalewski and Duba in 1983 has minimized these effects so it has ensure reducing the reflectance value. In this idea, it is aimed to collect collimation with multiple reflections by reflecting from one detector to another and reflecting on another [54].

Small changes in reflectance of identical surfaces do not change the total absorbance for the entire system. The radiation non-absorbed Φ_{na} is associated with reflectance is given by.

$$\Phi_{\mathrm{na}} = \Phi_0 \rho^{\mathrm{n}} \tag{2.6}$$

where ρ is the reflectance, n is the number of reflections, and Φ_0 is the incident flux [49]. Since ρ is typically about 0.2, Φ_{na} is a small fraction of the incident flux for $n \geq 3$. Typically, big part of the light is absorbed and converted to electrical signal [32].

2.3.1.2 Trap Detectors

The trap detectors proposed by Zalewski and Duba are designed to create a more effective self-calibration procedure and to reduce the reflectance value [54]. There are two types of trap detectors in this regard. These are reflection and transmission types trap detectors. The reflection rates in both designs are significantly reduced when compared to the single mode detector. Figure 2.8 shows that the difference in the reflectance measurements for the S1337 silicon detector. It has reflectance values less than 1 percent above 400 nm wavelength. In the reflection trap detector, the incident radiation is reflected successively from the three detectors at 45°, 45°, 0°, 45°, 45° until the residual radiation emerges from the trap back along the direction of incidence. In the transmission trap detector, the radiation is transmitted through the trap co-axially with the incident beam, after suffering six successive reflections at 45°. In addition, the glass on the front surfaces of the sensors is removed to reduce the interference effects on the trap sensors. After this process, it is possible to perform detector calibration in air or vacuum. In addition, trap detectors are approximately independent of polarization. This is an important detail because the laser radiation for a trap detector to be used as a transfer standard has a very high polarization dependence. [40, 55 - 57] The reflection type trap detector used in this study is examined by performing measurements and characterization procedures in the subtitles of the next chapters.

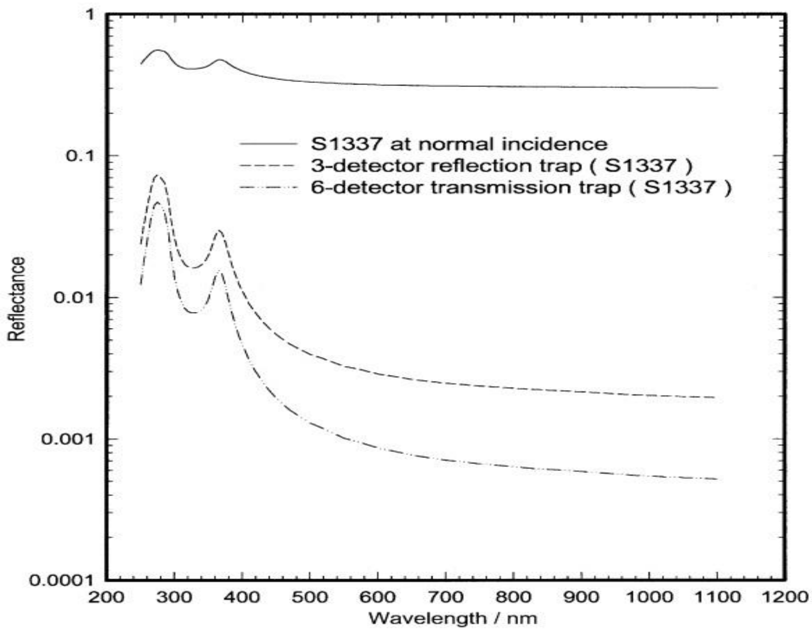

Figure 2.8 Reflection differences of silicone based reflection and transmission-type trap detectors and single element detector [40].

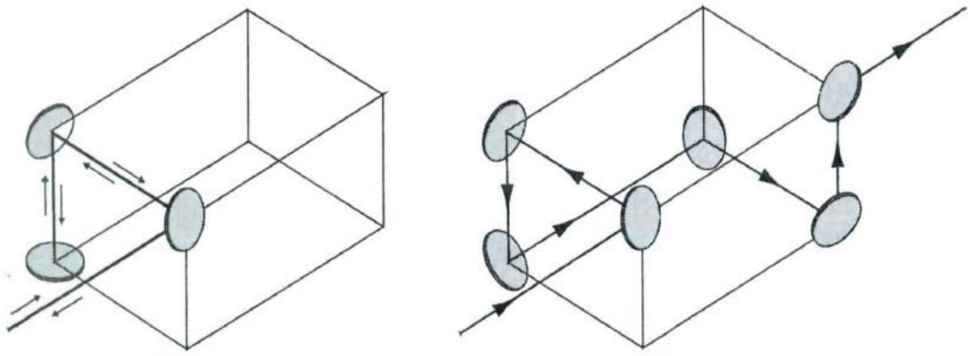

(a) (b)

Figure 2.9 Trap detectors configurations a) reflection b) transmission type [40]

2.3.1.3 Electrical Substitution Radiometers (ESRs)

Electrical Substitution Radiometry (ESR) device measures the same amount of electrical power against optic power and uses a cavity designed to collect optic radiation while doing this. In the National Institute of Standard and Technology (NIST) Albert C. Parr shows a schematic diagram of the ESR as shown in the Figure 2.10 [58].

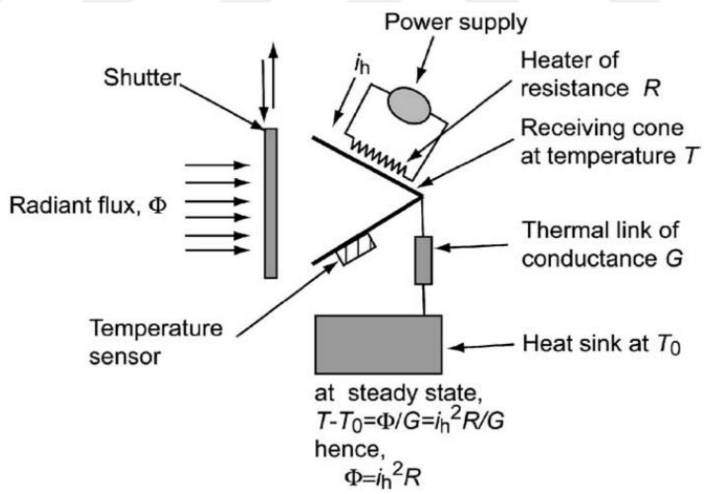

Figure 2.10 Schematic diagram of the ESR [45]

As shown in Figure 2.10, cavity behind the shutter is exposed by radiation flux Φ. Cavity can actually be described as a receiver, and it is connected to a heat sink with a G thermal conductor at constant temperature, i.e. at reference temperature T_0. When some stray, thermal radiations are ignored temperature equilibrium increase as given in

$$T - T_0 = \frac{\Phi}{G} \quad (2.7)$$

The equivalent amount of power provided by an electrical heater would have the same effect. Practically, by maintaining the receiving cavity at a constant temperature with the electrical heater, ESR performance could be improved. To create a specific temperature rise, power is supplied to the heater when a shutter is imposed to stop the light beam. A feedback loop decreases the electrical power when the shutter is opened. This feedback is involved to keep the same cavity temperature. By ignoring corrections and losses, the radiant power is given by:

$$\Phi = \left(i_{closed}^2 - i_{open}^2\right)R \tag{2.8}$$

where i_{closed} is the current applied from the resistance part when the shutter is closed, and i_{open} is the current applied when the shutter is open, also R is heater of resistance.

ESRs are used for many years [59] but the main idea is used for detector calibration, which is used to measure the power and energies of lasers. In recent years, a new design is made by lowering the liquid helium absolute temperature in order to minimize the loss of convection or radiation losses in order to ensure the progress in solid-state sensors in characterization [60]

During the 1970s and 1980s, the limited wavelength range with solid-state detector promotes the development of much-improved ESRs. A new significant design and construction of an ESR was innovated during this period that operated at cryogenic temperatures. This resulted in an increased responsivity with lower uncertainties due to convective and radiative losses.

2.3.1.4 Cryogenic Radiometer

Cryogenic radiometry is a radiometer used to reduce uncertainty by minimizing external factors in optic power measurements at the available lowest liquid helium temperature. Many NMI laboratories use cryogenic radiometry as the primary standard and it is applied at approximately 4.2K [14-16, 50]. ESRs, operating at cryogenic temperatures, work by compensating the electrical power requirement despite the temperature increase created by optic power in the cavity by using ohmic resistive heating [52]. The connection between these powers is determined in watts.

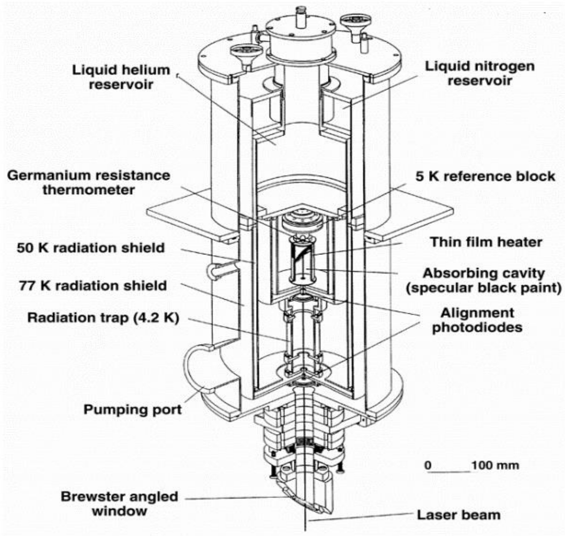

Figure 2.11 National Institute Standard of Technology (NIST) electrical substitution cryogenic radiometry schematic diagram [48].

The graphic representation of the Electrical Substitution Cryogenic Radiometer system in the National Institute Standard of Technology (NIST) publications by Albert C. Parr is described in Figure 2.11. [48]

Cryogenic Radiometer system brings several advantages together as it operates in liquid helium temperature. Since the low temperature reduces the heat capacity of the copper material used, it allows the use of a relatively larger cavity, which provides high absorption with low time constant. In addition, the conventional temperature released around cause miscarriage from distribution [4, 61, 62]. It also allows use of superconducting such as lead that has self-heating properties. [48].

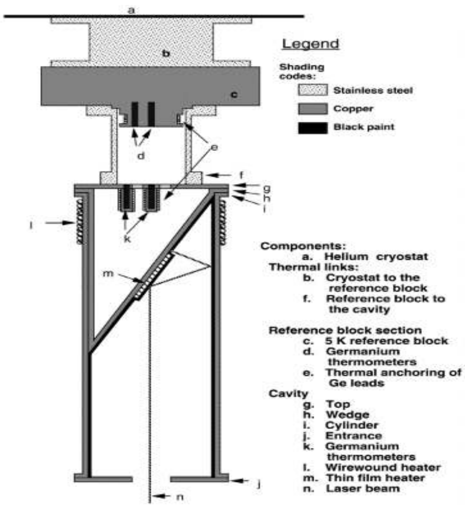

Figure 2.12 Schematic representation of the absorbing cavity of the cryogenic radiometry system [48].

2.3.2 Spectral Power Responsivity

One of the primary objectives of many National Metrology Institute's (NMI) is to identify spectral power responsivity of the photodetectors [32, 14, 16]. This knowledge is essential and is the basis for all radiometric, photometric, colorimetric applications.

Spectral power responsivity of the photodetector defined as the radio of generated photocurrent to the amount of the optical power is expressed as.

$$R(\lambda) = \frac{I(\lambda)}{\Phi(\lambda)} \tag{2.9}$$

where spectral power responsivity $R(\lambda)$ generally refers to the electrical signal $I(\lambda)$ produced by a photodetectors over radiation flux or power at specific wavelength.

Photodetectors are calibrated on behalf of spectral power responsivities in near infrared, visible and ultraviolet region defined as optic region [4, 35, 63]. The energy of each photon emitted from a radiation source with a spectral power value of $\Phi(\lambda)$ is given as hν. The number of photons reaching the detector in a unit time can be described as $\Phi(\lambda)$ / hν. Considering that each of these photons form an electron hole pairs, than the number of signal produced by each electron hole pair per unit time is given as n= η $\Phi(\lambda)$ / h and η represent quantum efficiency that is defined as the ratio number of generated electron hole pairs to the number of incident photons. If each signal contributes to the output current, then the electronic current is nq, where q is the electronic charge. The current is given as.

$$I(\lambda) = \left(\frac{\eta q}{h\upsilon}\right)\Phi(\lambda) \tag{2.10}$$

In the simplest case, the spectral power responsivity value for the photodetector calibrated by the radiation from a radiation source with a $\Phi(\lambda)$ flux value can be described using Eqns. (2.9) and (2.10) as in the form.

$$R(\lambda) = \frac{I(\lambda)}{\Phi(\lambda)} = \frac{\eta q}{h\upsilon} \tag{2.11}$$

The spectral responsivity is given by Eqn. (2.11) is rearranged by substituting $\nu = c/\lambda$ and $\eta = 1$ for an ideal photodetector and in the form,

$$R(\lambda) = \frac{\lambda}{1240} \quad (2.12)$$

where λ is given nm. The graph of the Eqn. (2.12) is given in the Figure 2.13a, it is seen that the responsivity value of the photodiode is limited at a wavelength, this value is cut off wavelength λ_g value and the forbidden energy range of the materials is determined using energy band gap denoted by E_g. It is expressed as $E_g = hc/\lambda$. Energy band gap of the semiconductor material determines wavelength limitation.

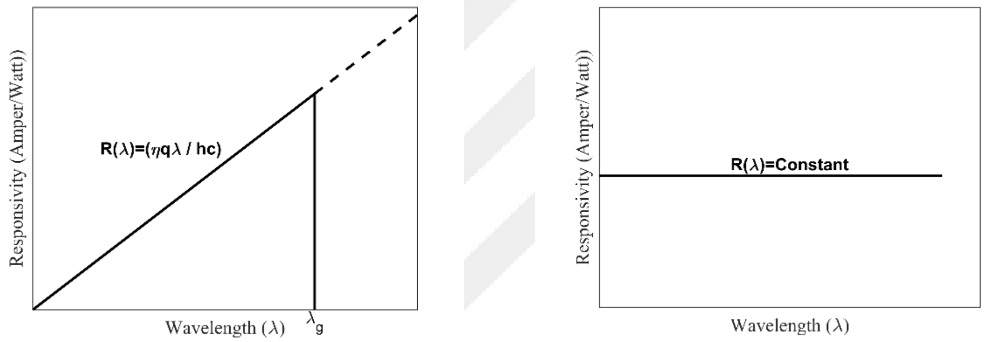

a b

Figure 2.13 Ideal detector responsivity for a) photon b) thermal [37]

The energy band range of Si photodetectors at room temperature is 1.12 eV and the corresponding cutoff wavelength is about 1100nm. For short wavelength, however the degree of light absorption within the surface diffusion layer becomes very large. Therefore, how thin diffusion layer and closer the PN junction surface, the sensitivity is so high. For normal Si photodiode, short wavelengths are around 320 nm, but some new photodetectors go down to 190nm. These are defined as UV-enhanced detectors. [64, 65].

2.3.3 Laser Based Method

Laser based methods are one of the most common methods used by NMIs to obtain the highest accuracy needed in metrology uncertainty measurements [66]. This is due to the laser's radiation characteristic structures. The wavelength accuracy used during laser-based calibration is a very high radiation. They have very small bandwidth age and high spectral purity. Since they have high-energy radiation, they are especially important in calibration and traceability measurements with the high signal to noise ratio needed during measurements. They also have a very low stray beam level. There are cases of very serious power swings in laser radiation, but by using some electronic and optical stabilizers these oscillations can be reduced to zero. Thanks to opto-mechanical and an electronic device used in measurements, good beam geometry, low beam divergence and easy alignment, convenience is solid.

The use of adjustable lasers in resource-based measurement systems leads to the avoidance of traditional balk body radiometer and increased resolution during calibration with detector-based measurement systems.

2.3.4 Black Body Radiator

At any temperature above 0 K (absolute zero), any non-transparent body emits thermal radiation. For an arbitrary body, the emitted radiant power cannot be predicted as a function of temperature and wavelength without further knowledge of material properties. However, for a hypothetical ‘‘blackbody’’ in thermodynamically equilibrium, which completely absorbs all incoming radiation (absorptivity α=1), Kirchhoff found in 1860 that the spectrum of emitted radiation becomes a function of wavelength and temperature alone, independent of the shape and material of the body. Based on the second law of thermodynamics, Kirchhoff concluded that the emissivity ε has to be equal to the absorptivity α for every-body under the same conditions of temperature, wavelength, and direction. The emissivity, which indicates the ability of a body to emit thermal radiation, therefore is unity for a blackbody, and cannot be greater than that for any other body at the same temperature. Based on Kirchhoff's findings, the search for an analytical description of the blackbody radiance spectrum became a major challenge to theoretical physics in the latter part of the 19^{th} century. Although general properties of the blackbody spectrum such as the Stefan–Boltzmann law (1879/1884) and Wien's displacement law (1893) were discovered during the next decades, the correct mathematical expression describing the spectrum could not be derived with the help of thermodynamics or classical statistical mechanics. Thus, the ‘‘mystery of thermal radiation’’ was the most prominent unresolved problem of physics at the end of the 19^{th} century [40].

With the measurements of the later scientists did not attain their original objective, the experimental confirmation of Wien's radiation law. Instead, they set up a milestone on the way to the correct blackbody radiation law, which was found by Planck in the following years, and was first presented in a session of the German Physical Society in Berlin on 19 October 1900 [67, 68]. Eight weeks later, on 14 December 1900, in another session of the Physical Society [68, 69], Planck presented the derivation of his radiation law based on the ''quantum hypothesis''. This was the birth of quantum physics. In addition, Planck's law and the work of the Germany NMI also provided the basis of radiometry as a new field of metrology.

The black body is defined as an object that absorbs electromagnetic radiation from all directions. [11, 46, 47]. One of the source-based measurements systems, the black body radiator system is used as primary standards [70]. However, due to some restrictions at high temperatures, these standards have become incompatible with other traceable standards produced with lower uncertainties.

CHAPTER 3

THE LASER BASED SPECTRAL RADIANCE SYSTEM

This established measuring system is a completely laser-based measuring system. This laser-based system, consisting of optical, opto-mechanical and opto-electronic parts, is a system that provides spectral radiance of unknown radiation sources or radiation surfaces. In addition, it enables to derive from the basic unit radiance to other radiometric and photometric quantities.

This study is based on determining the transfer function of the system created at certain laser wavelengths. The system defined for certain laser wavelengths is generalized between 350 nm and 1100 nm with reference radiance source, and becomes part of the traceability chain.

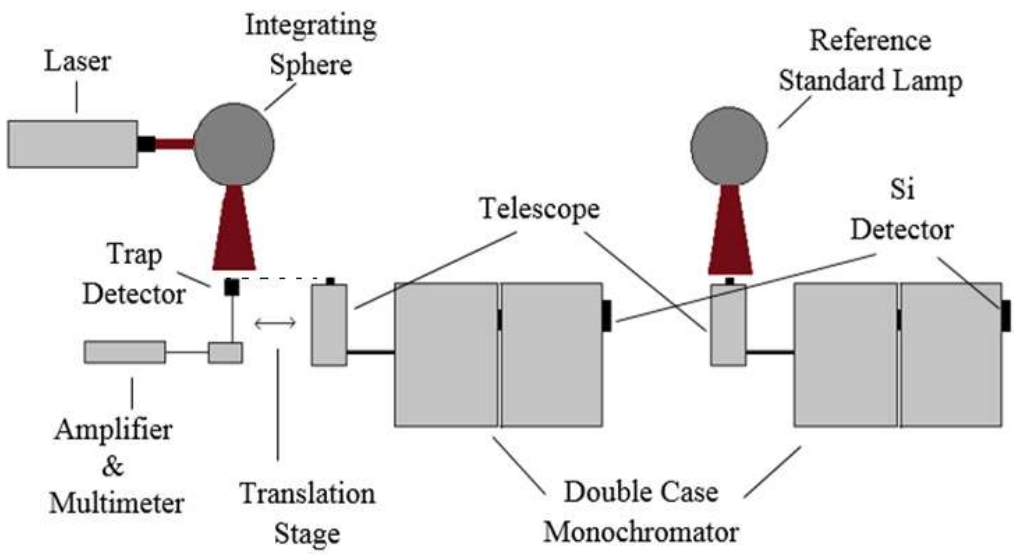

(a) (b)

Figure 3.1 Laser based spectral system a) spectral radiance and radiance responsivity of the spectroradiometer b) radiance measurement of the reference standard radiation source with calibrated spectroradiometer.

As shown in Figure 3.1, the laser-based system provides the light source with the Lambertian distribution sent on the reflection-type trap detector with a well-calibrated aperture, determining the radiance values by calculating the necessary geometric parameters. After that, for that radiance value, spectral radiance responsivity of the spectroradiometric system is derived and finally spectral radiance values of unknown radiation sources can be obtained easily.

This laser-based measurement system starts from the radiation source, integrating sphere, new generating reflection type 3 element trap detector, telescope with different field of view (FOV) mrad values, fiber optic cable, double case monochromator system, single element silicone detector. Also opto-mechanical and electronic devices and halogen lamp with reference polychromatic Lambertian distribution to control this entire system is operated for all measurement.

3.1 Lasers

In this study, different type continuous tunable gas lasers are used. These lasers systems cover form 457 nm to 1064 nm at specific wavelength regions. Most important part of the spectral radiance measurement system is to be laser-based system. This system with laser source has a lower uncertainty, while the signal to-noise ratio (SNR) of the output of the monochromator with polychromatic source causes high uncertainty in the transfer function within the required resolution range for the measurements. In recent years, a method that is developed to solve this problem, and which is used in metrology laboratories, is the use of a laser radiation source instead of a polychromatic radiation source. This approach has helped to obtain the radiation scale and to determine the monochromator transfer function with low uncertainty. By using laser radiation, these problems can be greatly reduced as more stable, narrow-band, and high-powered beams can be obtained compared with polychromatic radiation sources [4, 19-21, 35].

Argon-Ion gas laser (457, 477,488 and 514 nm), He-Ne (543, 594, 604, 612 and 632.8 nm), Nd-Yag (532 and 1064 nm) and He-Ne single (632.8 nm) continuous gas lasers are used in the laser based radiance measurement system as shown in the Figure 3.2.

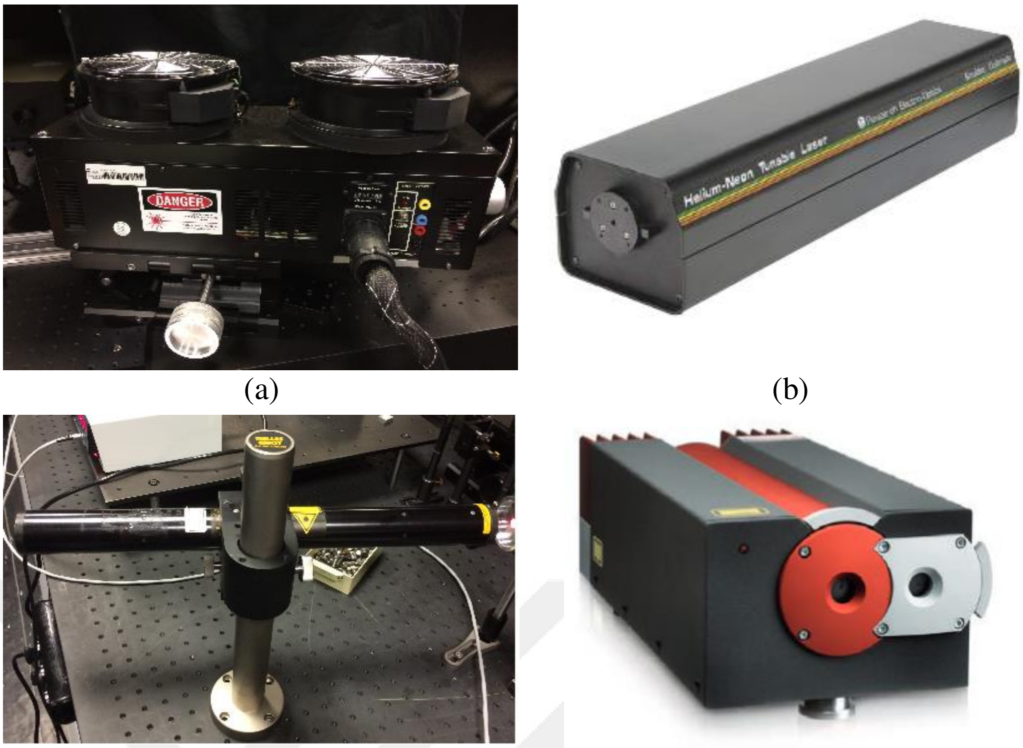

(a) (b)

(c) (d)

Figure 3.2 Laser based spectral radiance facility system has some lasers source a) Argon-ion b) He-Ne tunable c) He-Ne single d) Nd-Yag.

3.2 Integrating Spheres

Spherical shell-shaped optical equipment covered with special material with high reflective ability is called an integrating sphere. The integrating spheres have a uniform projection ability in almost all directions and positions. The radiation entering from the input port provides many internal reflections (uniformly diffuse) and a beam of light with an almost Lambertian radiant distribution from the output port. There are spheres in different sizes and different port numbers according to the application areas and are generally used in radiometry and photometry applications in optics [71-75].

Small-scale spheres can be used for entrance port of monochromator in the 30 - 100 mm diameter, middle scale spheres can be used for uniform radiance source in the 300 - 500 mm diameter and large scale ones can be used for total flux in the photometer in the 1000 - 5000 mm diameter. In addition, the spheres are classified according to the number of ports, their sizes and the arrangement of the ports. In some reflection measurements, the reflective ability of the radiation on the material is tested at 8 degrees or 45 degrees [11, 73]. Sphere and port sizes are a very important parameter in terms of the usefulness of the sphere. The optical properties of the spheres are described by transmittance and reflectance. It transmits the radiation that falls into it through multiple reflections and transmits it through the output port. Transmittance of an integrating sphere is calculated by total flux in the exit port divided total flux in the incident port.

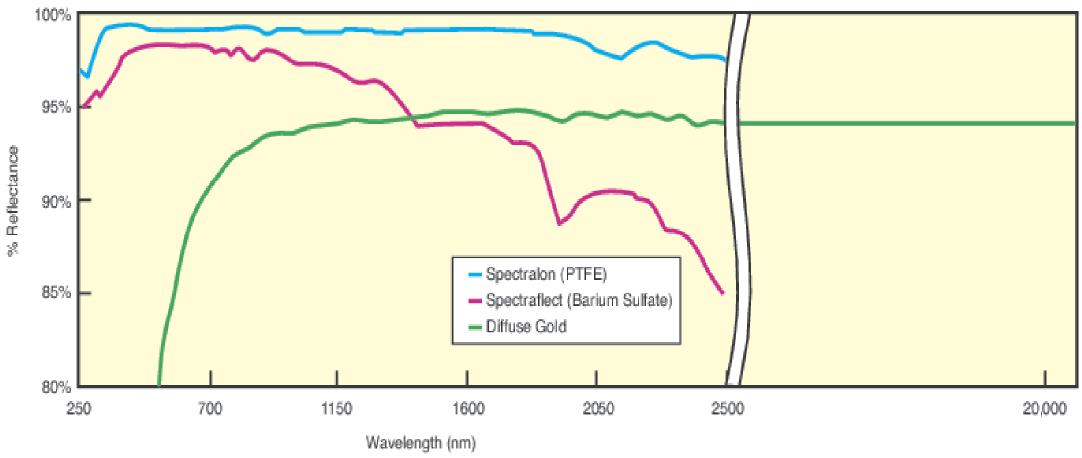

Figure 3.3 Reflectance values of the three different material coated inside of the integrating sphere [76].

There are different types of spheres for applications as well as integrating spheres with different reflectance coatings. These are Bariumsulfate (BaSO4), polytrafluoreethylene (PTFE) and gold (Au) coating materials. As shown in Figure 3.3, it is seen that different materials show different properties for different wavelengths.

PTFE based integrating spheres can be used in more demanding environments, including underwater and high or low temperature processes. At the same time, reflectance exceeding 95% from 250–2500 nm, 98% from 310–2100 nm, and 99% from 400–1500 nm make them ideal for even the most demanding measurements from the ultraviolet to the near infrared [76].

Barium sulfate integrating sphere coating has an effective range from 300 nm to 2400 nm, with reflectivity greater than 97% at 600 nm. It is a cost effective and adequate for most of radiation measurement applications. The unmatched environmental stability and high-performance based spheres are derived from their rugged monolithic thermoplastic material and are superior to coated integrating spheres. In addition, their high damage threshold surface can be cleaned with distilled water [76].

The diffuse gold coatings on gold spheres exhibit superior reflectance characteristics in the long IR region when compared with coatings on existing barium sulfate and PTFE integrating spheres. The typical reflectance of gold is >94% up to 20 µm, while reflectance deteriorates rapidly after 2500 nm for both barium sulfate and PTFE. This makes gold spheres an ideal choice for mid- to far-IR applications [76].

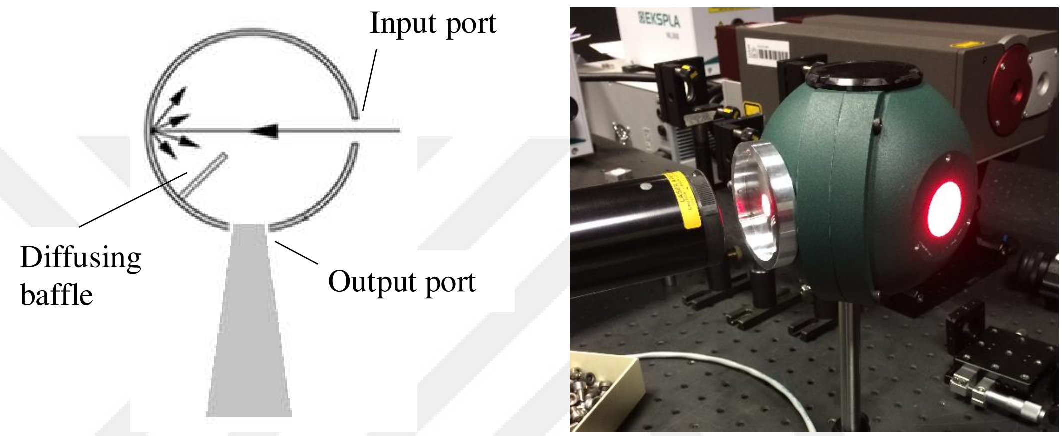

Figure 3.4 Integrating sphere used in the spectral radiance measurement system

In our spectral radiance measurement system used integrating sphere, has 0.15 m diameter size, three port 0, 90 and 90 (North Pole) degree and BaSO4 reflectance coating. In addition, input port is 0.01 m and exit port is 0.025 m diameter size as shown in Figure 3.4.

3.3 Trap Detector

Detectors used in the radiometric measurements are divided two groups depending on application areas such as thermal and photon detectors. Because the interaction rate, responsivity, linearity of the responsivity, sensitivity, quantum efficiency, spatial homogeneity, noise equivalent power (NEP), of the photon detectors are higher in accordance with thermal detectors. Therefore, in the spectroradiometric measurements photon detectors are more preferred.

Photon detectors, according to the working principle and structure, photo resistor, phototransistor and photodiode are divided into three groups. Photo resistor is a semiconductor that has not a junction. Phototransistor without base connection works like a photodiode; otherwise, it is a current raising detector. In addition, photodiodes are divided two groups in itself produce of current (photoconductor) and voltage (photovoltaic cell and solar cell). In the spectroradiometric applications photodiodes generating current are used as shown in the Figure 3.5.

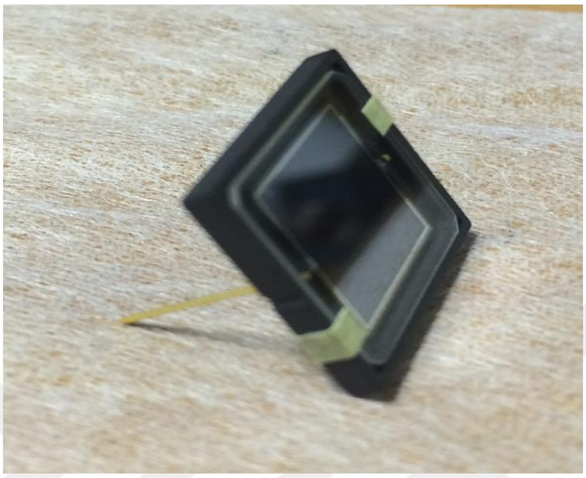

Figure 3.5 Reflection type Silicon Photo Diode Hamamatsu S1337.

The high reflection losses and dependence of the polarizations of these detectors restricts the using in the spectroradiometric applications. In this study, the number and placement of shapes of the photodiode can reduce the reflection losses (< % 1) and polarization dependence and these type photodiode sensors called trap detector as shown in Figure 3.6. In this kind of trap detectors incoming beam undergoes five reflections where most of the radiation is being absorbed by photodiodes and the remaining beam returns back along the incoming beam. Due to these reasons the response of the detector to incident light can be determined more effectively [30].

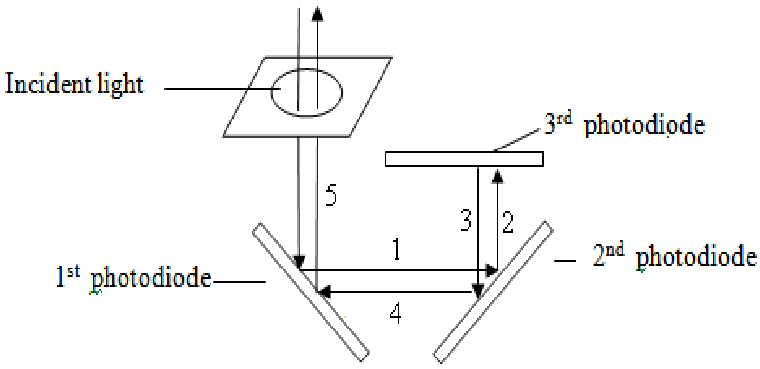

Figure 3.6 Reflection type Silicon trap detector schematically representation.

In this study, reflection type silicon-based trap detector is designed and manufactured for use in spectroradiometric measurement.

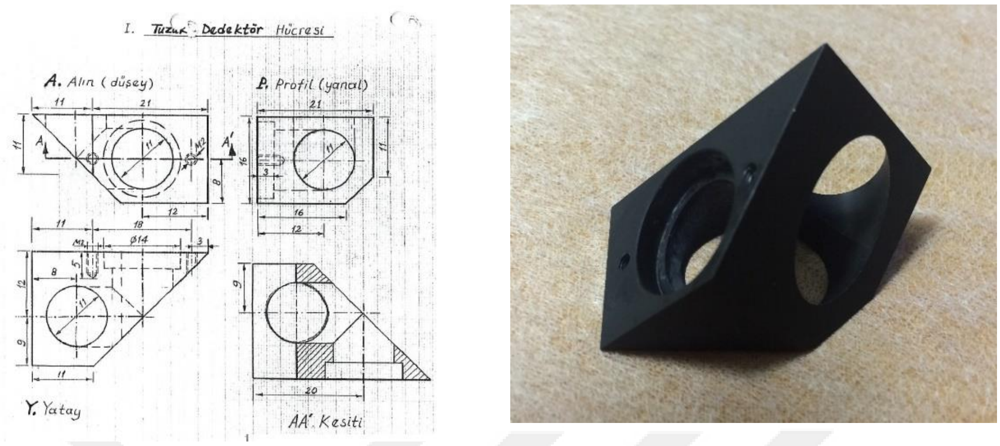

Figure 3.7 Trap detector bottom holder and schematic display.

The detector holding section, which is schematically drawn in three dimensions, is designed as seen in the Figure 3.7 to combine three identical silicon-based photodiodes which are two of them are 90 degrees to each other and other ones is 45 degrees each other. In addition, in order to be used in radiometric measurements, the entrance area is designed with a precision aperture of 0.01 m as a top and bottom cover in Figure 3.8.

Figure 3.8 Trap detector front-back cover and protective outer shell.

By using bottom holder of the detectors obtained, three identical Si-based photodiode (Hamamatsu S1337) is fixed carefully to holder. Following this operation, the connections of the detectors are connected in a parallel form to each other as shown in the following Figure 3.9.

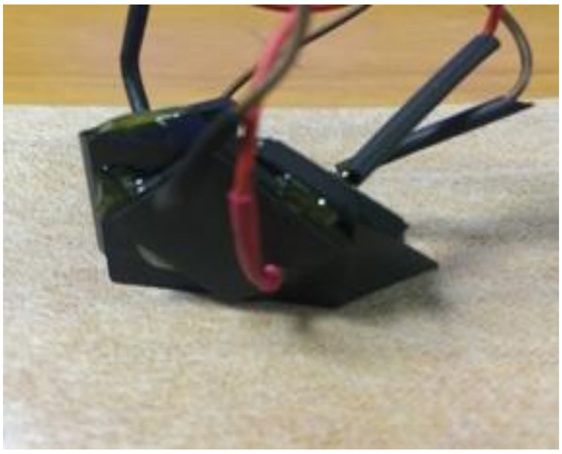

Figure 3.9 Trap detector

3.4 Reference Radiance Source

SRS12 reference radiance source is shown in the Figure 3.10. This reference standard source can been used as the calibrated radiance source to the determination of spectral radiometric and photometric quantities. The units are of mW / m^2 sr nm over a wavelength range of 250 nm to 2500 nm in intervals of 5 nm. Results are provided with an associated uncertainty using coverage factor k=2 to provide a 95.45% level of confidence. The lamp is operated from a power supply at 8.5A, and run for twenty minutes warm up time before measurements commenced. Measurement conditions are conducted at a temperature of 20°C and relative humidity of 65%. Photometric values are correlated color temperature 3310 K and Luminance – 20889.169 cd/m^2

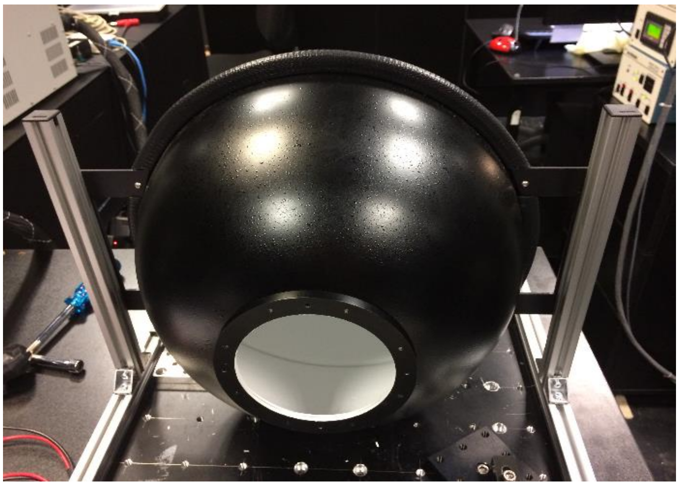

Figure 3.10 SRS12 reference radiance source.

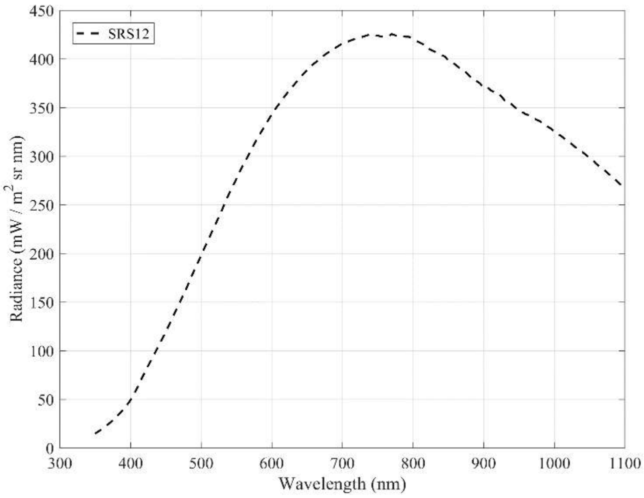

Figure 3.11 Spectral radiance distribution of the SRS12 reference standard source.

The spectral radiance responsivity values obtained with the laser sources used for spectral radiance measurement system are controlled by using SRS12 reference standard source. Although this source is a certified radiance of 250 nm to 2500 nm, only 350 nm to 1100 nm is used in the measurements. Certified spectral radiance values are given in Figure 3.11.

3.5 Telescope

TEL310, allowing the radiation measurement using defined vision areas related to measurement standard, computer controlled stepper motor-driven focus and clarity with the selection, direct-sighted telescope. USB camera-based viewer shows the user a measurement stage; measurement range is connected to any monochromator through a quartz fiber bundle. The telescope displays the measurement scene from an aperture for measurement to the aperture plane where only the selected portion of the scene is transmitted. Radians corresponding field of view, is the ratio of the distance between the lens and the aperture diameter of the aperture. Sources according to standard 200 mm depending on the application or resource 500 lux (only 200 mm) measured at a distance to produce an illumination. In practice, the measurement distance may be many meters. As the entrance lens, position is adjusted to obtain a focused image, the image distance changes, and, for a given aperture diameter, so changing the field of view. The TEL310 consists of a stepping motor driven periscope to change the image distance of the lens, and a stepping motor driven aperture wheel, which automatically selects the required aperture for a given field of view, to within 1% .

Laser based radiation source and reference standard radiation source are placed 200mm in front of TEL310 device and transferred to double monochromator system with fiber optic cable, as shown in Figure 3.12.

Figure 3.12 Bentham Company TEL310 telescope.

The TEL310 telescope used in the experiment has three different field of view (FOV) as 1.7-mrad, 5-mrad and 11-mrad. In this study, each FOV mrad is used and tested.

3.6 Monochromator

Monochromator is optical systems that transmit the radiation into separable wavelengths by using prisms or grating. Monochromator with grating are often preferred for spectrometric measurements due to capabilities such as wavelength selectivity, high resolution and low stray light [77, 78]. Before performing measurements like photometric, radiometric, atomic absorption and emission, wavelength calibration of the monochromator with grating should be accurately known [79].

Monochromator systems occurs spectral distribution in the UV(ultra-violet), Vis(Visible) and IR(Infra-Red) regions depending on light source and grating properties. This spectral region is about between 200 nm and 2500 nm. Blaze angle and power of the gratings used in the monochromator introduce this spectral diversity [80]. In monochromator where different gratings are used for each spectral region, besides in wavelength calibration the accuracy of the grating is a critical requirement for all wavelength-dependent measurement.

Monochromator is divided into two groups that are single and double optical diffraction side, according to their usage characteristics. When single monochromator part is connected with mechanical system of the other single monochromator part in series, it takes the form of a double monochromator given in Figure 3.13.

3.6.1 Double Monochromator System

In the wavelength-dependent measurements of radiometric units, monochromator systems with high spectral resolution, high wavelength selectivity and low stray light levels are preferred instead of filters [20]. While it makes light separation operation, it uses the diffraction grating, which is explained, in the following subsection.

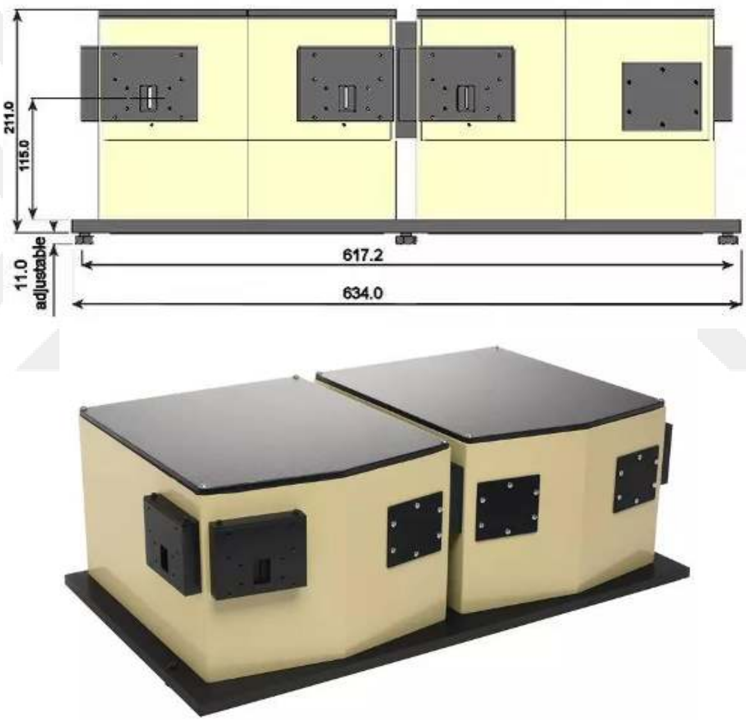

Figure 3.13 Double monochromator system.

In double monochromator system, theoretically, there are four-entrance and exit port, but since the exit port of one corresponds to entrance port of another, there are one entrance, one exit and one middle port. Double monochromator system can be used both single mode and double mode. Also double mode has different two types of operating characteristics. These are additive and subtractive mode. Additive means that light that is dispersed by the first monochromator is further dispersed by the second [81]. The dispersion is the wavelength range in nm in 1mm distance in the plane of the slit. Thus, if a single monochromator has a dispersion of 2 nm/mm, then the same type and design of a double additive monochromator would have a dispersion of 1 nm/mm. The second type is subtractive mode that is used also in two different measurement methods. The first one is used in situation where rapid measurement is necessary and other one is used in situations where spectral measurements of the detectors are required.

In the ideal a monochromator system, before starting this study, there are some calibration measurements. These measurements determine that the system is working properly whether or not. These are stray light measurement, set the band-pass (resolution), spectral radiation falling per mm and wavelength accuracy of the monochromator device. Making the monochromator, calibration ensures to take accurate measurements.

3.6.1.1 Stray Light

The exit beam from a typical monochromator should be monochromatic but usually it contains undesired light of other wavelengths. Filters can be used to block higher order diffracted wavelengths. Other unwanted light, called stray light, has several origins and it should be minimized. Stray light can be caused by diffraction, light scattering, or the machine may need to be repaired. All spectrophotometers have stray light. Higher end models have less stray light, but no machine is perfect. Usually, part of this unwanted light, called re-entrant spectra, is due to diffracted light being directed onto the entrance, collimating or focusing mirror, and back towards the grating [82].

3.6.1.2 The Band Pass

The band-pass is the width of the spectrum passed by a monochromator when illuminated by a light source with a continuous spectrum. In a monochromator, the band pass may be decreased by reducing the width of the slits until a limiting band pass is reached. The limiting band pass is called the resolution of the instrument. In spectral analysis, the resolution is a measure of the ability of the instrument to separate two spectral lines that are close together [82].

3.6.1.3 Spectral Band Width (SBW or FWHM)

When a monochromator is set to a particular wavelength, light with a Gaussian intensity distribution of wavelengths emerges from the exit slit. This intensity distribution is depicted in Figure 3.14. In this figure, λ and the dotted vertical line represent the wavelength set on the instrument. The heavy black line represents the distribution of light that reaches the sample. The spectral bandwidth is defined as the width of the band of light at one-half the peak maximum (or full width at half maximum (FWHM)) and is represented by the two vertical red lines and λ_{SB} on the wavelength axis. Spectral slit width is defined as the total spread of wavelengths represented by the blue lines and λ_{SSW}. The spectral bandwidth of the instrument is always narrower than the spectral slit width. The spectral bandwidth of a spectrophotometer is related to the physical slit-width of the monochromator and, therefore, to the resolution capabilities of the instrument.

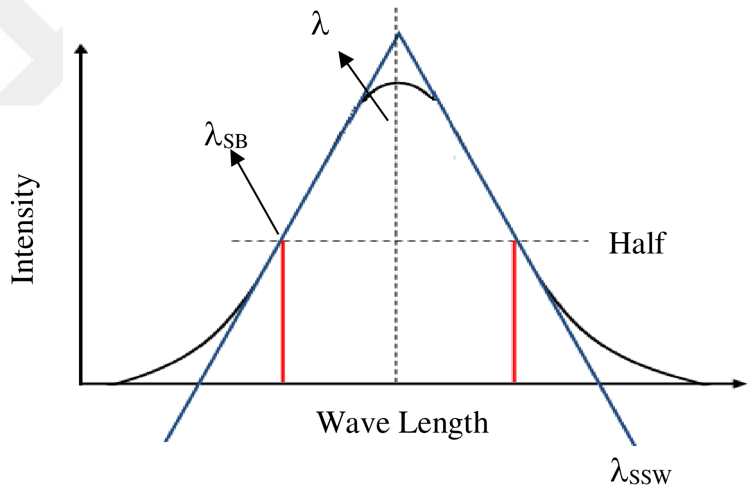

Figure 3.14 Gaussian intensity distribution of wavelengths emerging from the monochromator. The spectral bandwidth is defined by the red boundaries and λ_{SB}. The spectral slit width is depicted by the blue boundaries and λ_{SSW}.

3.6.1.4 Dispersion

The dispersion is defined as the 1nm of spectrum per mm of the slit width. That is the dispersion is the wavelength range in nm in 1 mm distance in the plane of the slit. Thus, if a single monochromator has a dispersion of 2 nm/mm, then the same type and design of a double monochromator would have a dispersion of 1 nm/mm. In addition, it is characterized as the bandwidth of the band per unit slit width. In the double monochromator system, there are two dispersion modes additive or subtractive. In addition, a double monochromator include an extra slit, the middle slit that is used for additive dispersion mode. The purpose of the middle slit is to reduce the amount of the stray light going from the first to second monochromator; and tracking problem between the component monochromator is to result.

3.6.1.5 Diffraction Grating

The equipment, which is used to separate the wave lengths of the radiations are such as prisms, filters and gratings. Filters and prisms do not provide optimum radiation feature in the desired wavelength, but gratings have maximum performance in the desired wavelength region. Gratings have linear distribution. Exit surface of the monochromatic rays change linearly with the wavelength but prisms do not have it.

Gratings are used to separate the wavelength of the broadband radiation and to adjust the band range. These devices are used in the monochromator parts of the spectrophotometer devices. In order to get good spectral results, correct grating must be chosen. There are two parameters of the grating such as “groove frequency” and “blaze angle” to determine the properties of it. In the grating surface opening channels is called “groove" is called and like saw tooth.

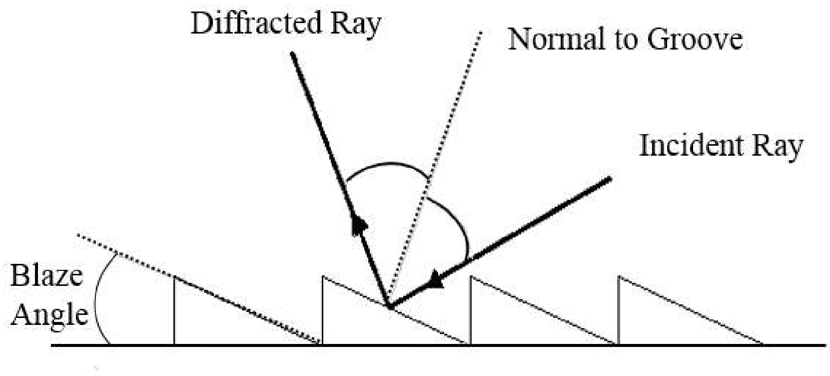

Figure 3.15 Diffraction grating representation and Blaze angle.

Most modern spectrophotometers contain gratings instead of prisms. These devices are made from glass blanks, onto which very narrow grooves are ruled. Traditionally, this task is done mechanically, but modern production methods use a holographic optical process. The dimensions of the grooves are of the same order as the wavelength of light to be dispersed. Finally, an aluminum coating is applied to create a reflecting source. Light falling on the grating is reflected at different angles, depending on the wavelength. Holographic gratings yield a linear angular dispersion with wavelength and are temperature insensitive.

Grating used in this study is shown in the Figure 3.15 and double monochromator has the triple diffraction grating system. Each parts of the grating are same groove over millimeter. In terms of the spectral region studied, different gratings are used in the Table 3.1 summarize the maximum recommended range of use in the monochromator most popular diffraction gratings. [81].

Table 3.1 Available maximum wavelength range of the gratings.

Line density (g/mm)	**Maximum λ Range (g/mm)**
2400	200-600nm (250nm Blaze)
1200	300-1200nm (500nm Blaze)
600	800-2500nm (1250nm Blaze)

3.6.1.6 Order Shorting Filter

Monochromator disperse light into its component wavelengths, and diffraction gratings spread light into a number of overlapping diffraction orders. All of these orders should be eliminated in order to obtain accurate spectral measurements. For example, at the grating position at which one finds first order 400nm, one also finds second order 800nm where the source emits light at the wavelength. This is a cause of concern where the photodetector or sample under test also responds at the higher order wavelength. Unwanted diffraction orders leaving from the output slit of the monochromator prevent with the circular motion filter mechanism as shown in Figure 3.16, depending on the wavelength setting of the monochromator.

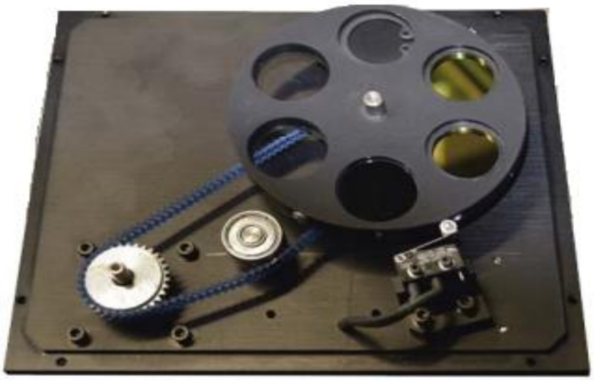

Figure 3.16 Order shorting filter of the monochromator system.

3.6.2 Monochromator Detector

Silicone photodiode, as shown in the Figure 3.17 is integrated into the double monochromator system. It is called DH-Si UV-enhanced silicon photodiode and it offers excellent linearity and low noise over the UV Vis NIR spectral range. It used in the double monochromator system has 0.01 x 0.01 m active area and it covers 200 - 1100 nm spectral range that enhanced UV region

Figure 3.17 DH-Si UV enhanced Bentham Company detector.

The detector shown in Figure 3.17 is a detector designed for brand double monochromator system. As shown in Figure 3.18, spectral power responsivity values in UV regions go up to 200 nm.

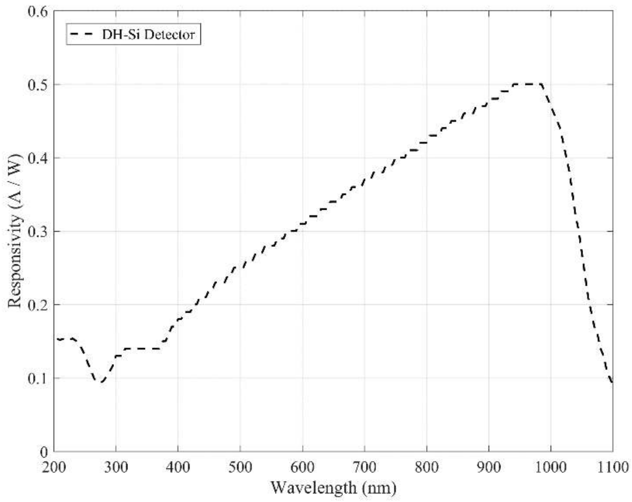

Figure 3.18 DH-Si UV detector power responsivity.

3.7 Amplifier and Multimeter

The radiation falling on the photodiode can create low current values on the detector from picoampere level to microampere level. This current is converted to voltage in a current-to-voltage amplifier, a so-called transimpedance amplifier. The size of the feedback resistor determines the size of the amplification, e.g. a 1 MΩ resistor cause an amplification of 10^6 V/A. For trap detector used in the system and for single detector behind the double monochromator are amplified by transimpedance amplifiers as shown in Figures 3.19 and 3.20 respectively.

Figure 3.19 Lab Kinetic Ltd SP042 amplifier.

Figure 3.20 Bentham Company 417 detection electronic system

Figure 3.21 HP 3458A digital Multimeter.

In the Figure 3.21 digital Multimeter output signal amplified coming from transimpedance amplifiers presents as a current without any loss. Labkinetic amplifier and Hp 3458A Multimeter used with together connected to trap detector. In addition, Bentham Company 417 detection electronic system has both amplifier and Multimeter combined together. These electronic devices have many properties and shows diversity according to the application used so not every property has defined about this device.

3.8 Theoretical Model for the Laser Based Radiance System

This study is modelled by using radiometric quantities and is followed some steps to calculate the spectral radiance of laser based source, spectral radiance responsivity of spectroradiometer system and unknown radiation source.

First, using geometric parameters given in the Figure 3.22 a model used for evaluation of laser based radiance measurement system is defined

Radiance is obtained numerically by analyzing the physical parameters between the source-detector given in Figure 3.22 for the measurement apparatus given in Figure 3.1.

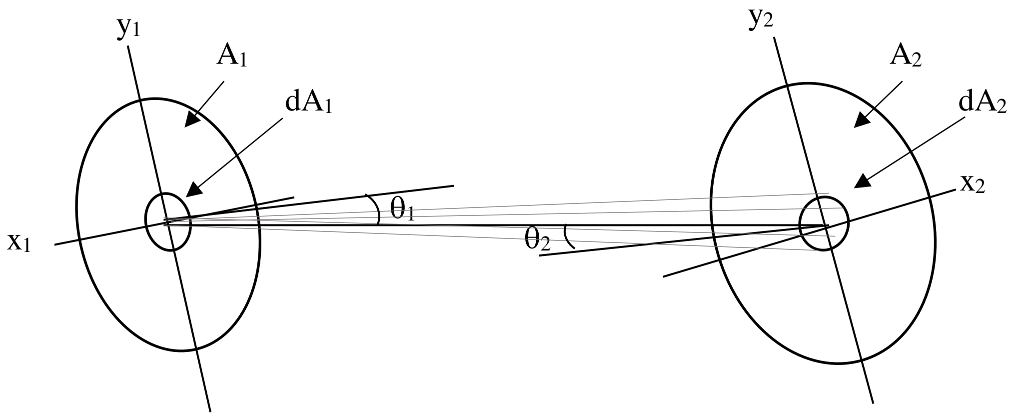

Figure 3.22 Geometric identification between source and detector.

The relation defined to the Eqn. (2.5) between the radiation flux (Φ) and the radiance (L) from the radiation source can be given as,

$$d^2\Phi(\lambda) = L(\lambda)\frac{dA_1 \cos\theta_1}{(x_2 - x_1)^2} dA_2 \cos\theta_2 \tag{3.1}$$

where, dA_1 and dA_2 is the differential area element of the source and detector respectively. x_1 and x_2.are the coordinate axes. Radiation flux defined in the Eqn. (3.1) is a function of the spatial and angular coordinates. Since source of radiometric interest can be considered Lambertian, they radiate a constant radiance in all directions into hemisphere. Because of that reason, some assumptions can be made and integral only depend on function of the wavelength [40].

The current I^s generated in the detector is expressed as follows,

$$I^S = \int R_s^*(\lambda)\ \phi(\lambda) d\lambda \tag{3.2}$$

where $R_s^*(\lambda)$ is the spectral power responsivity of the trap detector. By considering the required parameters and geometric values in Figure 4.1, the radiance formula is obtained as,

$$I^s = \frac{A_1 A_2 (1+\delta)}{(r_1^2 + m^2 + r_2^2)} \int L(\lambda)\ R_s^*(\lambda) d\lambda \tag{3.3a}$$

$$L(\lambda) = \frac{I^S}{R_s^*(\lambda)} \frac{D^2}{A_1 A_2 (1+\delta)} \tag{3.3b}$$

where $\delta = r_1^2 r_2^2 / D^4$ and $D^2 = r_1^2 + m^2 + r_2^2$ in Eqn. (3.3b), A_1 and A_2 are the active area of the radiation source and detector, respectively. m represents the distance between the radius of source r_1 and detector r_2. In addition, I^S is the measured spectral current, $L(\lambda)$ is the spectral radiance, and $R_s^*(\lambda)$ is the spectral power responsivity of the detector.

3.8.1 Spectral Radiance Responsivity of the Spectrophotometric System

When a radiation source with a known radiance value is transferred to the spectrometric measurement system, the transfer function of the system, namely the radiance responsivity value, can be determined. By performing unit analysis, the spectral radiance responsivity value is determined as follows from the spectral power responsivity value of the detector.

If unit analysis of the Eqn. (3.3b) is done and the geometric parameters are equal to a constant C, the Eqn. (3.4) is obtained as.

$$L(\lambda) = \frac{I^S}{R_s^*(\lambda)}\frac{1}{C} = \left[\frac{A}{A/W}\frac{1}{m^2\ sr}\right] = \left[\frac{W}{m^2\ sr}\right] \tag{3.4}$$

where current I^S in the trap detector is amper (A) unit and power responsivity $R_s^*(\lambda)$ of the trap detector is amper/watt (A/W) unit.

The spectral radiance responsivity $R_s(\lambda)$ can be changed using spectral power responsivity. $R_s^*(\lambda)$, with $R_s(\lambda) = R_s^*(\lambda)C$ the standard detector output signal can be obtained as follows,

$$I^S = \int R_s(\lambda)\, L(\lambda)\, d\lambda \tag{3.5}$$

where, $R_s(\lambda)$ is in A / (W / (m^2 sr nm)) unit and it called that spectral radiance responsivity of the laser source on the trap detector. Since laser radiation is very similar to monochromatic radiation, the integral of the delta function is taken over the wavelength of the laser.

Similar procedures are used to determine the spectral radiance responsiveness of the optical measurement system including telescope and monochromator. Firstly, the radiance field that is obtained is transferred to the optical system and the output signal of the monochromator is measured. This signal is dependent on the laser wavelength and the adjusted wavelength of the monochromator. The obtained signal becomes the spectral radiance responsivity function of the monochromator $R_M(\lambda_M,\lambda_L)$. Thus, the output signal of the monochromator I^M is described as.

$$I^M = \int R_M(\lambda_M, \lambda_L)\ L_{Laser,\lambda_L} d\lambda \tag{3.6}$$

where current I^M is the output current signal of the monochromator, $R_M(\lambda_M, \lambda_L)$ is the spectral radiance responsivity of the optical system depend on both laser wavelength and monochromator setting wavelength. Substituting for L_{Laser,λ_L} in Eqn. (3.5), the following equation for the unknown spectral radiance responsivity of monochromator $R_M(\lambda_M, \lambda_L)$ is obtained as:

$$R_M(\lambda_M, \lambda_L) = \frac{I^M R_s(\lambda_L)}{I^S} = \frac{I^M\ R_s^*(\lambda_L)\ \Delta C}{I^S} \tag{3.7}$$

where, I^M and I^S are the current created on the exit of the monochromator and trap detector respectively. $R_s^*(\lambda_L)$ is the spectral power responsivity and ΔC is the geometric parameters.

3.8.2 Evaluation of the Radiance for an Unknown Source

The radiance field that is obtained is transferred to the monochromator in three different fields of view (1.7-mrad, 5-mrad, and 11-mrad). A Tel310 telescope is used during the transmission of the radiance field. Therefore, the spectral radiance transfer function of the monochromator system is defined based on the telescope, fiber optic cable, double monochromator, and detector parameters.

The monochromator system to be defined as a transfer function is a double-case system, so three slit structures are available, namely the entrance, middle, and exit slits. In order for the transmitted radiance field to give the correct output signal, each slit range requires a suitable adjustment. Both in theory and practice, slit ranges can be set to the same values. However, in double monochromator systems, the entrance slit should be wider than the exit slit, and the middle slit should be wider than the entrance slit. The differences between the slit widths should not be significant. Each of the three slits has its own special significance. Therefore, as the exit slit is at the side where the image occurs, it needs a maximum SNR in the smallest slit value [32].

The radiance field resulting from a light source is transformed into an output signal depending on the wavelength of the monochromator λ_M, radiation source λ_L, and the spectral radiance responsivity function of the monochromator $R_M(\lambda_M, \lambda_L)$. Thus, if

Eqn. (3.6) is rearranged by using the output signal I^U of the unknown source from the monochromator and the wavelength adjustment of the monochromator λ_M, so $R_M(\lambda_M, \lambda_L) \rightarrow R_M(\lambda_M, \lambda_M)$ the result can be obtained as,

$$I^U = \int R_M(\lambda_M, \lambda_M)\, L^U(\lambda) d\lambda \tag{3.8}$$

where I^U is the monochromator output signal at the monochromator wavelength setting λ_M, and L^U is the spectral radiance of the unknown source. Because $L^U(\lambda)$ has a linear dependence as a function of the wavelength, $L^U(\lambda)$ can be moved outside the integral.

The spectral radiance responsivity of the monochromator is taken as the integral over the wavelength setting, by using Eqn. (3.7) the radiance formula of the unknown source is obtained in the form.

$$L^U(\lambda) = \frac{I^U \; I^S}{I^M \; R_s^*(\lambda_L)\; \Delta\lambda\; \Delta C} \tag{3.9}$$

where, $\Delta\lambda$ is the full width at half maximum (FWHM), which is the spectral band-pass value of the monochromator. The slit spacing of the double monochromator system is adjusted to calculate this band-pass value.

CHAPTER 4

MEASUREMENT OF SPECTRAL RADIANCE

To determine the spectral radiance of the unknown radiation source and reflection surfaces, a system is designed using the devices described in the Chapter 3. The spectral radiance measurement system to measure traceability of the radiometric and photometric quantities is shown in the Figure 4.1. This thesis is done in TUBITAK-UME optic laboratory. Firstly, calibration should be made and system characterization of the double monochromator system starts to measure spectral radiance responsivity. After that, lasers and reference source measurements are realized. In the last stage, errors and corrections made during the measurements is defined.

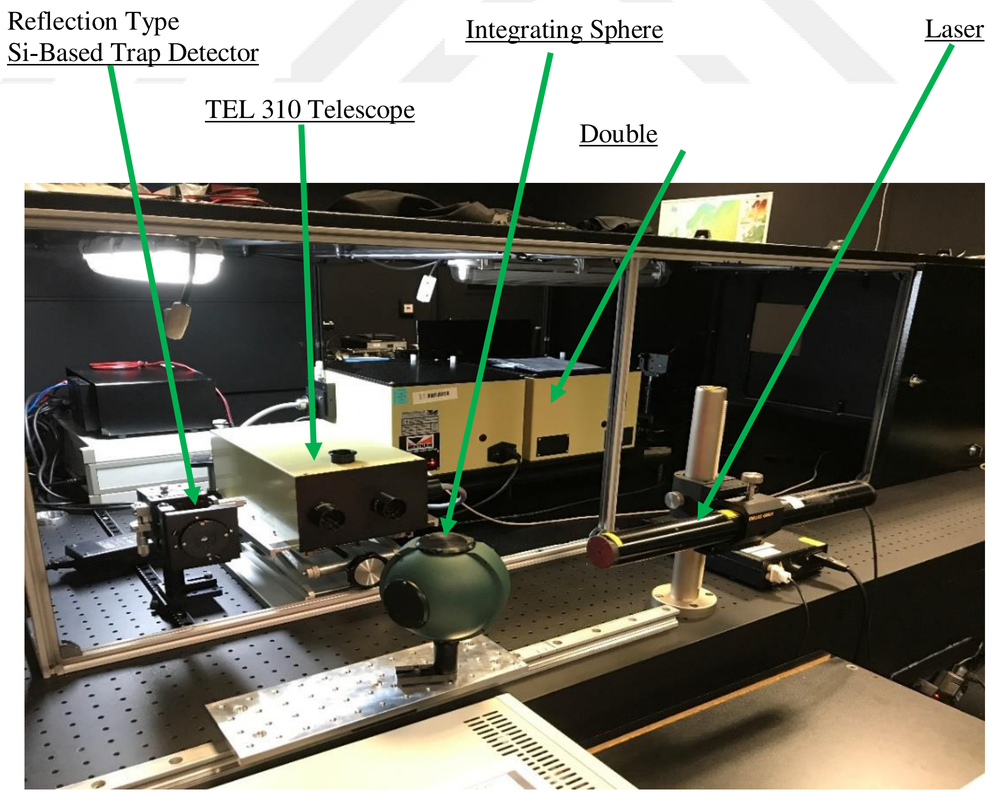

Figure 4.1 Spectral radiance measurement system.

The devices used for the spectral radiance measurement and their properties are described in the previous sections. Each electronic, mechanical and optical component used in the measurement system is calibrated and is ensured traceability in TUBITAK-UME optic laboratory. Before starting the measurements, production and characterization of the Si-based reflection-type trap detector is realized also all relevant information to this process is defined in Chapter 3.3.

Spectral radiance values with expanded estimated uncertainty values, is defined making geometrical corrections and calculations by using lasers and integrating sphere in given Eqn. (3.3). The radiance values determined for different laser wavelengths are transferred to the input slit of the double monochromator system and spectral radians responsivity value of it is determined in given Eqn. (3.7). Finally, spectral radiance value of the unknown radiation source is easily defined

4.1 System Characterization and Correction Factors

The spectral radiance formula defined in Eqn. (3.9) must include some uncertainty and correction factors caused by measurement setup in Figure 4.1. These are wavelength accuracy of the monochromator system, trap detector characterization, geometric correction factor due to conservation of radiance, monochromator wavelength sift and bandwidth.

The first of these correction parameters is the wavelength uncertainty of the monochromator. For each grating system in the double case monochromator system, the specified wavelength uncertainty of the scale is determined [33].

4.1.1 Calibration of the Monochromator System

Wavelength calibration measurements can be performed with some calibration equipment such as low-pressure pen-ray type calibration lamps, neutral density filters and lasers. Pen-ray type lamps have variations like mercury (Hg), mercury-argon (Hg (Ar)), mercury-neon (Hg (Ne)) and xenon (Xe). These lamps have characteristic emission peaks in the different spectral region and each lamp has its own unique emission peaks as fingerprints [83, 84]. Using diffraction orders, longer emission wavelength peaks can be achieved even though these calibrations lamps have emissions in the UV and Vis region under normal circumstances. On the other hand, neutral density filters can be used for some spectrometric calibration measurements such as wavelength calibration, resolution and stray light of the monochromator, but these type filters usually are used in the UV-Vis regions and they are not convenient for longer wavelength region. These are used to control the absorbance values at a certain wavelength region of the spectrophotometer systems with an invariant radiation source and detector [85]. Lasers are light sources that produce monochromatic radiation, have a very small spectral bandwidth, and high wavelength stability. Its diffraction orders can be used as standard wavelength calibration lamps [86]. Lasers and pen-ray-lamps are preferred instead of filters in extended wavelength calibrations due to diffraction order properties.

In the measurements, extended wavelength accuracy of the double monochromator with a focal length of 2 x 0.3 m is tested in between 200 nm and 2500 nm (UV-B and NIR spectral region). In the monochromator system, first orders for small wavelength region and diffraction orders for large wavelength regions are used to extend the calibration spectrum. In addition, different calibration lamps are preferred for monochromator systems. Therefore, Hg (Ar) and He-Ne Tunable laser wavelength are used in the double case monochromator. Consequently, the measurement difference from the Hg (Ar) is tested in terms of wavelength accuracy. In calibration measurements, integrating sphere is utilized homogeneously and practically transfers to the radiation to the input slit of the monochromator. This sphere in the setup is an optical device with specific ports attachment, coated with barium sulfate with 99 percent reflectivity.

The Double monochromator system has a triple grating system with a focal length of 0.3 m for each case. Diffraction gratings have three different groove density values 2400 g/mm, 1200 g/mm and 600 g/mm. They are preferred to cover the UV, Vis and IR region. Their maximum wavelength range varies between these regions 200 nm-600 nm (250 nm blaze angle), 300 nm-1200 nm (500 nm blaze angle) and 800 nm-2500 nm (1.25 μm blaze angle) respectively.

There are some sharp emission peaks of the pen-ray type Hg (Ar) lamp. Wavelength calibration is carried out by using these emission peaks of the Hg (Ar) pen-ray-lamp. The measurement results, differences and spectral bandwidth of the radiation are given in Tables 4.1, 4.2 and 4.3 for diffraction grating of 600 g/mm, 1200 g/mm and 2400 g/mm respectively.

Table 4.1 * is the Hg(Ar) spectral calibration lamp 3rd and 4th order emission peaks of 546.07 nm respectively for 600 g/mm grating.

Radiation Source	Reference Wavelength	Measured Wavelength	Difference (nm)	SBW(nm)
Hg(Ar)	1638.21*	1638.15	-0.06	0.68
	2184.28*	2184.19	-0.09	

Table 4.2 * is the Hg(Ar) spectral calibration lamp 2nd order emission peaks of 365.02 nm and 546.07 nm respectively for 1200 g/mm grating.

Radiation Source	Reference Wavelength	Measured Wavelength	Difference (nm)	SBW (nm)
Hg(Ar)	546.07	546.09	0.02	0.34
	730.04*	730.01	-0.03	
	1014.00	1013.9	-0.10	
	1092.14*	1092.03	-0.11	

Table 4.3 Hg(Ar) spectral calibration lamp 1st order emission peaks for 2400 g/mm grating.

Radiation Source	Reference Wavelength	Measured Wavelength	Difference (nm)	SBW (nm)
Hg(Ar)	184.91	184.97	0.06	0.17
	253.65	253.65	0.00	
	365.02	365.00	-0.02	
	404.62	404.72	0.06	

For the measurements of each grating, the fit functions between the reference and measured wavelength values are obtained. The fit function is a parameter used within the model function to calculate the uncertainty.

Table 4.4 Extended uncertainty of the triple grating double monochromator system.

Monochromator Type	Grating g/mm	Spectral Band Width (SBW-nm)	Result Uncertainty (nm)	Extended %95 (k=2) Uncertainty (nm)
Double	2400	0,17	0,146	0,291
	1200	0,34	0,138	0,275
	600	0,68	0,146	0,293

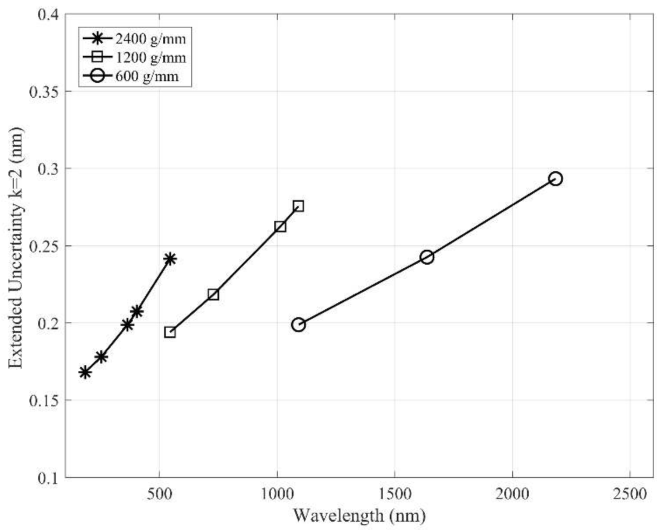

Figure 4.2 Double monochromator system k=2 extended uncertainties (See Appendix-A, for MatLab codes of wavelength accuracy calibration classical uncertainty calculation, and Monte Carlo calculation, also comparison of the them)

Uncertainty parameters used in the model function can be itemized as; slope of the reference and measured wavelength, the contribution of the accuracy of the current meter to wavelength, contribution to Lambertian radiation accuracy of the integrating sphere, repeatability and reproducibility.

In these calculations, focal length, grating types and structures of double monochromator systems with triple-grating wavelength uncertainty calculations are made. In consequence of the analysis, it is understood that the extended general uncertainty range of the results for each grating is in between 0.15 nm and 0.30 nm, which corresponds to 1 % difference approximately as shown in the Figure 4.2 [33]

Results conclude that, this practical and prompt analysis with emission orders enables the measurements in a wide spectrum with such a unique design and provides high precision measurements. It is a novel and proficient solution standing as a great alternative to conventional wavelength calibration methods.

4.1.1.1 Slit Function and Results

At each wavelength, the absolute slit function (or the band-pass) of the monochromator is determined either by tuning the laser wavelength through a fixed monochromator setting in the automated laser range or by scanning the monochromator over a fixed laser wavelength in the non-automated laser range. In practice, the slit function of the monochromator is determined by measuring the output signal of the monochromator as a function of scanning wavelength under monochromatic (laser) radiation [87, 88].

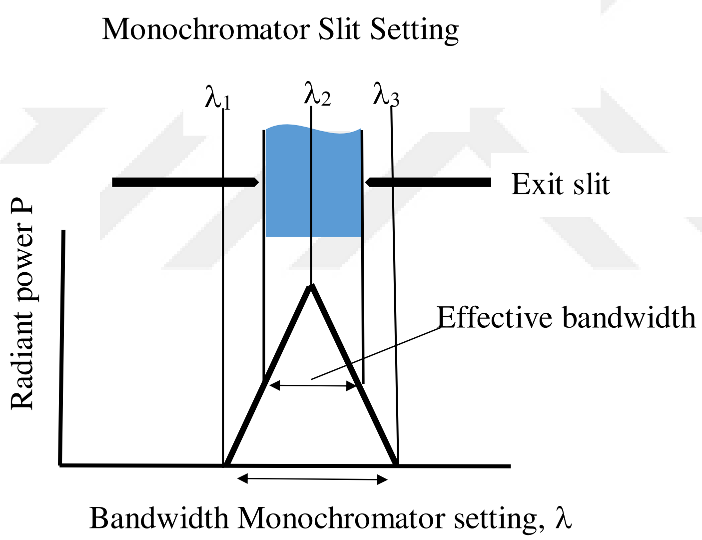

Figure 4.3 Slit function of the monochromator in the exact situation

In the double monochromator system, there are three slit structures available and they are entrance, middle and exit slits. The optimum expected result of the radiation sent to the system according to the output-slit interval of the monochromator should be as given in Figure 4.3, so signal to noise ratio must be large in the smallest slit range. It should be chosen nearly equal slits as it gives a nearly triangular slit function and provides the maximum signal.

$$SBW = \frac{wG}{2f\tan(\sin^{-1}(\frac{Gg}{2}))}x10^6 \quad (4.1)$$

As shown in Figure 4.4, Eqn. (4.1) is used to determine the correct spectral bandwidth for each monochromator system. This formula is re-acquired by using the grating blaze wavelength 'G' , the grating groove number 'g', the focal length of the monochromator 'f' and the exit slit width 'w' and the grating equations [89]. For each grating and monochromator, accurate slit spacing is determined by individual calculations and spectral bandwidth values are found.

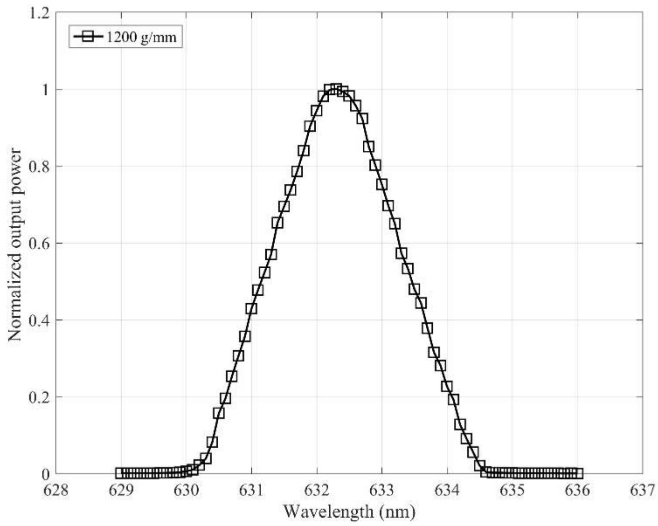

Figure 4.4 Slit function of the double monochromator with 1200g/mm grating is chosen max signal over noise ratio the minimum slit range by using 632.80 nm He-Ne laser wavelength.

It is chosen nearly equal slits (2.50 mm, 2.25 mm, 2.00 mm) as it gives a nearly triangular slit function and provides the maximum signal. The triangular shape is inexact, because of mirror aberrations leading to a non-perfect imaging of the entrance slit onto the exit slit. In the theory and practice, slit ranges can be set to the same values. However, in the double monochromator systems, entrance slit should be wider than exit slit and middle slit should be wider than the entrance slit. Differences in between the widths of slit should not be significant. Each of the three slits has its own special significance. Therefore, as exit slit is at sides of where the image occurs, it must have maximum signal to noise ratio in the smallest slit value.

4.1.2 Optical Characterization of Trap Detector

Spectral power responsivity of the regenerated reflection type silicon based trap detector is obtained comparatively with the trap detector, which is characterized against to electrical substitutions cryogenic radiometry at absolute zero temperature in the National Metrology Institute of Turkey (UME) [27].

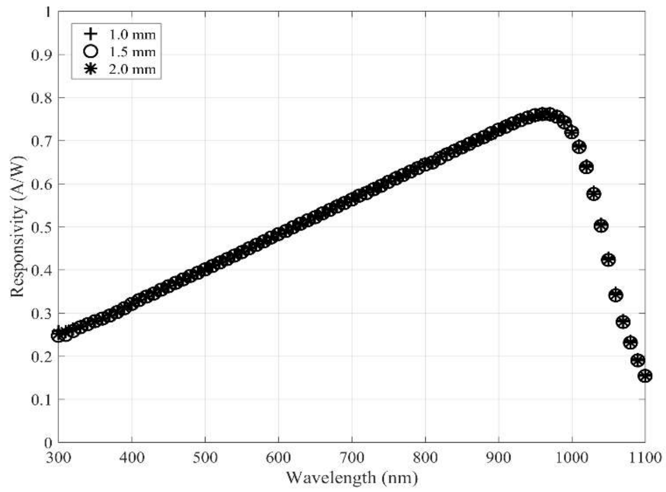

Figure 4.5 Spectral power responsivity of the reflective-type trap detector obtained at different output ranges of the monochromator.

The spectral power responsivity obtained at different output range of the monochromator as shown in the Figure 4.5 gives us information about the detector's linearity and homogeneity. When spectral responsivity of the detector is tested at specific constant wavelength, Figure 4.6 is obtained as a function of the power.

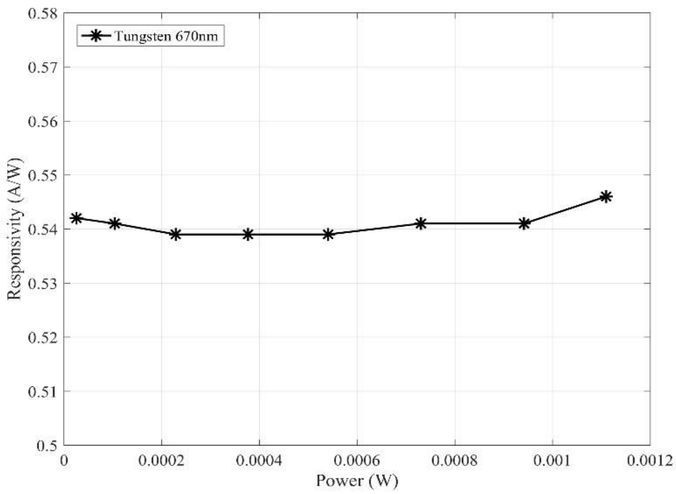

Figure 4.6 Spectral responsivity of the reflective-type trap detector at the power value obtained at specific constant wavelength.

In addition, the graphical change of the current values obtained in the trap detector versus the power change is shown in the below Figure 4.7.

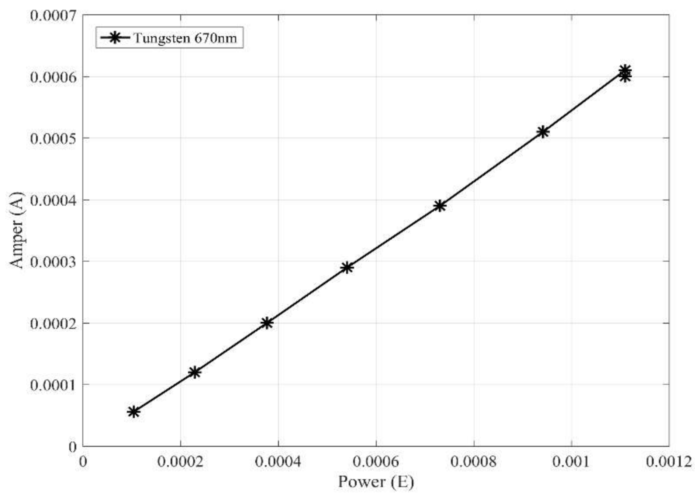

Figure 4.7 Changing power versus current obtained in the trap detector

Other optical measurements made for the designed trap detector are investigated in the following graphs, such as reproducibility, polarization dependency. Spectral power responsivity values of the trap detector are measured at different time is given in Figure 4.8. From this graph, it is seen that each measurement gives same responsivity values.

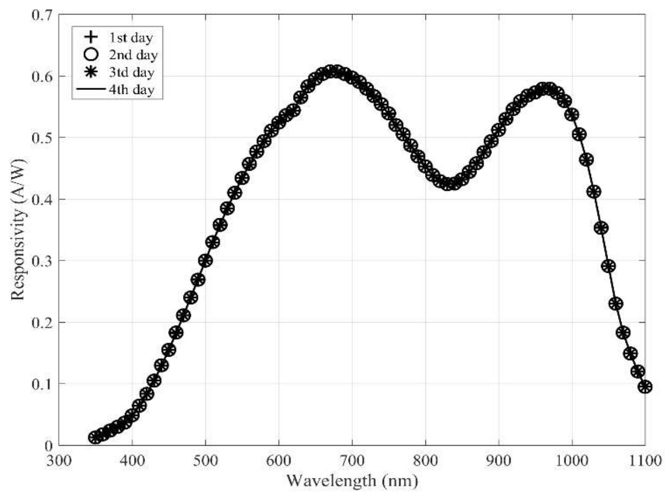

Figure 4.8 Responsivity values of the trap detector at different times

Current values are obtained by rotating the detector that become perpendicular to the source. The graph obtained from measurements made with 30-degree rotation steps and it is given Figure 4.9.

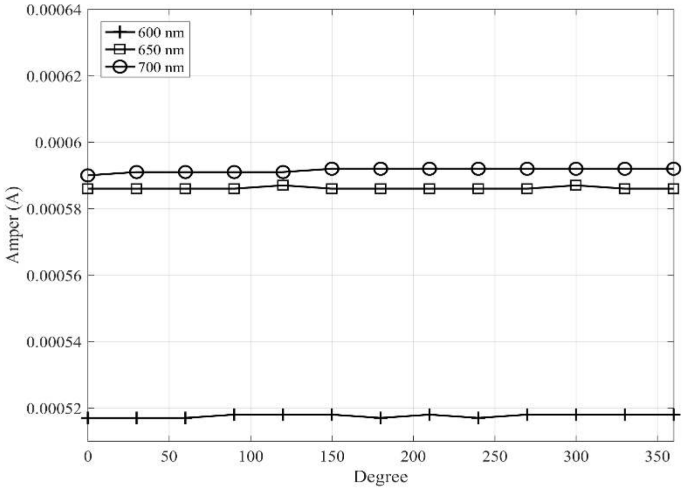

Figure 4.9 Polarization dependence

The realization of the spectral responsivity of silicon-based reflection-type trap detectors is studied in this working. Spectral power responsivity, reproducibility, response to optical power and polarization dependence are obtained. The results show that spectral power responsivity of the detector has stable values at 10^{-3} and polarization dependence has stable values at 10^{-4}. In the NMI of the Turkey optic laboratory, uncertainty values of the trap detector between 350 nm and 1100 nm is calculated within of 0.05% [5]. The measurement uncertainty for the detector in the k=2 extended measurement uncertainty is calculated as 1.5% in the wavelength range of 300 nm to 340nm, 1.1% in the wavelength range of 350 nm to 850 nm, and 1.4% in the wavelength range of 860 nm to 1100 nm.

4.1.3 Correction Factors

Another characterization parameter is the geometric correction factor, which is described according to the radiance conservation [40]. The approximate Lambertian radiation pattern that is obtained using the integrating sphere and the He-Ne 632.8 nm laser is measured by the trap detector at regular intervals from 0.05 m to 0.39 m. At each point, the radiance values are determined by using measured current values and geometric parameters. The equation $y = a * x^b + c$ is derived when the power series second-order curve fit is made with the graph of the radiance values as a function distance. Using the fit function, a specific two-point range where the changes of radiance values are constant is determined, and the new current values are normalized according to these points. Because of the new current values, the geometrical correction factor is found between 1.2392 ± 0.0156 and 1.2484 ± 0.0158 according to the law of invariance of radiance with a relative standard uncertainty.

When the radiance field that is obtained by using the integrating sphere is transmitted to the double monochromator system, there is a correction factor owing to the wavelength shift of the monochromator [90]. This wavelength shift is characterized and is given by formula,

$$\mathrm{CorFac_{WS}} = \frac{1 - \Delta\lambda_{WC} I'(\lambda)/I(\lambda)}{1 - \Delta\lambda_{WC} I'_T(\lambda)/I_T(\lambda)} \tag{4.2}$$

where, $\mathrm{CorFac_{WS}}$ is the correction factor of the wavelength shift. Here, $I(\lambda)$ and $I_T(\lambda)$ are the current values on the output of the double monochromator and trap detector, respectively. In addition, the quotation mark $I'(\lambda)$ represents the first derivation of $I(\lambda)$ by wavelength. The derivative operation is performed by applying numerical derivative rules. Interpolation and central difference approximation operations are performed, and the numerical derivative is applied to certain wavelength values. Because of the calculations for each field of view and the wavelength, the correction factors that are determined by the wavelength shift are defined as given in Table 4.5. In addition, the wavelength correction is, $\Delta\lambda_{WC} = \Delta\lambda_1 + \Delta\lambda_2$ where $\Delta\lambda_1$ is the result of the offset from the wavelength of the monochromator, and has a different value for each wavelength. The value defined as $\Delta\lambda_2$ is identical for each wavelength, and is caused by system repeatability.

The radiance field is transmitted along the telescope at three different fields of view (1.7-mrad, 5.0-mrad, and 11.0-mrad) to the monochromator system defined.

Table 4.5 Wavelength shift correction factor for all mrad field of view (FOV) values.

Wavelength	1.7-mrad		5-mrad		11-mrad	
	value	sigma	value	sigma	value	sigma
457	9.50E-01	3.53E-02	9.84E-01	3.23E-03	9.95E-01	3.20E-04
477	9.92E-01	1.35E-02	9.98E-01	8.48E-04	9.99E-01	4.05E-04
488	9.99E-01	2.56E-03	1.01E+00	4.04E-04	1.01E+00	3.47E-03
514	9.87E-01	3.58E-03	9.92E-01	7.45E-04	9.99E-01	2.30E-04
543	9.86E-01	3.00E-02	9.82E-01	1.26E-03	9.91E-01	5.89E-04
594	9.93E-01	5.07E-03	9.96E-01	7.52E-04	1.00E+00	5.68E-04
604	9.90E-01	8.34E-03	9.98E-01	1.18E-03	1.00E+00	1.11E-03
612	9.85E-01	3.89E-03	9.83E-01	7.79E-04	9.87E-01	4.57E-04
633	1.00E+00	3.82E-03	9.97E-01	6.11E-04	9.99E-01	2.51E-04
1064	1.00E+00	3.10E-03	1.00E+00	8.97E-04	9.98E-01	1.38E-03

Another correction factor for the monochromator bandwidth is called the $CorFac_{BW}$, and given by formula,

$$\mathrm{CorFac_{BW}} = \frac{1 - \Delta\lambda_{WC}{}^{2}\frac{1}{12}\mathrm{I}''(\lambda)/\mathrm{I}(\lambda)}{1 - \Delta\lambda_{WC}{}^{2}\frac{1}{12}\mathrm{I}''{}_{T}(\lambda)/\mathrm{I}_{T}(\lambda)} \tag{4.3}$$

This factor corrects the triangle slit function of the monochromator [90]. $I''(\lambda)$ refers to the 2nd derivation of the current as a function of the wavelength. For different fields of view, it is calculated as in Table 4.6.

Table 4.6 Monochromator bandwidth correction factor for all mrad FOV values.

Wavelength	1.7-mrad		5-mrad		11-mrad	
	value	sigma	value	sigma	value	sigma
457	1.00E+00	9.12E-03	1.00E+00	2.78E-03	1.00E+00	3.68E-04
477	1.01E+00	4.65E-03	1.00E+00	7.48E-04	1.00E+00	2.32E-04
488	1.00E+00	5.73E-04	1.00E+00	5.91E-05	1.00E+00	7.35E-04
514	1.00E+00	2.29E-03	1.00E+00	3.77E-04	1.00E+00	1.37E-04
543	9.99E-01	6.34E-03	1.00E+00	2.38E-03	1.00E+00	2.67E-04
594	1.01E+00	2.60E-03	1.00E+00	3.99E-04	1.00E+00	2.81E-04
604	9.88E-01	1.98E-03	1.00E+00	3.19E-04	1.00E+00	3.37E-04
612	1.01E+00	1.18E-03	1.01E+00	4.59E-04	1.00E+00	8.29E-05
633	1.00E+00	1.33E-03	1.00E+00	1.55E-04	1.00E+00	7.98E-05
1064	1.00E+00	3.08E-04	1.00E+00	5.64E-04	1.00E+00	4.60E-04

.

If the spectral radiance distribution formula of an unknown radiation defined as in Eqn. (3.9) is redefined (see appendix-B for more information), it is given as

$$L_{\lambda}^{U}(\lambda) = \frac{I^{U}(\lambda_M)\ I^{s}}{I^{M}(\lambda_M)\ R_s^{*}(\lambda_L)\ \Delta\lambda\ \Delta C} \mathrm{CorFac} \tag{4.4}$$

For correction factor measurements that are based on the wavelength shift and bandwidth, the reason for which the uncertainties are smaller in large mrad values than the small mrad values and besides the radiation intensities of different laser sources are different for each laser wavelength. The increase in the uncertainty of laser sources with low radiation intensity at a low FOV is due to a reduction in the radiation intensity when passing through the integrating sphere and through the monochromator system

4.2 Spectral Radiance Responsivity for the Measurement System

When Eqns. (3.7) and (4.4) are reconsidered, the spectral radiance responsivity function (transfer function) for the measurement system is reproduced as a function of a known radiation source. The formula defined in Eqn. (3.7) is the spectral radiance responsivity value obtained by using laser-based radiation. By separately applying these two equations, spectral radiance responsivity values are obtained for the same system and is given,

$$R_M^{\wedge}(\lambda_M, \lambda_M) = \frac{I^{\wedge}}{L^{\wedge}(\lambda_M)\ \Delta\lambda} \mathrm{CorFac} \tag{4.5}$$

where $L^{\wedge}(\lambda_M)$ and $I^{\wedge}$ are the certificate radiance value and the current value of the monochromator output signal, respectively. The SRS-12 reference standard has radiance certification values at 5nm intervals wavelength compared to the source laser wavelengths. The radiance values at these points are compared with the expanded uncertainty values with the laser-based system and generalized to the branch length region of 300 nm and 1100 nm. The use of the SRS-12 reference radiation source alone for the system to define the transfer function is not accurate for the control of traceability from a metrological point of view. Therefore, it is more accurate to use SRS-12 only for generalizing and solidifying measurements.

Eqns. (4.8) and (4.5) are handled for the same system and used in there results of the measurement with laser and SRS-12 radiation sources, respectively. The results are calculated with specific standard uncertainty as shown in Figure 4.10. When the results of two measurements are evaluated, it is determined that k = 1 sigma uncertainty values are in the same range.

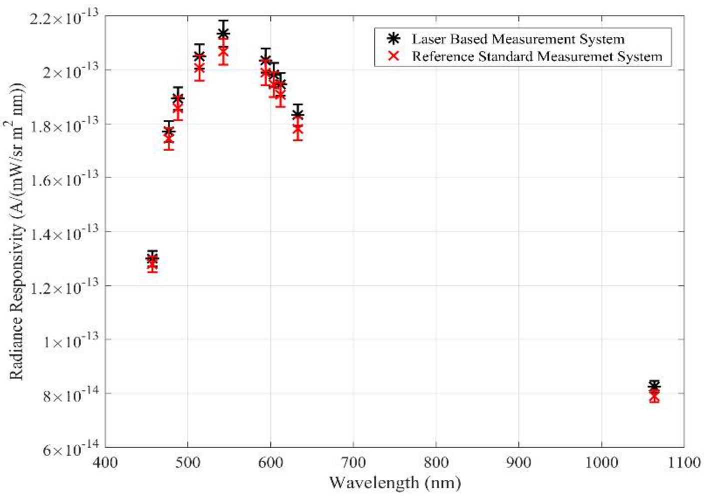

Figure 4.10 Spectral radiance responsivity with relative standard uncertainty both laser based and reference standard measurement system for 11-mrad FOV.

In the calculations made for each mrad FOV, it is seen that in the k = 1 sigma uncertainty range, the laser based system is in the same range with reference standard SRS-12 source values. Following graphs Figures 4.11 and 4.12 show that spectral radiance responsivity values of the radiance measurement system in the 5-mrad and 1.7-mrad respectively.

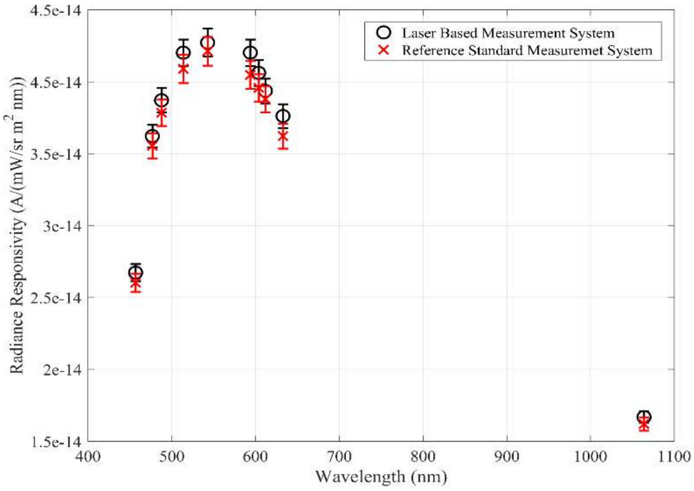

Figure 4.11 Spectral radiance responsivity with relative standard uncertainty both laser based and reference standard measurement system for 5-mrad FOV.

Each laser wavelength used in laser-based measurement system has different power values. This is due to tunable laser wavelengths and different laser sources. Therefore, the decrease in mrad value of the aperture of the Tel310 telescope system causes an increase in the uncertainty value of the laser source simultaneously. As seen in Figure 4.11, 1.7-mrad value is a very small FOV range. The reduction in radiant intensity increases our uncertainty.

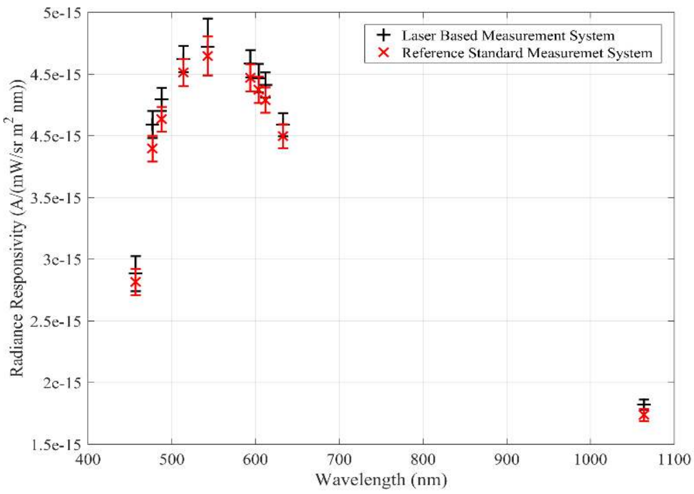

Figure 4.12 Spectral radiance responsivity with relative standard uncertainty both laser based and reference standard measurement system for 1.7-mrad FOV.

The spectral radiance responsivity values that are obtained for all three mrad FOV values are investigated in the same wavelength range for both the laser-based measurement system and the SRS12 reference-source measurement system.

These drawn graphs describe the transfer function for the measurement system consisting of a Tel-310 telescope, fiber-optic cable, the monochromator, and the Si-based trap detector. By using this transfer function, the spectral radiance of an unknown radiation source can be defined and further radiometric and photometric quantities can be transferred. Figure 4.13 illustrates the overall measurements for all mrad FOV values for which the measurement and results are defined.

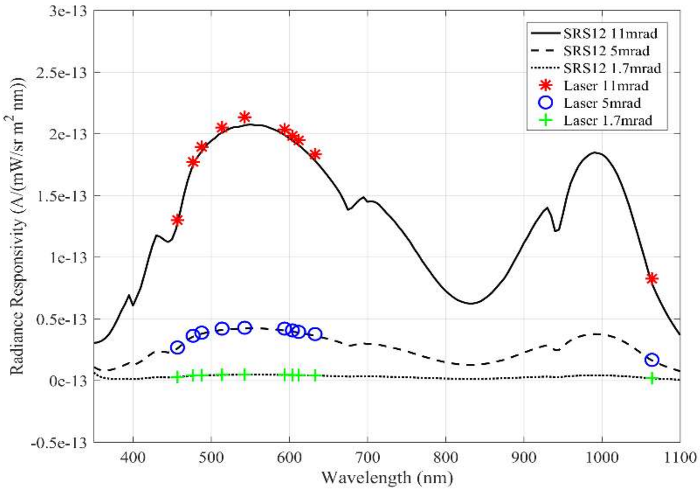

Figure 4.13 Spectral radiance responsivity both laser based and reference standard measurement system for all mrad FOV.

As it is known, the SRS-12 source is a radiation source, which has a certificate value, and its spectral radiance values are known. With the Spectral Radiance measurement chain established for this study, both this reference source and the laser radiation source are measured and it is shown one by one in the above graphs that the same FOV values are in the same uncertainty range. For each mrad between 350 nm and 1100 nm, the generalized spectral radiation responsivity of the system is as shown in Figure 4.13 where ten-laser wavelength point is tested.

4.3 Spectral Radiance of the SRS12 Reference Source

The equation described in Eqn. (4.4) is the generalized radiance equation for an unknown radiation source. The equation that includes both Eqn. (3.7) and Eqn. (4.5) that describes the transfer function of the system is a general equation. The spectral radiance values of SRS12 with sigma-1 uncertainty and the radiance values obtained by laser based transfer function are compared to the same range as seen in Figure 4.14.

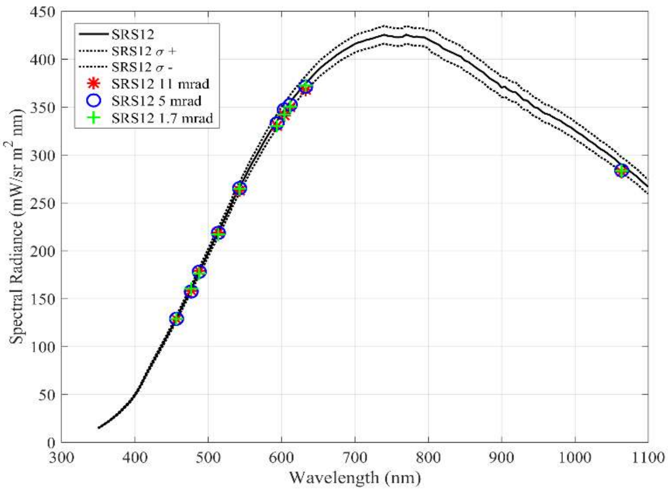

Figure 4.14 Spectral radiance of the SRS12 reference source for all mrad FOV

When the values obtained from laser-based measurements and SRS-12 reference standard source measurements and certification values are examined, it is seen that laser-based measurement values are among the specific values of the reference source. It is concluded that the radiance measurements made with the spectral radiance measurement system established remain in the same range SRS-12 with the certificate reference radiance source and k = 1 sigma value. In the next chapter, an uncertainty budget is created for each wavelength value in each mrad value. These calculations are compared using both classical uncertainty calculations and Monte Carlo uncertainty calculations by using Eqn. (4.4).

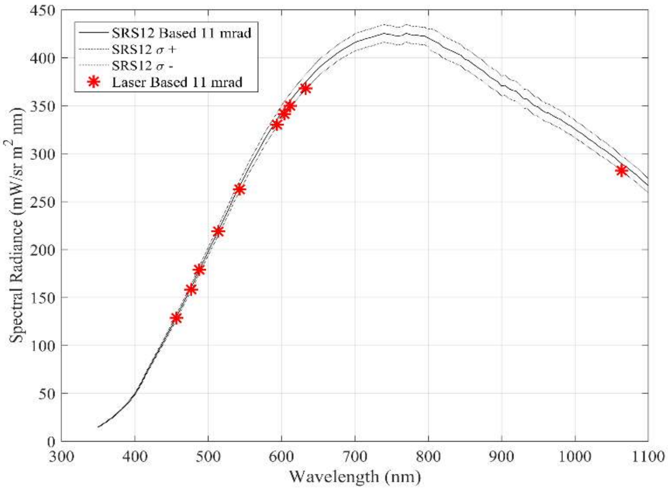

Figure 4.15 Spectral radiance values of the SRS-12 source with k=1 sigma uncertainty and laser based for 11-mrad FOV.

The measurements are repeated for an unknown source of radiation to obtain the graph given in Figure 4.15. Different laser wavelengths and different mrad values can be considered as an unknown source of radiation. Figures 4.16 and 4.17 show the spectral radiance measurement results obtained at different mrad values.

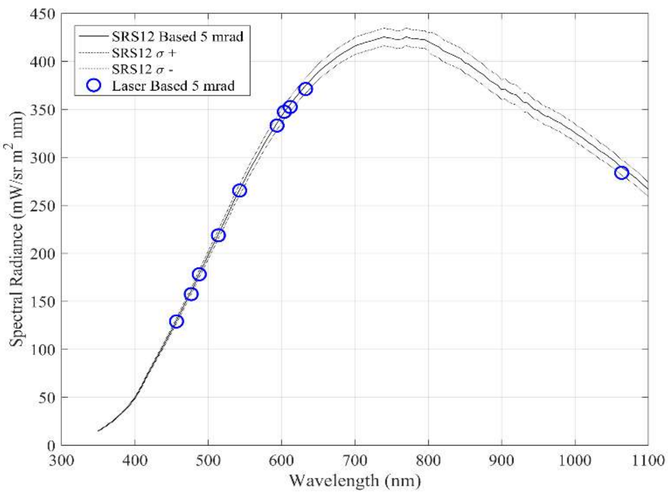

Figure 4.16 Spectral radiance values of the SRS-12 source with k=1 sigma uncertainty and laser based for 5-mrad FOV.

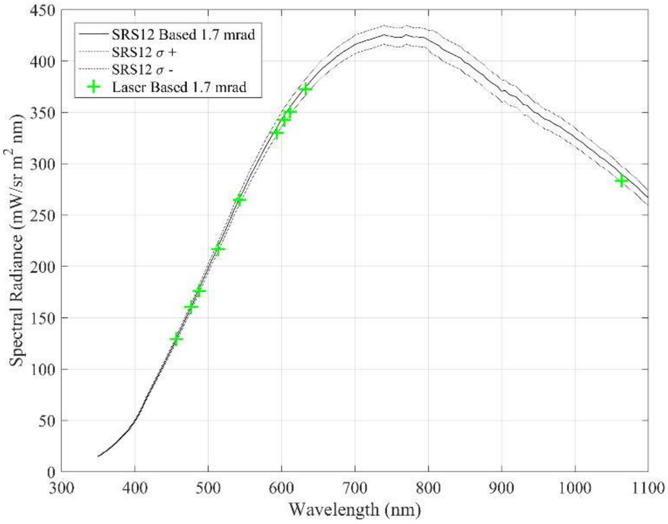

Figure 4.17 Spectral radiance values of the SRS-12 source with k=1 sigma uncertainty and laser based for 1.7-mrad FOV.

CHAPTER 5

MEASUREMENT UNCERTAINTY

The uncertainty is defined as a result of a measurement actually describes the lack of precise information on the end of the measured quantity. The uncertainty here actually means doubt for the quantities measured. During the measurement, the result obtained due to random effects and systematic ethics give us an estimated result of the value of the measured quantity.

If a measurement is done in terms of metrology, making the uncertainty analysis and giving the result with this analysis is an important situation for both the metrology and the user. [91-94].

Guide to the Expression of Uncertainty in Measurement" (GUM) published for the first time in 1993 is the preferred method by many metrology laboratories all over the world and the most preferred method for evaluating and expressing measurement uncertainty [91]. For the definition of the uncertainty of the measurement, alternative model in 2008 was improved. This method enables faster and more practical uncertainty calculations and it is called that Monte Carlo uncertainty method (GUM Supplement-1) [92]. In this study, both methods are used to compare the measurement uncertainty.

5.1 Calculation of the Measurement Uncertainty according to GUM

GUM methods are supported by the International Organization for Standardization (ISO) and CIE-2006 [91, 94]. The first step in the GUM method is to define the measurement size, since you cannot measure the Y component directly; it is obtained by measuring N from other quantities such as X_1, X_2, X_3...X_N through a function f:

$$Y = f(X_1, X_2, \ldots\ldots X_N). \tag{5.1}$$

After measuring each X values for the Y component in Eqn. (5.1), secondly, the uncertainty of each quantity should be evaluated. The GUM method defines this uncertainty assessment in two groups. These are Type-A and Type-B groups. The Type-A assessment standard uncertainty is generally input amount X is obtained by the standard deviation of the distribution of random errors and by means of repeated observations. This means that the repeatability u_A of the measurement can be found with the experimental standard deviation $\bar{x}$, as given,

$$u_A(x) = s(\bar{x}) = \frac{1}{\sqrt{n}} \sqrt{\frac{1}{n-1} \sum_{i=1}^{n} (x - \bar{x})^2} \tag{5.2}$$

Type-B uncertainty assessment of the GUM method is the evaluation process that includes all cognitive definitions except statistical analysis. The probability distribution may be Gaussian, rectangular, triangular.

$u_c(y)$ is the combined standard uncertainty obtained by combining quantities whose standard uncertainty is u_i, and they can be Type-A and Type-B.
That is

$$u_c^2(y) = \sum_{i=1}^{N} \left[\left(\frac{\partial f}{\partial x_i} \right)^2 u^2(x_i) \right] + 2 \sum_{i=1}^{N-1} \sum_{j=i+1}^{N} \frac{\partial f}{\partial x_i} \frac{\partial f}{\partial x_j} u(x_i) u(x_j) r(x_i x_j) \tag{5.3}$$

The propagation of the uncertainty is actually the first order Taylor series distribution. The derivation of "f" with dependence on "x" is the sensitivity coefficients and $u(x_i)$ and $u(x_j)$ are the standard uncertainties associated to the inputs quantities x_i and x_j, respectively, and $r(x_i, x_j)$ is the correlation coefficient. The correlation coefficient $r(x_i, x_j)$ defines the correlation between x_i and x_j and can take values between +1 and -1. If there is no relationship between them, this value goes to zero and Eqn. (5.3) is written as in the form,

$$u_c^2(y) = \sum_{i=1}^{N} \left(\frac{\partial f}{\partial x_i} \right)^2 u^2(x_i) \tag{5.4}$$

Eqn. (5.4) is the most general form of uncertainty calculations and is defined by assuming that not all measurement variables are correlated.

$u_c(y)$ which is the combined standard uncertainty can be used to describe the uncertainty of a measurement result y in many uncertainty measurement. When the Y value is intended to measured, it is generally seen that the probability distribution is $y-u_c(y) \leq Y \leq y+u_c(y)$ at a confidence level p between the uncertainty of the measurement result and the combined standard uncertainty values. The confidence interval of the standard uncertainty value for many measurements is expected to be at 95.45%. The uncertainty of the last measurement is usually described by the expanded uncertainty U (y) and is obtained by multiplying $u_c(y)$ by a coverage factor k is given as.

$$U(y) = k(v, p) * u_c(y) \qquad (5.5)$$

The coverage factor k (v, p) depends on the "degree of freedom" v of the output quantity and the confidence levels p wished or required in the application."

5.2 Calculation of the Measurement Uncertainty by using Monte Carlo Method

By using pseudo random numbers, by defining the Probability Density Function (PDF) for each input in the measurement result, uncertainty calculation becomes possible with Monte Carlo (MC) simulation method.

In cases where the mathematical formula defining the experimentally measured quantity is non-linear, the Monte Carlo simulation method offers a more practical and easy solution than the classical uncertainty calculation (GUM) method. The standard GUM method is valid only for "linear" models. It means, that the signs of the partial derivatives $(\partial y/\partial x_i)$ of the output quantity y determined with respect to all input quantities x_i must not change within the intervals limited by (at minimum) twice the associated standard uncertainties $(x_i \pm 2u(x_i))$ [94].

The Monte Carlo method is adopted and described by International Organization for Standardization (ISO) and CIE-2006. The value and the associated uncertainty of the output quantity Y, represented by y, are assigned by a large number of simulated observations as seen in the Figure 5.1. The values of the output quantity y are evaluated from the values of the input quantities xi with the associated standard uncertainty $u(x_i)$ [92, 94].

The shape of the probability distribution of such quantities may be Gaussian rectangular or any other type. The related probability distributions are generated by means of random values.

As an example, for a single input quantity $N_{i,j} = N_j(x_i, u(x_i))$ the output quantity $y_{i,j} = f(x_1, x_2,..N_{i,j},..,x_N)$ can be evaluated for 1 < j < m. Thus, the variance u_i^2 of the simulated values can be seen as the combined uncertainty of the mean values y_i.

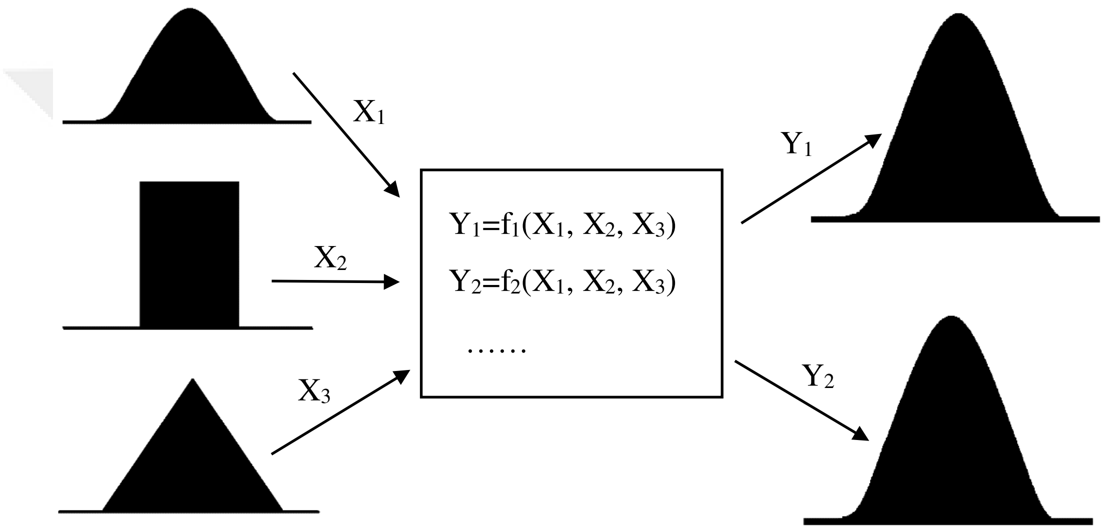

Figure 5.1 Principle of the Monte Carlo method.

For doing numerical simulation, first, a complete set of random input variables X_i with appropriate distributions are generated. Second, the generated input variables X_i are used to calculate all results Y_j. Third, all-important variable and results are stored. The cycle is repeated several times until an appropriated distribution function is reached. The stored results may use to calculate the standard deviation, the distribution functions and correlations between the input or output quantities [90].

The values of all input quantities are simulated independently and in order to form an appropriate distribution, m is chosen often higher than 10000. Thus, from the simulated values of the output quantity, the mean value y and its associated variance u(y) are calculated by:

$$y = \frac{1}{m}\sum_{j=1}^{m} f\left(N_{1,j}, N_{2,j}, \dots. N_{i,j}, \dots. N_{N,j}\right) \tag{5.6}$$

$$u(y) = \sqrt{\frac{1}{m(m-1)}\sum_{j=1}^{m.N}\left[f\left(N_{1,j}, N_{2,j}, \dots. N_{i,j}, \dots. N_{N,j}\right) - y\right]^2} \tag{5.7}$$

5.3 Determination of Spectral Radiance Value for GUM Method

In this section, the uncertainties of the measurements, certificate values, and other parameters in the calibration according to the GUM [91] method are evaluated as TYPE-A and TYPE B. The resultant measurement and accompanying systematic or random uncertainty values are calculated and placed separately within the uncertainty budget. Finally, the uncertainty budget is completed by calculating the sensitivity coefficient value.

Table 5.1 k=2 extended standard uncertainty budget for 632.8 nm in the 11-mrad

Uncertainty Component (X_i)	Sym	Measured Values (x_i)	Unit	Standard Measurement Uncertainty ($u(x_i)$)	Unit	Sensitivity Coefficient (C_i)	Unit	Uncertainty Contribution ($u_i(y)$)	Variance ($u_i^2(y)$)
Trap Detector Responsivity	R^*	3.3170e-01	A/W	3.6487e-03	A/W	-1.0316e+00	W^2/ A m^2sr nm	-3.7640e-03	1.4167e-05
Geometric Constant	ΔC	6.1421e-07	m^2 sr	1.2536e-08	m^2 sr	-5.5711e+05	W/(m^2 sr)^2 nm	-6.9841e-03	4.8777e-05
Detector Output Signal	I^s	2.3811e-07	A	7.8377e-11	A	1.4371e+06	W/A m^2sr nm	1.1263e-04	1.2687e-08
Spectrometer Output Signal	I^m	2.8013e-10	A	1.9801e-13	A	-1.2215e+09	W/A m^2sr nm	-2.4187e-04	5.8500e-08
Unknown Output Signal	I^u	1.7669e-10	A	6.4885e-13	A	1.9366e+09	W/A m^2sr nm	1.2566e-03	1.5790e-06
Wavelength Band pass	$\Delta\lambda$	2.6500e+00	nm	1.0000e-02	nm	-1.2912e-01	W/m^2sr nm^2	-1.2912e-03	1.6673e-06
Correction Factors	δR	1.2301e+00	-	3.7718e-04	-	1.0000e+00	-	3.7718e-04	1.4227e-07
Repeatability	δR	3.6793e-01	W/m^2sr nm	5.5423e-04	W/m^2sr nm	1.0000e+00	-	5.5423e-04	3.0717e-07
								Sum (W/m^2sr nm)	**6.6711e-05**
								Total measurement uncertainty (W/m^2sr nm) $u(L(\lambda))$	**0.0081**
								Extended measurement uncertainty (W/m^2sr nm) $U(L(\lambda))$	**0.0163**

Table 5.2 k=2 extended standard uncertainty budget for 632.8 nm in the 5-mrad

Uncertainty Component (X_i)	Sym	Measured Values (x_i)	Unit	Standard Measurement Uncertainty ($u(x_i)$)	Unit	Sensitivity Coefficient (C_i)	Unit	Uncertainty Contribution ($u_i(y)$)	Variance ($u_i^2(y)$)
Trap Detector Responsivity	R^*	3.3170e-01	A/W	3.6487e-03	A/W	-1.0628e+00	W^2/ A m^2sr nm	-3.8877e-03	1.5036e-05
Geometric Constant	ΔC	6.1421e-07	m^2 sr	1.2536e-08	m^2 sr	-5.7385e+05	W/(m^2 sr)^2 nm	-7.1951e-03	5.1769e-05
Detector Output Signal	I^s	2.3811e-07	A	7.8377e-11	A	1.4805e+06	W/A m^2sr nm	1.1604e-04	1.3465e-08
Spectrometer Output Signal	I^m	5.5235e-11	A	1.4094e-13	A	-6.3822e+09	W/A m^2sr nm	-8.9952e-04	8.0913e-07
Unknown Output Signal	I^u	3.5941e-11	A	2.8636e-13	A	9.8083e+09	W/A m^2sr nm	2.8087e-03	7.8888e-06
Wavelength Band pass	$\Delta\lambda$	2.6500e+00	nm	1e-02	nm	-1.3303e-01	W/m^2sr nm^2	-1.3303e-03	1.7696e-06
Correction Factors	δR	1.2284e+00	-	7.9986e-04	-	1.0000e+00	-	7.9986e-04	6.3977e-07
Repeatability	δR	3.7107e-1	W/m^2sr nm	5.5423e-04	W/m^2sr nm	1.0000e+00	-	5.5423e-04	3.0717e-07
Sum (W/m^2sr nm)									**7.8234e-05**
Total measurement uncertainty (W/m^2sr nm) u(L(λ))									**0.008845**
Extended measurement uncertainty (W/m^2sr nm) U(L(λ))									**0.01769**

Table 5.3 k=2 extended standard uncertainty budget for 632.8 nm in the 1.7-mrad

Uncertainty Component (X_i)	**Sym**	**Measured Values (x_i)**	**Unit**	**Standard Measurement Uncertainty ($u(x_i)$)**	**Unit**	**Sensitivity Coefficient (C_i)**	**Unit**	**Uncertainty Contribution ($u_i(y)$)**	**Variance ($u_i^2(y)$)**
Trap Detector Responsivity	R^*	3.3170e-01	A/W	3.6487e-03	A/W	-1.0445e+00	W^2/ A m^2sr nm	-3.8110e-03	1.4524e-05
Geometric Constant	ΔC	6.1421e-07	m^2 sr	1.2536e-08	m^2 sr	-5.6408e+05	W/(m^2 sr)^2 nm	-7.0714e-03	5.0005e-05
Detector Output Signal	I^s	2.3811e-07	A	7.8377e-11	A	1.4551e+06	W/A m^2sr nm	1.1404e-04	1.3006e-08
Spectrometer Output Signal	I^m	6.2325e-12	A	3.8156e-14	A	-5.5589e+10	W/A m^2sr nm	-2.1211e-03	4.4989e-06
Unknown Output Signal	I^u	3.9656e-12	A	3.0489e-14	A	8.7365e+10	W/A m^2sr nm	2.6637e-03	7.0950e-06
Wavelength Band pass	Δλ	2.6500e+00	nm	1.0000e-02	nm	-1.3074e-01	W/m^2sr nm^2	-1.3074e-03	1.7093e-06
Correction Factors	δR	1.2346e+00	-	4.9915e-03	-	1.0000e+00	-	4.9915e-03	2.4915e-05
Repeatability	δR	3.7254e-01	W/m^2sr nm	5.5423e-04	W/m^2sr nm	1.0000e+00	-	5.5423e-04	3.0717e-07
Sum (W/m^2sr nm)									**1.0307e-04**
Total measurement uncertainty (W/m^2sr nm) u(L(λ))									**0.01015**
Extended measurement uncertainty (W/m^2sr nm) U(L(λ))									**0.02030**

Uncertainty values for each laser wavelength and three different mrad FOVs used in the measurement are calculated as a function of the wavelength and is given in Table 5.1, Table 5.2 and Table 5.3. Only for the 632.8-nm He-Ne laser wavelength is the uncertainty budget defined and the spectral radiance values are determined in the 95% confidence level of the k = 2 extended uncertainties (See appendix C1)

5.4 Determination of Spectral Radiance Value for Monte Carlo Method

When the function that defines the measurement system is linear, the GUM method offers an easy solution, but when the function that defines the system is not linear, the Monte Carlo [92] method is more practical because the partial derivation of the output quantities according to each input quantity makes the calculations difficult. In addition, all of the uncertainty components in the GUM method need to be defined within the uncertainty budget, and these are more complex than the Monte Carlo method.

Each measurement quantity y and the accompanying u (y) sigma values are defined by a PDF with random numbers according to the type of change, and the sigma value of the Gaussian function formed after its replacement in the function describing the system gives us the associated measurement uncertainty value.

For each mrad FOV, a Monte Carlo operation is performed, and the uncertainties corresponding to spectral radiance values at the laser wavelength are calculated. A histogram distribution is also defined for the radiance value obtained for 633 nm, as shown in Figure 5.2, and a Gaussian fit function is applied to it.

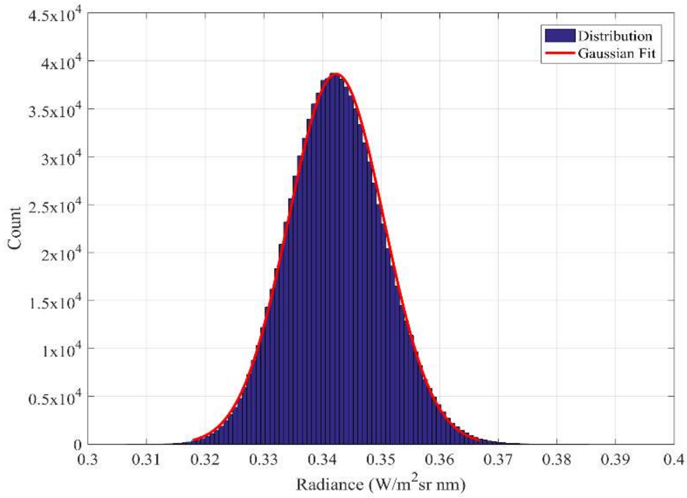

Figure 5.2 Plot showing 633 nm spectral radiance histogram distribution and associated Gaussian fit function. The mean value of the function is the spectral radiance value 0.34238 ($Wm^{-2}sr^{-1}nm^{-1}$), and one sigma value of it is 0.008155 ($Wm^{-2}sr^{-1}nm^{-1}$).

Calculations made with Monte Carlo uncertainty method are investigated for each mrad and each wavelength. The results given for laser wavelengths of 633 nm, which are calculated with the classical uncertainty method and given in Tables 5.2 and 5.3, are shown in Figures 5.3 and 5.4 by the Monte Carlo method.

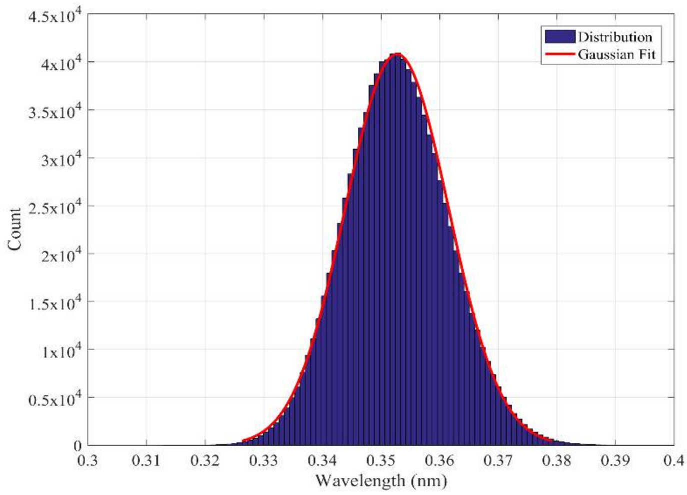

Figure 5.3 Plot showing 633 nm spectral radiance histogram distribution and associated Gaussian fit function. The mean value of the function is the spectral radiance value 0.35271 ($Wm^{-2}sr^{-1}nm^{-1}$), and one sigma value of it is 0.008809 ($Wm^{-2}sr^{-1}nm^{-1}$).

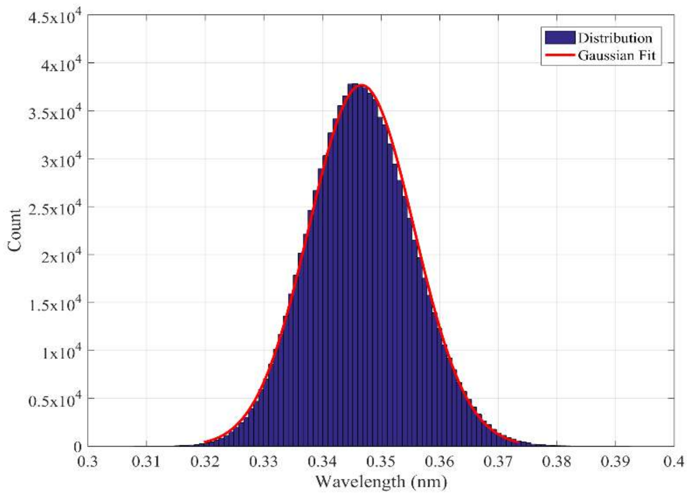

Figure 5.4 Plot showing 633 nm spectral radiance histogram distribution and associated Gaussian fit function. The mean value of the function is the spectral radiance value 0.3468 ($Wm^{-2}sr^{-1}nm^{-1}$), and one sigma value of it is 0.008939 ($Wm^{-2}sr^{-1}nm^{-1}$).

Monte Carlo uncertainty calculations using 10^6 random numbers are tested for different mrad values. The results of the uncertainty values produced by the classic and Monte Carlo method are given comparatively in the Table 6.1. Program calculating these uncertainty values are given in appendix C2.

.

CHAPTER 6
RESULTS AND DISCUSSION

The spectral radiation values of an unknown light source are determined by defining the spectral transfer function of the measurement system, and the extended uncertainty value that is associated with the radiance value is defined using both the classical approach and the Monte Carlo approach.

In this study, a laser-based spectral radiance system is established, and this system is transferred to a system that has a telescope, a double monochromator system, and a silicone detector; thus, the spectral radiance transfer function of the system is obtained. By using this transfer function, the spectral radiance value of any radiation source having homogeneous radiation can be obtained. During the radiance measurements, three different types of gas laser radiation are sent to the integrating sphere, which has a 0.15-m surrounding diameter, a 0.02-m exit port diameter, and is covered inside with BaSO4 (barium sulfate has the ability to reflect 99%). The radiation emitted from the output port of the integrating sphere is has an approximate Lambertian radiation distribution. This radiation having a Lambertian distribution is sent over a reflection-type silicon-based trap detector with an aperture diameter of 0.08 m from a certain geometric distance to obtain radiance values at each laser wavelength point.

The radiance measurements made by using certain laser wavelengths and the uncertainty measurements of it are determined using both the classical uncertainty calculation method and the Monte Carlo method. There are 3 different FOVs that collect the radiation in the optical measurement system used. Table 6.1 contains only the comparison results for 11 mrad FOV. The results obtained in other mrad FOVs are given in Table 6.2 and Table 6.3.

Table 6.1 k=2 Extended standard uncertainty for 11-mrad FOV in terms of both GUM and Monte Carlo Method.

Wavelength (nm)	GUM		Monte Carlo		Ratio of the two calculations
	Calculated Radiance (W/m^2sr nm)	k=2 Extended measurement uncertainty (W/m^2sr nm)	Calculated Radiance (W/m^2sr nm)	k=2 Extended measurement uncertainty (W/m^2sr nm)	
457	0.11952	0.0058	0.11953	0.0057	1.0229
477	0.14892	0.0072	0.14887	0.0071	1.0198
488	0.16825	0.0119	0.16819	0.0108	1.0998
514	0.19524	0.0094	0.19483	0.0093	1.0086
543	0.24632	0.0122	0.24708	0.0121	1.0099
594	0.32095	0.0153	0.32041	0.0153	1.0033
604	0.33359	0.0165	0.33469	0.0162	1.0204
612	0.32635	0.0155	0.32543	0.0155	0.9980
633	0.34347	0.0163	0.34237	0.0163	0.9993
1064	0.25589	0.0150	0.25424	0.0146	1.0253

The spectral radiance values obtained are determined using a laser based radiation source. It is expected that the same radiance values are obtained within the different FOVs used while the laser radiation is transferred to the double case monochromator system. Table 6.2 is obtained using a smaller FOV (5 mrad) than the first measurement and the results are found to be close.

Table 6.2 k=2 Extended standard uncertainty for 5-mrad FOV in terms of both GUM and Monte Carlo Method.

Wavelength (nm)	GUM		Monte Carlo		Ratio of the two calculations
	Calculated Radiance (W/m^2sr nm)	k=2 Extended measurement uncertainty (W/m^2sr nm)	Calculated Radiance (W/m^2sr nm)	k=2 Extended measurement uncertainty (W/m^2sr nm)	
457	0.12895	0.01207	0.11741	0.00614	1.0982
477	0.15740	0.00799	0.14804	0.00747	1.0632
488	0.17804	0.00849	0.16745	0.00840	1.0633
514	0.21865	0.00959	0.18596	0.00936	1.1758
543	0.26527	0.01454	0.25481	0.01306	1.0410
594	0.33301	0.01589	0.31653	0.01577	1.0521
604	0.34733	0.01690	0.33015	0.01660	1.0520
612	0.35233	0.01682	0.33490	0.01670	1.0521
633	0.37107	0.01769	0.35273	0.01761	1.0520
1064	0.28379	0.01448	0.25559	0.01426	1.1103

Table 6.3, obtained by using a smaller FOV, gives similar results with the Tables 6.1 and 6.2. However, when the radiation of a light source or a surface is inspected, the uncertainty of the measurements made in very small FOVs causes the uncertainty to be high due to the low light intensity. It can be seen that the results with less uncertainty are at 11 mrad FOV.

The results obtained with this measurement have some differences in the FOVs at the same wavelength, which is due to a decrease in laser power values and a decrease in the FOV values. In order to determine the radiance value of a radiation source, a spectral transfer function that is obtained is used for different FOVs. Figure 5.14 shows that spectral radiance values are obtained using both the transfer function of the system and certificate values of the SRS12 spectral reference radiance source. The results show that both the certificate and the measurement results have very close values. This measurement setup can be used not only for the radiation source but also for the surface where the radiation reflected.

Table 6.3 k=2 Extended standard uncertainty for 1.7-mrad FOV in terms of both GUM and Monte Carlo Method.

Wavelength (nm)	GUM		Monte Carlo		Ratio of the two calculations
	Calculated Radiance (W/m^2sr nm)	k=2 Extended measurement uncertainty (W/m^2sr nm)	Calculated Radiance (W/m^2sr nm)	k=2 Extended measurement uncertainty (W/m^2sr nm)	
457	0.12895	0.09002	0.12650	0.01299	1.0983
477	0.16031	0.03619	0.15076	0.00883	1.0829
488	0.17603	0.01050	0.16555	0.00829	1.0512
514	0.21678	0.01416	0.19088	0.00972	1.1657
543	0.26461	0.07786	0.25441	0.02554	1.0385
594	0.33002	0.02123	0.30710	0.01631	1.0426
604	0.34226	0.02733	0.32536	0.01849	1.0367
612	0.35046	0.01943	0.32614	0.01688	1.0465
633	0.37254	0.02030	0.34667	0.01788	1.0561
1064	0.28327	0.01566	0.24944	0.01376	1.1083

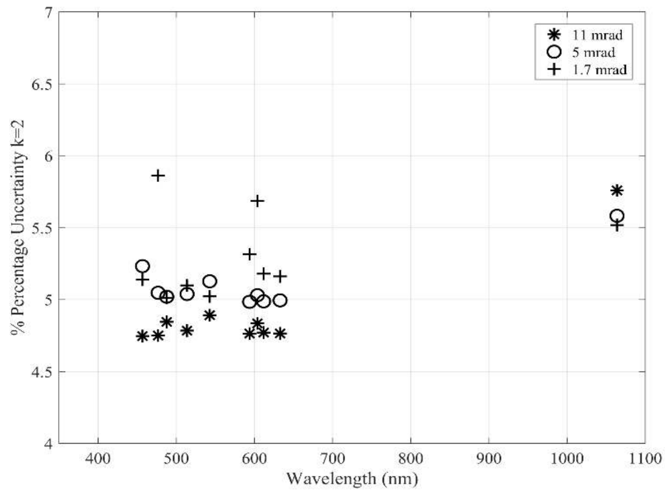

Figure 6.1 Percentage uncertainty distribution of spectral radiance of the unknown radiation source for all mrad FOV values.

Because lasers have low power at some wavelengths, the power transmitted to the system at small FOVs are less, so the uncertainty is high in some regions but it is small in some wavelength regions as given in Figure 6.1. Consequently, it is seen from the Figure 6.1 the distribution of uncertainty is obtained between 4.5% and 6%.

This study is an internal project in the TUBITAK-UME optical laboratory. In our country's radiometry and photometry fields aims to eliminate the dependence on foreign sources by creating a traceability chain. In this way, the correct radiometric and photometric measurements of all radiating materials can be calculated by measuring the conversion to all units with low uncertainty.

As a result, the spectral radiance responsivity (transfer function) for 11-mrad FOV between 350 nm and 1100 nm is determined as in Figure 7.2 because of the measurements and calculations. SRS-12 reference source, which is a source whose certificate is prepared and calibrated by external service, cannot directly provide the traceability of the measurement system. Because, in order to be traceable, it is necessary to provide the calibration in the laboratory setting. Over time, there are changes in the radiance value of the resource with the duration of usage. However, every mechanical, electronic and optical materials in the measurement system can be traced within TUBİTAK-UME.

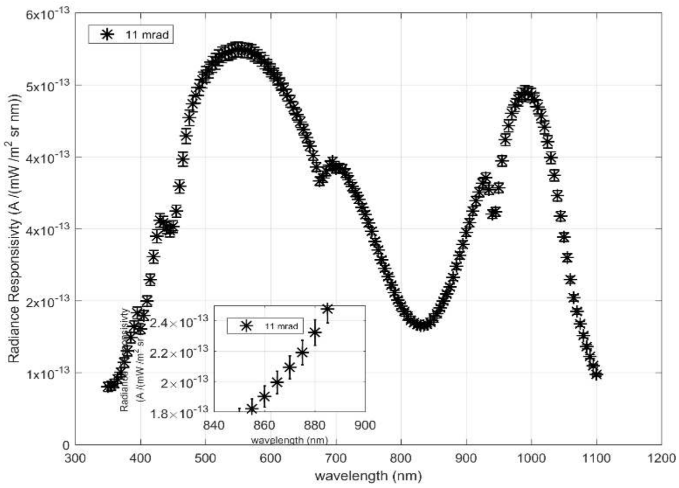

Figure 6.2 Spectral radiance responsivity functions of the measurement system for 11-mrad and zoom graph of the some range of the figure.

The k = 2 sigma confidence interval is the optimized version of the certificate value of the reference source and the uncertainty value obtained by using laser source.

By including all uncertainty components, the spectral radiance responsivity (transfer function) formula of the measurement system is given as,

$$L_{\lambda}^{U}(\lambda) = \frac{I^{U}(\lambda_M)\ I^{s}}{I^{M}(\lambda_M)\ R_s^{*}(\lambda_L)\ \Delta\lambda\ \Delta C} \mathrm{CorFac} \tag{6.1a}$$

$$R_M(\lambda_M, \lambda_M) = \frac{I^{M}(\lambda_M)\ R_s^{*}(\lambda_L)\ \Delta\lambda\ \Delta C}{I^{s}\ \mathrm{CorFac}} \tag{6.1b}$$

$$L_{M}^{U}(\lambda_M) = \frac{I^{U}(\lambda_M)}{R_M(\lambda_M, \lambda_M)} \tag{6.1c}$$

where, R_M (λ_M, λ_M) is the transfer function of the related FOV. By using, the Eqn. (6.1c) spectral radiance values of the unknown radiation source or surface can be obtained by measuring currents from radiance measurement system.

The spectral radiance responsivity function of the measurement system is obtained and is given in Figure 6.2 by using calibrated mechanical, electronic and optical materials of TUBİTAK-UME optics laboratory.

By placing an unknown radiation source at a distance of 0.2 m in front of the measurement system and writing the spectral current values measured at the 11-mrad FOV in Eqn. (6.1c), the spectral radiance value can be easily determined**.**

After obtaining the current values for each radiant source in Eqn. (6.1c), the radiance values of different radiant sources for 11-mrad FOV are given in Figure 6.3.

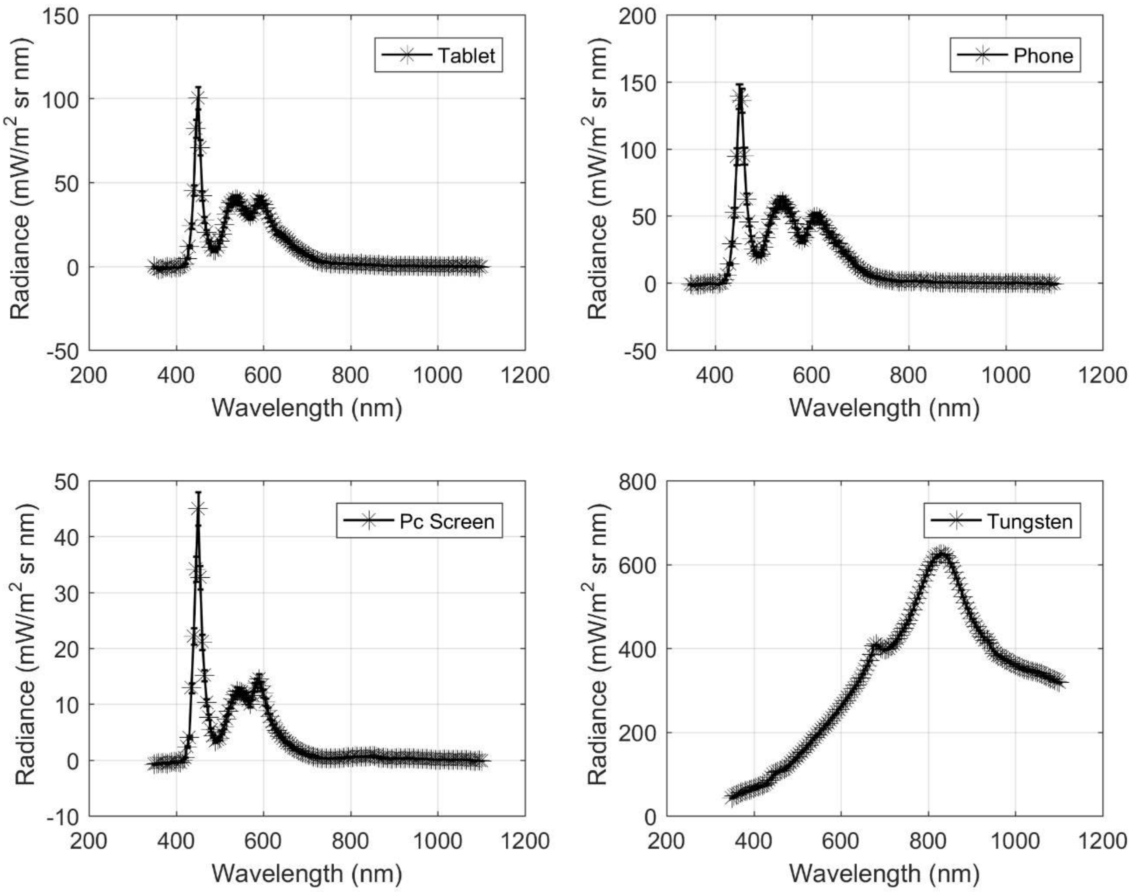

Figure 6.3 Spectral radiance distribution of the some radiation source and surface for 11-mrad FOV with k=2 sigma expanded relative uncertainty.

Spectral radiance distribution of the four different radiation source is represented in the Figure 6.3. By using obtained radiance responsivity of the measurement system, they that have different radiation properties indicate different radiance distribution. As expected, the tablet phone and pc screen shows a strong glow in the blue area like a Light Emitting Diode (LED). In fact, it is natural that such LED type structures show a predominant distribution of RGB (Red Green Blue). However, when we look at the tungsten polychromatic lamp, it shows an expected distribution in the spectral region. Because of certain standards, radiation measurements are desired all over the world. The determination of radiance distribution for different source is very important for human health.

CHAPTER 7

CONCLUSION

In recent years, scientific studies in many fields have an indisputable importance. The demand for science and technology is increasing to develop new technologies. Self-parked cars, aircraft landed itself into an airport and military systems without users can be give as examples of new technologies. The most important common part of these studies, even in different fields, is the effort to obtain accurate and precise measurements. In order to keep up with advancing technologies, the development of optical measurement techniques in such systems has increased the quality of the studies. Because of these situations, optic metrology becomes important.

This study tries to contribute to the development of optical measurement methods and to reduce the measurement uncertainty to the lowest levels. For this reason, a high-resolution measurement system is established to perform these studies. Optical, mechanical and electronic parts are characterized and calibrated with high accuracy and low uncertainty. Wavelength accuracy of the monochromator system is investigated. Characterization of the reflection-type trap detector is tested and calibrated against to the ESCR and it is obtained correctly in the uncertainty scales of the TUBITAK-UME. By using laser radiation sources, the spectral radiance responsivity values of the measurement system set up under good optical characterization conditions and the radiance values of the unknown radiation sources are obtained. In addition, by using the spectral radiance responsivity value obtained, it is easily ensured that all light sources or surfaces are converted into the requested radiometric and photometric quantities.

After the measuring system is characterized, a laser based radiation source with Lambertian distribution is obtained to form of a spectral radiance traceability chain by using integrating sphere. This obtained beam distribution is very important to measure radiance homogeneously. This radiation source is obtained by using an integrated sphere and laser source at different wavelength. Radiance values are calculated by using geometrical parameters at exit port of the integrating sphere. This process is repeated and calculated for each different laser source so at the specific laser wavelength limited spectral radiance distribution is obtained. These radiance values without breaking the alignment of the integrating sphere are transfer through TEL310 telescope system to double monochromator system. When the radiance values calculated on the trap detector are transferred to the spectroradiometric system, the spectral radiance responsivity of the system is obtained for limited laser wavelengths.

Laser based measurements is done and then, SRS-12 polychromatic reference standard radiation source, whose radiance values between 350 nm and 1100 nm are formed at 5 nm intervals, are sent to the same spectroradiometric system using the same TEL310 telescope. By means of this process, another transfer function is obtained for the same system between 350 nm and 1100 nm with a known uncertainty source. It is seen that the transfer function achieved by using the polychromatic radiation source and the transfer function obtained in laser wavelengths are in the same uncertainty scale. The spectral radiance responsivity value obtained with both different radiation source enables the spectral radiance value of an unknown radiation source. In addition, the standard relative uncertainty range of the spectral radiance responsivity of the radiance measurement system is defined for 95.45% k = 2-sigma confidence level with both classical and Monte Carlo uncertainty calculation methods and an innovation is added to the measurement and calculation methods.

By determining the standard relative uncertainty values of the spectral radiance responsivity of the measurement system, the traceability chain for spectral radiance measurements is obtained in TUBITAK-UME optical laboratory. Spectral radiance scale with detector based by using laser source standard, which is described in Figure 2.7, is enable the determination of spectral radiance values for unknown radiant sources or surfaces.

The spectral radiance measurement system, whose uncertainty values are determined, can be used in both technology production and testing of existing technology. In this way, the radiance distributions of phone, tablet and computer that are frequently used in daily life and that make screen radiation are tested. In terms of human eye health, the radiation of such devices is brought to a point that can be evaluated, besides the benefit from many areas so it is also beneficial for health studies in this sense.

This measurement setup can be used not only for radiation source but also for surface where radiation reflected. In our country's radiometry and photometry fields, it is aimed to eliminate the dependence of foreign sources by creating a traceability chain. In this way, the correct radiometric and photometric measurements of all radiating materials can be calculated by measuring the conversion to all units with low uncertainty.

It is concluded that both radiometric and photometric measurements of the radiation sources or radiant surfaces are possible to make within the borders of the country. This thesis is decrease scientifically foreign dependency in optical measurement. In addition, it provides the measurement basis with low uncertainty measurement systems.

This study is a guide towards the derivation of radiometric and photometric measurement units, which are the basis for all optical power measurement systems equipment in laboratories serving, military, metrology, healthcare field, or industry.

REFERENCES

[1] National Institute Standard and Technology (NIST). (2009). *Optical Radiation Measurements Based on Detector Standards.* NIST Technical Note: USA. **1621**.

[2] Nicodemus, F. E. (1969). Optical Resource Letter on Radiometry, *Journal of the optical society of America*, **59(3)**, 243-248.

[3] Kaufman, J. E., Christensen, J. F. (1984). *IES Lighting Handbook Reference Volume*. Illuminating Engineering Society of North America: New York.

[4] Brown, S.W., Eppeldauer, G. P., Lykke, K. R. (2006). Facility for Spectral Irradiance and Radiance Responsivity Calibrations Using Uniform Sources, *OSA publishing, Applied Optics.* **45(32)**, 8218-8237.

[5] Yoon, H.W., Gibson, C. G., Barnes, P.Y. (2002). Realization of the National Institute of Standard and Technology Detector-Based Spectral Irradiance Scale, *OSA publishing, Applied Optics.* **41(28)**, 5879-5890.

[6] Kirchhoff, G. (1860). About the Relationship between the Emissivity and the Absorption Capacity of the Body for Heat and Light, *Ann. Phys*. **19(3)**, 275-301.

[7] Schaefer, A. S., Saunders, R. D. (1984). Inter-Comparison between Silicon and Blackbody-Based Radiometry Using a Silicon Photodiode/Filter Radiometer, *Applied Optics Vol*. **23(14)**, 2224-2226.

[8] Metzdorf, J. (1993). Network and Traceability of the Radiometric and Photometric Standards at the PTB, *Metrologia*, **30(1)**, 403-408.

[9] Chu, B., McEvoy, H. C., Andrews, J. W. (1994). The NPL Reference Sources of Blackbody Radiation, *Meas. Sci. and Tech*. **5(1)**, 12-19.

[10] Sapritski, V. I. (1996). Blackbody Radiometry, *Metrologia.* **32(1)**, 411-417.

[11] Woolliams, E. (2003). *Development and Evaluation of a High Temperature Blackbody Source for the Realization of NPL's Primary Spectral Irradiance Scale*, Ph.D. thesis. University of Manchester: United Kingdom.

[12] Schaefer, A. R., Eckerle, K. L. (1984). Spectrophotometric Tests Using a Dye-Laser-Based Radiometric Characterization Facility, *Applied Optic*. ***23(2)***, 250–256.

[13] Schaefer, A. R., Saunders, R. D., Hughey, L R. (1986). Intercomparison Between Independent Irradiance Scales Based on Silicon Photodiodes Physics, Gold-Point Blackbody Radiation, Synchrotron Radiation, *Opt. Eng*. **25(7)**, 892–896.

[14] Martin, J. E., Fox, N. P., Key, P. J. (1985). A Cryogenic Radiometer for Absolute Radiometric Measurements, *Metrologia.* **21(3),** 147-155.

[15] Hoyt, C. C., Foukal, P. V. (1991). Cryogenic Radiometers and Their Application to Metrology, *Metrologia*. **28(3)**, 163-170.

[16] Bazkir, O., Ugur, S., Samedov, F., Esendemir, E. (2005). High-Accuracy Optical Power Measurements by Using Electrical Substitution Cryogenic Radiometer, *Optical Engineering.* **44(1)**, 64011-6.

[17] Van der Ham, E. W. M., Bos, H. C. D., Schrama, C. A. (2003). Primary Realizations of a Spectral Irradiance Scale Employing Monochromator-Based Cryogenic Radiometry between 200 nm and 20 μm, *Metrologia.* **40(1)**, 177–180.

[18] Keawprasert, T., Anhalt, K., Taubert, R. D., Abd-Elmageed, A., Sperling, A., Hartmann, J. (2008). Absolute Calibration of Spectral Responsivity for a Radiation Thermometer, *10th International Conference on New Developments and Applications in Optical Radiometry Daejeon.* NEWRAD.

[19] Anderson, V. E., Fox, N. P., Nettleton, D. H. (1992). Highly Stable, Monochromatic and Tunable Optical Radiation Source and Its Application to High Accuracy Spectrophotometry, *Applied Optics.* **31(4)**, 536-545.

[20] Abd-Elmageed, A., Winter, S., Nevas, S., Sperfeld, P., Kück, S., Sperling, A. (2010). Detector Based Traceability Chain for Spectral Irradiance Using Tunable Lasers, Independent From Blackbody Radiators, *Proceeding of BulLight.* 1314-0787.

[21] Keawprasert, T., Anhalt, K., Taubert, R. D., Abd-Elmageed A., Sperling A., Hartmann J. (2011). Monochromator Based Absolute Calibration of Radiation Thermometers, *International Journal of Thermophysics.* **32(7),** 1697-1706.

[22] Zalewski, E. F., Geist, J. (1980). Silicon Photodiode Absolute Spectral Self-Calibration, *OSA publishing, Applied Optics.* **19(8)**, 1214-1216.

[23] Geist, J., Zalewski, E. F., Schaefer, A. R. (1980). Spectral Response Self-Calibration and Interpolation of Silicon Photodiodes, *OSA publishing, Applied Optics.* **19(22)**, 3795-3799.

[24] Mart, N. (2005). Development of Detectors and Calibration Methods for Spectral Irradiance and Radiometric Temperature Measurement, *Metrology Research Institute Report.* **25(38),** 1237-3281.

[25] Varpula, T., Seppa, H., Saari, J. M. (1989). Optical Power Calibrator Based on a Stabilized Green He-Ne Laser and a Cryogenic Radiometer, *IEEE trans, Instrum Meas.* **38(2)**, 558-564.

[26] Touayar, O., Reyn, H., Bastie, J., Varpula, T. (1995). Indirect Comparison of Cryogenic Radiometers from the INM (France) and VTT (Finland) with a QEB-200 from VSL (Netherlands), *Metrologia.* **32(6)**, 561-564.

[27] Ozcan, B., Ferhad, S. (2004). Electrical Substitution Cryogenic Radiometer Based Spectral Responsivity Scale Between 250-2500nm Wavelength, *Optics and Lasers in Engineering*. **34(3)**, 427–438.

[28] Fox, N. P. (1991). Trap Detectors and Their Properties (E. F. Zalewski, personal communication), *Metrologia.* **28(3)**, 197-202**.**

[29] Köhler, R., Goebel, R., Pello, R. (1995). Results of an International Comparison of Spectral Responsivity of Silicon Photodetectors, *Metrologia.* **32(6)**, 463-468.

[30] Ozcan B., Ferhad S. (2005). Characterization of Silicon Photodiode-Based Trap Detectors and Establishment of Spectral Responsivity Scale, *Optic and Lasers in Enginnering.* **43(2),** 131-141**.**

[31] Kuchnerus, P., Rabus, H., Richter, M., Scholze, F., Werner L., Ulm G. (1998). Characterization of Photodiodes as Transfer Detector Standards in the 120 nm to 600 nm Spectral Range, *Metrologia.* **35(4)**, 355-362.

[32] Abd-Elmageed, A. (2011). *Detector-Based Traceability Chain for Spectral Irradiance using Tunable Laser-Based Facility at PTB*, PhD Thesis. PTB: Germany.

[33] Kilin, M., Tutunculer, H., Meric, S. (2019). Effective Measurement of the Wavelength Accuracy Calibration by Using Monte Carlo Uncertainty Calculation, *AIP Conference Proceedings.* 2178, 030008.

[34] Friedrich, R., Fischer, J. (2000). New Spectral Radiance Scale from 220 nm to 2500 nm, *Metrologia.* **37(5)**, 539-542.

[35] Eppeldauer, G. P., Brown, S. W., Larason, T. C., R´acz, M., Lykke, K. R. (2000). Realization of a Spectral Radiance Responsivity Scale with a Laser-Based Source and Si Radiance Meters, *Metrologia.* **37(5),** 531-534.

[36] Palmer, J. M., Grant, B. G. (2009). *PM184, the Art of Radiometry, Appendix V Radiometry and Photometry*. SPIE press book: USA

[37] BIPM. (2019). *Principles Governing Photometry*, 2nd edition. Rapport BIPM: France.

[38] CIE, D001. (1988). *Disc Version of CIE Photometric and Colorimetric*. Data Publication. **18(2),** 86-95.

[39] Hunt, R. W. G. (2004). *The Reproduction of Color, Spectral Luminous Efficiency Functions*, Appendix 7, 6th Edition. *New York*: United States.

[40] Parr, A.C., Datla, R. U., Gardner, J.L. (2005). *Optical Radiometry*, Volume 41. *Elsevier Academy Press:* USA.

[41] Blevin, W. R., Steiner, B. (1975). Redefinition of the Candela and the Lumen, *Metrologia.* **11(3)**, 97–104.

[42] Blevin, W. R. (1979). The Candela and the Watt, *CIE Proceedings*. Kyoto: Japan, **79-102**.

[43] Grum, F., Becherer, R. (1979). *Optical Radiation Measurements, volume 1*, 1st edition. *Academic Press*: New York,

[44] Quinn, T. J., Martin, J. E. (1991). Blackbody Source in the +50 to +200 ºC Range for the Calibration of Radiometers and Radiation Thermometers, *OSA Publishing Appl. Opt.* **30(31)**, 4486-4488.

[45] James, H. W., Robert, D. S., Albert T. H. (1987). Spectral Radiance Calibrations, *National Bureau of Standards Special Publication, NBS.* **250(20)**, 1-102.

[46] Sperfeld, P., Metzdorf, J., Yousef, S., Stock, K., Möller, W. (1998). Improvement and Extension of the Black-Body Based Spectral Irradiance Scale, *Metrologia*. **35(4)**, 267-271.

[47] Sperfeld, P., Pape, S., Khlevnoy, B., Burdakin, A. (2009). Performance Limitations of Carbon-Cavity Blackbodies Due to Absorption Bands at the Highest Temperatures, *Metrologia.* **46(4)**, 170-173.

[48] Parr, A. C. (2000). The Candela and Photometric and Radiometric Measurements, *J. Res. Natl. Inst. Stand. Technol*. **106(1)**, 151-186.

[49] Haapalinna, A. (2004). *Characterization Methods for Silicon Photodiode and Silicon Sub-Surface Properties*, Ph.D thesis. Helsinki University of Technology: Finland.

[50] Werner, L., Friedrich, R., Johannsen, U., Steiger, A. (2000), Precise Scale of Spectral Responsivity for Ingaas Detectors Based on a Cryogenic Radiometer and Several Laser Sources, *Metrologia*. **37(5),** 523–526.

[51] Cromer, C. L., Eppeldauer, G., Hardis, J. E., Larason, T. C., Parr, A. C. (1993). Detector-Based Photometric Scale, *Applied Optics*. **32(16)**, 2936-2948.

[52] Schrama, C. A., Bosma, R., Gibb, K., Reijn, H., Bloembergen, P. (1998). Comparison of Monochromator-Based and Laser-Based Cryogenic Radiometry, *Metrologia.* **35(4)**, 431–435**.**

[53] Ahtee, V., Brown, S. W., Larason, T. C., Lykke, K. R., Ikonen, E., Noorma, M. (2007). Comparison of Absolute Spectral Irradiance Responsivity Measurement Techniques Using Wavelength-Tunable Lasers, *OSA Publishing Applied Optics*. **46(20),** 4228-4236.

[54] Zalewski, E. F., Duda, C. R. (1983). Silicon Photodiode Device with 100 % External Quantum Efficiency, *OSA Publishing Applied Optics.* **22(18),** 2867-2873.

[55] Walker, J., Saunders, R. D., Hattenburg, A. T. (1987). *Spectral Radiance Calibrations*, National Bureau of Standards (NBS). Special publication: France.

[56] Kübarsepp, T., Kärhä, P., Ikonen, E. (1997). Characterization of a Polarization Independent Transmission Trap Detector, *Applied Optics.* **36(13)**, 2807-2812.

[57] Goebel, R., Yilmaz, S., Pello, R. (1996). Polarization Dependence of Trap Detectors, *Metrologia.* **33(3)**, 207–213.

[58] Parr, A. C. (1996). *A National Measurement System for Radiometry, Photometry, and Pyrometry Based upon Absolute Detectors*, Technical Note 1421. NIST: USA.

[59] Hengstberger, F. (1989). *Absolute Radiometry*, Academic Press, Inc,: Boston, 0-12-340810-5

[60] Coblentz, W. W. Emerson, W. B. (1916). *Studies of Instruments for Measuring Radiant Energy in Absolute Value*, An Absolute Thermopile, 12th edition. Bulletin of the Bureau of Standards: USA

[61] National Institute of Standards and Technology. (2008). *Spectroradiometric Detector Measurements, Ultraviolet, Visible, and near Infrared Detectors for Spectral Power*, 1st edition. NIST special publication: USA. 250-41.

[62] Lei, F., Fischer, J. (1993). Characterization of Photodiodes in the UV and Visible Spectral Region Based on Cryogenic Radiometry, *Metrologia.* **30(4)**, 297–303.

[63] Shaw, P., Larason, T. C., Gupta, R., Brown, S. W., Lykke, K. R. (2000). Improved Near-Infrared Spectral Responsivity Scale, *J. Res. Natl. Inst. Stand. Technol*. **105(5)**, 689-700.

[64] Hamamatsu Company. (2017). *Chapter-2 Si Photodiodes Handbook*. Hamamatsu Publication: Japan.

[65] Johnson, M. (2003). *Photodetection and Measurement Maximizing Performance in Optical Systems*. McGraw-Hill companies: USA.

[66] Kilin, M., Tutunculer, H., Bazkir, O., Meric, S. (2020). Realization of the Radiance Scale Using Transfer Function of the Laser Based Optical System, *International Journal of Optics.* **2020(1)**, 1-10.

[67] Planck, M. (1900). Ueber Eine Verbesserung Der Wienschen Spektralgleichung, Verhandlungen Der Deutschen Physikalischen Gesellschaft, *Pergamon Press.* **2(1)**, 202–204.

[68] Planck, M. (1997). *Die Ableitung der Strahlungsgesetze, Ostwalds Klassiker der exakten Wissenschaften*, Verlag Harri Deutsch. Bad 206: Thun und Frankfurt am Main.

[69] Planck, M. (1900). Zur Theorie des Gesetzes der Energieverteilung im Normalspektrum, *Verhandlungen der Deutschen Physikalischen Gesellschaft* **2(1)**, 237–245.

[70] Santa Cruz Institute for Particle Physics (SCIPP), http://scipp.ucsc.edu 15.08.2019.

[71] Hauer, K., Höpe, A. (2009). High-Grade Uniform Light Source for Radiometric and Photometric Applications, *MAPAN*. **24(3)**, 175-182.

[72] Knee, P. C. (1999). Investigation of the Uniformity and Ageing of Integrating Spheres, *Analytica Chimica Acta.* **380(1),** 391-399.

[73] Kostkowski, H. J. (1997). *Reliable Spectroradiometry*, Spectroradiometry Consulting. La Plata: Maryland.

[74] Brown, S. W., Eppeldauer, G. P., Lykke, K. R. (2000). NIST Facility for Spectral Irradiance and Radiance Responsivity Calibrations with Uniform Sources, *Metrologia*. **37(5),** 579-582.

[75] Shaw, P., Li, Z. (2008). On the Fluorescence from Integrating Spheres, *Applied Optics.* **47(21),** 3962-3967.

[76] Oriel integrating sphere, http://www.newport.com, 15.07.2019.

[77] Sagberg, H., Lacolle, M., Johansen, I. R., Lovhaugen, O., Belikov, R., Solgaard, O., Sudbo, A. S. (2004). Micro Chemical Grating for Visible and Near-Infrared Spectroscopy, *IEEE Journal of Selected Topic in Quantum Electronics*. **10(3)**, 604-613.

[78] Simonov, A.N., Grabamik, S., Vdovin, G. (2007). Stretchable Diffraction Grating for Spectrometry, *Optic Express*. **15(15),** 9784-9792.

[79] Sameh, M. R., Alaa-Eldin, A. A. (2012). On the Use of Spectral Lamp Line in the Monochromator Calibration, *Science Road Publishing Corporation*. **4(1),** 22-25.

[80] Kneubühl, F. (1969). Diffraction Grating Spectroscopy, *Applied Optic*, **8(3)**, 505-519.

[81] DeCusatis, C. (1998). *Handbook of Applied Photometry*. Optical Society: America.

[82] Owen, T. (1996). *Fundamentals of UV-Visible Spectroscopy*. Hewlett-Packard Company: USA.

[83] Craig, J. S., Marc, L. S., Joseph, R. (1996). Wavelength of Spectral Lines in Mercury Pencil Lamps, *Applied Optic.* **35(1)**, 74-77.

[84] Reader, J., Sansonetti, C. J. (1999). Modern Wavelength Standards in the Ultraviolet and Vacuum Ultraviolet, *Conference on Ultraviolet Atmospheric and Space Remoting-Methods and Instrumentation II (SPIE) proceeding and abstract*. 2-8.

[85] Andor, G., Dezsi, G. (1998). New Standard Reference Material Set for UV Spectrophotometer Linearity Test, *SPIE-Optika '98 - 5th congress on modern optics proceeding and abstract.* 335-338.

[86] Liu, H., Ying, C., Chen, K., Wang, H., Jiang, B., Wu, B., Wang, H. F., Huo, M. (2016). Research on Calibration Technology of the Wide Spectrum Grating Monochromator Wavelength Accuracy, *URSI Asia-Pacific Radio Science Conference proceeding and abstract.* 1744-1747.

[87] Boivin, L. (2002). Study of Bandwidth Effects in Monochromator-Based Spectral Responsivity Measurements, *Applied Optics.* **41(10)**, 1929-1935.

[88] Saunders, R. D., Shumaker, J. B. (1986). Apparatus Function of a Prism-Grating Double Monochromator, *Applied Optics.* **25(20)**, 3710-3714.

[89] Palmer, C. (2002). *Diffraction Grating Handbook, fifth edition*. Thermo Richard Grating Laboratory: New York.

[90] Winter, S., Sperling, A. (2006). Uncertainty Analysis of a Photometer Calibration at the DSR Setup of the PTB, *2nd Expert Symposium on Measurement Uncertainty*, Braunschweig, Germany CIE. x029-2006.

[91] BIPM. (2008). Joint *Committee for Guides in Metrology, Evaluation of Measurement Data—Guide to Expression of the Uncertainty in Measurement (GUM 1995 Minor Corrections), Vol. 100*. BIPM Joint Committee for Guides in Metrology, Sevres: France.

[92] BIPM. (2006). *Joint Committee for Guides in Metrology, Evaluation of measurement data—Supplement 1 to the Guide to Expression of the Uncertainty in Measurement—Propagation of Distribution Using a Monte Carlo Method.* BIPM Joint Committee for Guides in Metrology, Sevres: France.

[93] NIST. (1994). *Guidelines for Evaluating and Expressing the Uncertainty of NIST Measurement Results*. NIST Technical Note 1297: USA.

[94] CIE. (2006). Measurement Uncertainty, *Proceedings of the 2nd CIE Expert Symposium*. Braunschweig: Germany.

[95] López, M., (2008). *Optical Characterization of Ge- and InGaAs-Semiconductor Detectors for High Accuracy Optical Radiant Power Measurements in the Near Infrared*, Ph.D Thesis. Braunschweig University: Germany.

APPENDIX

Appendix-A

There are three grating system of the each turret mechanism of the double monochromator system such as 600 gr/mm, 1200 gr/mm and 2400 gr/mm. There are wavelength resolution regions in which each grating is active. Calculation MatLab computer programs codes made for the Table 4.4 and Figure 4.2 is given A1 and A2 section. Also Monte Carlo uncertainty calculation of the same system is defined and compared in the A3 and A4 section.

A1

Table 4.4 is obtained by using computer program codes for each grating and each wavelength. The following codes are given for 600 g/mm and it is same for other grating that is it has made same calculation procedure for other grating.

```
clear; clc;
% monochromator resolution
resol=0.05/sqrt(3);
% reference wavelengths
L_ref=[546.07 730.04 1013.98 1092.14 1638.21 2184.28];
% measurement data
data546 =load ('546_07.txt');
data730 =load ('730_04.txt');
data1013 =load ('1013_98.txt');
data1092 =load ('1092_14.txt');
data1638 =load ('1638_21.txt');
data2184 =load ('2184_28.txt');
% measurement wavelength range
L_546 =data546 (:,1);
L_730 =data730 (:,1);
L_1013 =data1013 (:,1);
L_1092 =data1092 (:,1);
L_1638 =data1638 (:,1);
L_2184 =data2184 (:,1);
```

```
% zeros matrix
I_546 =zeros(32,10);
I_730 =zeros(38,10);
I_1013 =zeros(21,10);
I_1092 =zeros(34,10);
I_1638 =zeros(35,10);
I_2184 =zeros(27,10);
k=2;
for i=1:10;
  I_546(:,i)=data546(:,k) + data546(:,k)*0.02/100;
  I_730(:,i)=data730(:,k) + data730(:,k)*0.02/100;
  I_1013(:,i)=data1013(:,k) + data1013(:,k)*0.02/100;
  I_1092(:,i)=data1092(:,k) + data1092(:,k)*0.02/100;
  I_1638(:,i)=data1638(:,k) + data1638(:,k)*0.02/100;
  I_2184(:,i)=data2184(:,k) + data2184(:,k)*0.02/100;
  k=k+1;
end
for j=1:10
  L_546_all_Pik(:,j)=sum(L_546.*I_546(:,j))./sum(I_546(:,j));
  L_730_all_Pik(:,j)=sum(L_730.*I_730(:,j))./sum(I_730(:,j));
  L_1013_all_Pik(:,j)=sum(L_1013.*I_1013(:,j))./sum(I_1013(:,j));
  L_1092_all_Pik(:,j)=sum(L_1092.*I_1092(:,j))./sum(I_1092(:,j));
  L_1638_all_Pik(:,j)=sum(L_1638.*I_1638(:,j))./sum(I_1638(:,j));
  L_2184_all_Pik(:,j)=sum(L_2184.*I_2184(:,j))./sum(I_2184(:,j));
end
L_546_pik=mean(L_546_all_Pik);
L_546_pik_std=sqrt(std(L_546_all_Pik).^2 + resol^2);
L_730_pik=mean(L_730_all_Pik);
L_730_pik_std=sqrt(std(L_730_all_Pik).^2 + resol^2);
L_1013_pik=mean(L_1013_all_Pik);
L_1013_pik_std=sqrt(std(L_1013_all_Pik).^2 + resol^2);
L_1092_pik=mean(L_1092_all_Pik);
L_1092_pik_std=sqrt(std(L_1092_all_Pik).^2 + resol^2);
L_1638_pik=mean(L_1638_all_Pik);
L_1638_pik_std=sqrt(std(L_1638_all_Pik).^2 + resol^2);
L_2184_pik=mean(L_2184_all_Pik);
L_2184_pik_std=sqrt(std(L_2184_all_Pik).^2 + resol^2);
```

```
L_pik=[L_546_pik   L_730_pik   L_1013_pik   L_1092_pik   L_1638_pik
L_2184_pik ];
S_L_pik=(1/sqrt(3)).*[L_546_pik_std   L_730_pik_std   L_1013_pik_std
L_1092_pik_std L_1638_pik_std  L_2184_pik_std];
[xData, yData] = prepareCurveData( L_ref, L_pik );
% Set up fittype and options.
ft = fittype( 'poly1' );
% Fit model to data.
[fitresult, gof] = fit( xData, yData, ft );
p1=fitresult.p1;
p2=fitresult.p2;
s=confint(fitresult,0.95);
s_p1=(1/sqrt(3)).*(abs(s(2,1)'-s(1,1)')/4);
s_p2=(1/sqrt(3)).*(abs(s(2,2)'-s(1,2)')/4);
Un_1=S_L_pik.^2 + L_pik.^2.*s_p1.^2 + s_p2.^2;
Un_2=sqrt(Un_1);
[L_ref' Un_2' 2*Un_2']
```

A2

Figure 4.2 has given the wavelength uncertainty distribution of the double monochromator system with triple grating.

```
clear all; clc;
C_2400=load('Ben_Clas_2400.txt');
C_1200=load('Ben_Clas_1200.txt');
C_600=load('Ben_Clas_600.txt');
x1=C_2400(:,1);
y2=C_2400(:,2);
x11=C_1200(:,1);
y22=C_1200(:,2);
x111=C_600(:,1);
y222=C_600(:,2);
plot(x1,y2,'k*-','MarkerSize',10,'LineWidth',1.5)
hold on
grid on
plot(x11,y22,'ks-','MarkerSize',10,'LineWidth',1.5)
plot(x111,y222,'ko-','MarkerSize',10,'LineWidth',1.5)
axis([100 2600 0.1 0.4])
title('For   Double   Monochromator   with   Triple   Grating   System
```

```
Uncertainty Distribution','FontSize',13,'FontName','times')
xlabel('Wavelength (nm)')
ylabel('Extended Uncertainty k=2 (nm) ')
legend('2400 g/mm','1200 g/mm','600 g/mm' ...
        ,'Location','NorthWest','fontSize',10)
size=[2400 1800];
res=300;
set(gca,'FontName','times');
set(gca,'FontSize',13);
set(gcf,'paperunits','inches','paperposition',[0 0 size/res]);
print('Figure_5_1.tiff','-dtiff',['-r' num2str(res)]);
```

A3

Definitions made in the appendix A1 and A2 are repeated calculating also with Monte Carlo uncertainty and they are compared with one other. This MatLab source code gives the Monte Carlo uncertainty calculation of the wavelength calibration of the double monochromator system. By the way, the following codes are given for 600 g/mm and it is same for other grating that is it has made same calculation procedure for other grating.

```
clear; clc;
% resolution of the monochromator
resol=0.05/sqrt(3);
% referance wavelengths
L_ref=[546.07 730.04 1013.98 1092.14 1638.21 2184.28];
% measurement data
data546 =load('546_07.txt');
data730 =load('730_04.txt');
data1013 =load('1013_98.txt');
data1092 =load('1092_14.txt');
data1638 =load('1638_21.txt');
data2184 =load('2184_28.txt');
% measurement wavelength range
L_546 =data546(:,1);
L_730 =data730(:,1);
L_1013 =data1013(:,1);
L_1092 =data1092(:,1);
L_1638 =data1638(:,1);
```

```
L_2184 =data2184(:,1);
% zeros matrix
I_546 =zeros(32,10);
I_730 =zeros(38,10);
I_1013 =zeros(21,10);
I_1092 =zeros(34,10);
I_1638 =zeros(35,10);
I_2184 =zeros(27,10);
k=2;
for i=1:10;
  I_546(:,i)=data546(:,k) + data546(:,k)*0.02/100;
  I_730(:,i)=data730(:,k) + data730(:,k)*0.02/100;
  I_1013(:,i)=data1013(:,k) + data1013(:,k)*0.02/100;
  I_1092(:,i)=data1092(:,k) + data1092(:,k)*0.02/100;
  I_1638(:,i)=data1638(:,k) + data1638(:,k)*0.02/100;
  I_2184(:,i)=data2184(:,k) + data2184(:,k)*0.02/100;
  k=k+1;
end
for j=1:10
  L_546_all_Pik(:,j)=sum(L_546.*I_546(:,j))./sum(I_546(:,j));
  L_730_all_Pik(:,j)=sum(L_730.*I_730(:,j))./sum(I_730(:,j));
  L_1013_all_Pik(:,j)=sum(L_1013.*I_1013(:,j))./sum(I_1013(:,j));
  L_1092_all_Pik(:,j)=sum(L_1092.*I_1092(:,j))./sum(I_1092(:,j));
  L_1638_all_Pik(:,j)=sum(L_1638.*I_1638(:,j))./sum(I_1638(:,j));
  L_2184_all_Pik(:,j)=sum(L_2184.*I_2184(:,j))./sum(I_2184(:,j));
  end
L_546_pik=mean(L_546_all_Pik);
L_546_pik_std=sqrt(std(L_546_all_Pik).^2 + resol^2);
L_730_pik=mean(L_730_all_Pik);
L_730_pik_std=sqrt(std(L_730_all_Pik).^2 + resol^2);
L_1013_pik=mean(L_1013_all_Pik);
L_1013_pik_std=sqrt(std(L_1013_all_Pik).^2 + resol^2);
L_1092_pik=mean(L_1092_all_Pik);
L_1092_pik_std=sqrt(std(L_1092_all_Pik).^2 + resol^2);
L_1638_pik=mean(L_1638_all_Pik);
L_1638_pik_std=sqrt(std(L_1638_all_Pik).^2 + resol^2);
L_2184_pik=mean(L_2184_all_Pik);
L_2184_pik_std=sqrt(std(L_2184_all_Pik).^2 + resol^2);
```

```
L_pik=[L_546_pik   L_730_pik   L_1013_pik   L_1092_pik   L_1638_pik
L_2184_pik ];

S_L_pik=(1/sqrt(3)).*[L_546_pik_std   L_730_pik_std   L_1013_pik_std
L_1092_pik_std L_1638_pik_std  L_2184_pik_std];

[xData, yData] = prepareCurveData( L_ref, L_pik );

% Set up fittype and options.
ft = fittype( 'poly1' );

% Fit model to data.
[fitresult, gof] = fit( xData, yData, ft );

p1=fitresult.p1;
p2=fitresult.p2;
s=confint(fitresult,0.95);
s_p1=(1/sqrt(3)).*(abs(s(2,1)'-s(1,1)')/4);
s_p2=(1/sqrt(3)).*(abs(s(2,2)'-s(1,2)')/4);

for i=1:6
 n=1e6;
 MC_L=normrnd(L_pik(i),S_L_pik(i),1,n);
 MC_p1=normrnd(p1,s_p1,1,n);
 MC_p2=normrnd(p2,s_p2,1,n);
 LL=(MC_p1.*MC_L)+MC_p2;
 MC_LL=fitdist(LL','Normal');
 MC_LL_Mu(i)=MC_LL.mu;
 MC_LL_sigma(i)=MC_LL.sigma;
end
 [L_ref' MC_LL_sigma' 2*MC_LL_sigma']
```

A4

When the calculation has repeated in the appendix A1 and A3, following figure is obtained. It shows us both MC and classical calculations results in the same graphs.

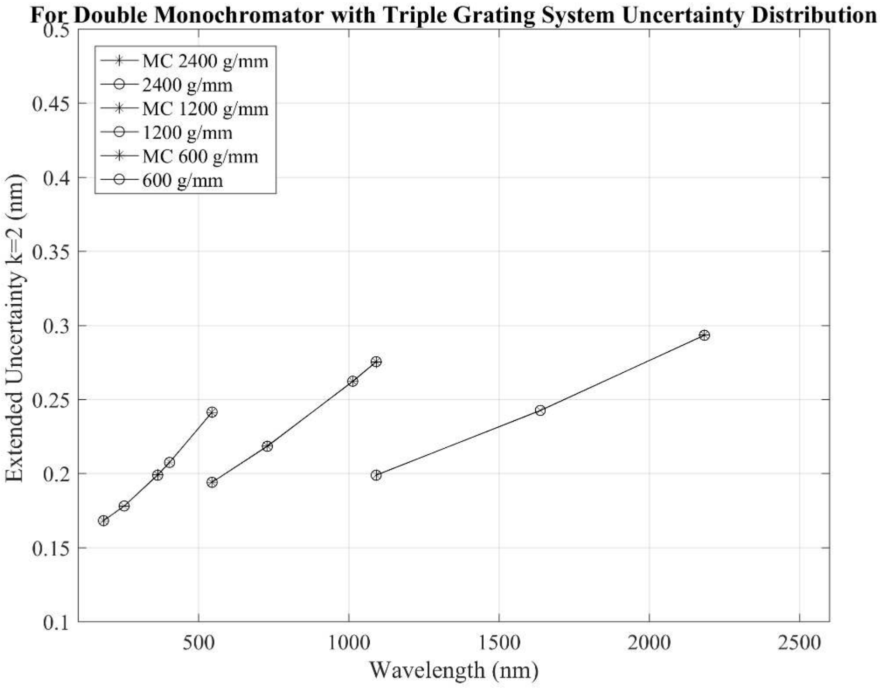

Figure A.1: by using classical uncertainty and Monte Carlo uncertainty, for double monochromator system with triple grating system comparatively wavelength calibration analysis.

Appendix-B

Correction factor subsection in the Chapter 4 is section 4.1.3. In here, calculation of the correction factor caused by measurement errors is explained. Firstly, by using conservation of the radiance, after that wavelength shift and finally monochromator's bandwidth correction factor are calculated and given following appendix sections B1, B2 (Table 4.5) and B3 (Table 4.6) respectively.

B1

```
clear all ; clc;
format short;
% from 0.05m to 0.39m distance 0.02m step
d=load('Distance.txt');
% as a function of distance, current values in ampere unit 10 time
disamp=load('Distance_Amper.txt');
s=sum(disamp,2);
Amper=s./10;             % mean current results
```

```
res=0.33158;   % 632.8 nm detector responsivity
rs=1.25e-2;    % integreating sphere output port radius in meter unit
rd=4.0e-3;     % detector actice area radius in meter unit
D2=d.*d+rs^2+rd^2;
sigma=(rs^2*rd^2)./(D2.*D2);
cons=D2./((pi^2*rd^2*rs^2)*(1+sigma));   % geomtric constant
Radiance=Amper.*cons/res; % Radiance (W / sr m^2 )
    % Fit Results a*d^b + b
    %    a  =   0.03031  (0.02467, 0.03594)
    %    b  =   -1.949   (-2.011, -1.887)
    %    c  =   3.009    (2.94, 3.078
% previous line radiance function fit function
f=inline('0.03031*x^-1.949 + 3.009');
% Open a file and type there of the results
fileID=fopen('Radiance1.txt','w');
for x=0.05:0.02:1.1;
    f(x);
    fprintf(fileID,'%f %f\n',x,f(x));
end
fclose(fileID);
data=load('Radiance1.txt');
% at extreme point radiance value by using fit function
RefRad=min(data(:,2));
NewAmpers=RefRad*res./cons;
Cor=NewAmpers./Amper;
CorFac=1/(Cor(8)+0.01*(Cor(9)-Cor(8))/0.02)
```

B2

```
clear all; clc;
format short
D17=load('Delta_Lambda_1.7mrad.txt');
D5=load('Delta_Lambda_5mrad.txt');
D11=load('Delta_Lambda_11mrad.txt');
IT17=load('I_Trap_1.7mrad_1st_Der.txt');
IT5=load('I_Trap_5mrad_1st_Der.txt');
IT11=load('I_Trap_11mrad_1st_Der.txt');
IM17=load('I_Mono_1.7mrad_1st_Der.txt');
IM5=load('I_Mono_5mrad_1st_Der.txt');
```

```
IM11=load('I_Mono_11mrad_1st_Der.txt');
Cor17=(1-((D17(:,2).*IM17(:,4))./IM17(:,2)))./ …
      (1 ((D17(:,2).*IT17(:,4))./IT17(:,2)));
Cor5=(1-(D5(:,2).*IM5(:,4))./IM5(:,2))./…
     (1-(D5(:,2).*IT5(:,4))./IT5(:,2));
Cor11=(1-(D11(:,2).*IM11(:,4))./IM11(:,2))./…
      (1-(D11(:,2).*IT11(:,4))./IT11(:,2));

a17=D17(:,2);
b17=IM17(:,4);
c17=IM17(:,2);
d17=IT17(:,4);
e17=IT17(:,2);
corb17=  a17./(c17.*((a17.*d17)./e17 - 1));
corc17= -(a17.*b17)./(c17.^2.*((a17.*d17)./e17 - 1));
cord17= -(a17.*((a17.*b17)./c17 - 1))./…
         (e17.*((a17.*d17)./e17 - 1).^2);
core17=  (a17.*d17.*((a17.*b17)./c17 - 1))./…
         (e17.^2.*((a17.*d17)./e17 - 1).^2);
sigmab17=IM17(:,5);
sigmac17=IM17(:,3);
sigmad17=IT17(:,5);
sigmae17=IT17(:,3);
a5=D5(:,2);
b5=IM5(:,4);
c5=IM5(:,2);
d5=IT5(:,4);
e5=IT5(:,2);
corb5=a5./(c5.*((a5.*d5)./e5 - 1));
corc5=-(a5.*b5)./(c5.^2.*((a5.*d5)./e5 - 1));
cord5=-(a5.*((a5.*b5)./c5 - 1))./(e5.*((a5.*d5)./e5 - 1).^2);
core5=(a5.*d5.*((a5.*b5)./c5 - 1))./(e5.^2.*((a5.*d5)./e5 - 1).^2);
sigmab5=IM5(:,5);
sigmac5=IM5(:,3);
sigmad5=IT5(:,5);
sigmae5=IT5(:,3);
a11=D11(:,2);
b11=IM11(:,4);
```

```
c11=IM11(:,2);
d11=IT11(:,4);
e11=IT11(:,2);
corb11=   a11./(c11.*((a11.*d11)./e11 - 1));
corc11=  -(a11.*b11)./(c11.^2.*((a11.*d11)./e11 - 1));
cord11=  -(a11.*((a11.*b11)./c11 - 1))./…
          (e11.*((a11.*d11)./e11 - 1).^2);
core11=   (a11.*d11.*((a11.*b11)./c11 - 1))./…
          (e11.^2.*((a11.*d11)./e11 - 1).^2);
sigmab11=IM11(:,5);
sigmac11=IM11(:,3);
sigmad11=IT11(:,5);
sigmae11=IT11(:,3);
sigma17=sqrt(corb17.^2.*sigmab17.^2+corc17.^2.*sigmac17.^2+cord17.^2
.*sigmad17.^2+core17.^2.*sigmae17.^2);

sigma5=sqrt(corb5.^2.*sigmab5.^2+corc5.^2.*sigmac5.^2+cord5.^2.*sigm
ad5.^2+core5.^2.*sigmae5.^2);

sigma11=sqrt(corb11.^2.*sigmab11.^2+corc11.^2.*sigmac11.^2+cord11.^2
.*sigmad11.^2+core11.^2.*sigmae11.^2);

format shortE
[Cor17 sigma17 Cor5 sigma5 Cor11 sigma11]
```

B3

```
clear all; clc;
format short
D17=load('Delta_Lambda_1.7mrad.txt');
D5=load('Delta_Lambda_5mrad.txt');
D11=load('Delta_Lambda_11mrad.txt');
IT17=load('I_Trap_1.7mrad_2nd_Der.txt');
IT5=load('I_Trap_5mrad_2nd_Der.txt');
IT11=load('I_Trap_11mrad_2nd_Der.txt');
IM17=load('I_Mono_1.7mrad_2nd_Der.txt');
IM5=load('I_Mono_5mrad_2nd_Der.txt');
IM11=load('I_Mono_11mrad_2nd_Der.txt');
Cor17= (1-(D17(:,2).^2.*IM17(:,4))./(12*IM17(:,2)))./(1-
       (D17(:,2).^2.*IT17(:,4))./(12*IT17(:,2)));
```

```
Cor5=  (1-(D5(:,2).^2.*IM5(:,4))./(12*IM5(:,2)))./(1-
       (D5(:,2).^2.*IT5(:,4))./(12*IT5(:,2)));
Cor11= (1-(D11(:,2).^2.*IM11(:,4))./(12*IM11(:,2)))./(1-
       (D11(:,2).^2.*IT11(:,4))./(12*IT11(:,2)));
a17=D17(:,2);
b17=IM17(:,4);
c17=IM17(:,2);
d17=IT17(:,4);
e17=IT17(:,2);
corb17=  a17.^2./(12*c17.*((d17.*a17.^2)./(12*e17) - 1));
corc17= -(a17.^2.*b17)./(12*c17.^2.*((d17.*a17.^2)./(12*e17) - 1));
cord17= -(a17.^2.*((b17.*a17.^2)./(12*c17) -
         1))./(12*e17.*((a17.^2.*d17)./(12*e17) - 1).^2);
core17=  (a17.^2.*d17.*((b17.*a17.^2)./(12*c17) -
         1))./(12*e17.^2.*((a17.^2.*d17)./(12*e17) - 1).^2);
sigmab17=IM17(:,5);
sigmac17=IM17(:,3);
sigmad17=IT17(:,5);
sigmae17=IT17(:,3);
a5=D5(:,2);
b5=IM5(:,4);
c5=IM5(:,2);
d5=IT5(:,4);
e5=IT5(:,2);
corb5= a5.^2./(12*c5.*((d5.*a5.^2)./(12*e5) - 1));
corc5= -(a5.^2.*b5)./(12*c5.^2.*((d5.*a5.^2)./(12*e5) - 1));
cord5= -(a5.^2.*((b5.*a5.^2)./(12*c5) -
        1))./(12*e5.*((a5.^2.*d5)./(12*e5) - 1).^2);
core5= (a5.^2.*d5.*((b5.*a5.^2)./(12*c5) -
       1))./(12*e5.^2.*((a5.^2.*d5)./(12*e5) - 1).^2);
sigmab5=IM5(:,5);
sigmac5=IM5(:,3);
sigmad5=IT5(:,5);
sigmae5=IT5(:,3);
a11=D11(:,2);
b11=IM11(:,4);
c11=IM11(:,2);
d11=IT11(:,4);
e11=IT11(:,2);
```

```
corb11= a11.^2./(12*c11.*((d11.*a11.^2)./(12*e11) - 1));
corc11= -(a11.^2.*b11)./(12*c11.^2.*((d11.*a11.^2)./(12*e11) - 1));
cord11= -(a11.^2.*((b11.*a11.^2)./(12*c11) -
         1))./(12*e11.*((a11.^2.*d11)./(12*e11) - 1).^2);
core11= (a11.^2.*d11.*((b11.*a11.^2)./(12*c11) -
        1))./(12*e11.^2.*((a11.^2.*d11)./(12*e11) - 1).^2);
sigmab11=IM11(:,5);
sigmac11=IM11(:,3);
sigmad11=IT11(:,5);
sigmae11=IT11(:,3);
sigma17= sqrt(corb17.^2.*sigmab17.^2+corc17.^2.*sigmac17.^2+
         cord17.^2.*sigmad17.^2+core17.^2.*sigmae17.^2);
sigma5=  sqrt(corb5.^2.*sigmab5.^2+corc5.^2.*sigmac5.^2+
         cord5.^2.*sigmad5.^2+core5.^2.*sigmae5.^2);
sigma11= sqrt(corb11.^2.*sigmab11.^2+corc11.^2.*sigmac11.^2+
         cord11.^2.*sigmad11.^2+core11.^2.*sigmae11.^2);
format shortE
[Cor17 sigma17 Cor5 sigma5 Cor11 sigma11]
```

Appendix-C

The results of the spectral radiance measurements are calculated both using classical uncertainty and Monte Carlo uncertainty. In the Table 5.1, 5.2 and 5.3 model function results are obtained for 632.8 nm He-Ne laser in the three different FOV. Following computer program code by using generalized classical uncertainty calculation is design for each parameters with k=1 sigma uncertainty value at 11-mrad FOV.

C1

```
clear all; clc;
Cor1=[1.23 ;1.933e-4]';                 % unitless
Cor2=load('Cor_Uncer_Datas_2.txt');     % unitless 1st column is
                                        wavelength 1.7 5 11
                                        respectivelty with sigma_1
Cor3=load('Cor_Uncer_Datas_3.txt');     % unitless 1st column is
                                        wavelength 1.7 5 11
                                        respectivelty with sigma_1
D_C=[6.14206e-7 ;1.25363e-8]';          % unit is (m^2 sr)
```

```
D_Res=load('det_resposivity.txt');        % unir is Amper/Watt 1st
                                          column is wavelength 2nd and
                                          3th value and sigma
D_L=[2.65 ;0.01]';                        % unit is nm
Is=load('I_Trap_11mrad_1st_Der.txt');     % unit is Amper 1st column
                                          is wavelength 2nd and 3th
                                          value and sigma
Im=load('I_Mono_11mrad_1st_Der.txt');     % unit is Amper 1st column
                                          is wavelength 2nd and 3th
                                          value and sigma
Iu=load('SRS12_Amper_11mrad_10data.txt'); % unit is Amper 1st and 2nd
                                           value and sigma
R11=load('SRS12_NewRad_11mrad.txt');       % unit is mW/m^2 sr nm  1st
                                           column is wavelength
R5=load('SRS12_NewRad_5mrad.txt');         % unit is mW/m^2 sr nm  1st
                                           column is wavelength
R17=load('SRS12_NewRad_1_7mrad.txt');      % unit is mW/m^2 sr nm  1st
                                           column is wavelength

format shortE
%  Radiance :      L = (Iu*Is*Cor1*Cor2*Cor3)/(Im*D_Res*D_C*D_L)

C_Iu= ((Is(:,2).*Cor1(:,1).*Cor2(:,6).*Cor3(:,6))./(
      Im(:,2).*D_Res(:,2).*D_C(:,1).*D_L(:,1) ) );
S_Iu= Iu(:,2).*C_Iu;
C_Is= ((Iu(:,1).*Cor1(:,1).*Cor2(:,6).*Cor3(:,6))./(
      Im(:,2).*D_Res(:,2).*D_C(:,1).*D_L(:,1) ) );
S_Is= Is(:,3).*C_Is;
C_Im= -((Iu(:,1).*Is(:,2).*Cor1(:,1).*Cor2(:,6).*Cor3(:,6))./(
      Im(:,2).^2.*D_Res(:,2).*D_C(:,1).*D_L(:,1) ) );
S_Im= Im(:,3).*C_Im;
C_D_Res=  -((Iu(:,1).*Is(:,2).*Cor1(:,1).*Cor2(:,6).*Cor3(:,6))./(
          Im(:,2).*D_Res(:,2).^2.*D_C(:,1).*D_L(:,1) ) );
S_D_Res=  D_Res(:,3).*C_D_Res;
C_D_C=    -((Iu(:,1).*Is(:,2).*Cor1(:,1).*Cor2(:,6).*Cor3(:,6))./(
          Im(:,2).*D_Res(:,2).*D_C(:,1).^2.*D_L(:,1) ) );
S_D_C=    D_C(:,2).*C_D_C;
C_D_L=    -((Iu(:,1).*Is(:,2).*Cor1(:,1).*Cor2(:,6).*Cor3(:,6))./(
          Im(:,2).*D_Res(:,2).*D_C(:,1).*D_L(:,1).^2 ) );
```

```
S_D_L=    D_L(:,2).*C_D_L;
for i=1:10;
  A=[R11(i,2) , R5(i,2) , R17(i,2)];
  Rp1=(std(A)/sqrt(3));
  Rp=Rp1/sqrt(6);
  Rep(i)=Rp; %num2str(Rp(:)) Unit is the radiance L= mW/sr m^2 nm
end
format shortE
ff=Cor1(1).*Cor2(:,6).*Cor3(:,6);        % corrections multiply
sff=   ff.*sqrt((Cor1(2)./Cor1(1)).^2 + (Cor2(:,7)./Cor2(:,6)).^2 +
       (Cor3(:,7)./Cor3(:,6)).^2);
[ff sff];

Variance_Sum=  (S_D_Res.^2 + S_D_C.^2 + S_Is.^2 + S_Im.^2 +
               S_Iu.^2 + S_D_L.^2 + sff.^2 + (Rep'*1e-3).^2);
format shortg
u=sqrt(Variance_Sum);
U=2*u;
[R11(:,1) 1e-3*R11(:,2) u U 100*U./(1e-3*R11(:,2))]
Un=U*1e3;
errorbar(R11(:,1), R11(:,2),Un,'*k')
hold on
grid on
title('Spectral Radiance for 11 mrad FOV with k=2 Standard
Uncertainty','FontSize',13,'FontName','times')
xlabel('Wavelength (nm)')
ylabel('Spectral Radiance (mW/sr m^2 nm )')
legend('SRS12 11mrad','location', 'NorthEast','fontSize',8)
size=[2400 1800];
res=300;
hold off
set(gca,'FontName','times');
set(gca,'FontSize',13);
set(gcf,'paperunits','inches','paperposition',[0 0 size/res]);
print('Radiance_11mrad_with_Uncertainty.tiff','-dtiff',['-r'
num2str(res)]);

[D_Res(9,2) D_Res(9,3) C_D_Res(9) S_D_Res(9) (S_D_Res(9))^2 ; ...
D_C(1) D_C(2) C_D_C(9) S_D_C(9) S_D_C(9)^2; ...
```

```
Is(9,2) Is(9,3) C_Is(9) S_Is(9) S_Is(9)^2 ; ...
Im(9,2) Im(9,3) C_Im(9) S_Im(9) S_Im(9)^2 ; ...
Iu(9,1) Iu(9,2) C_Iu(9) S_Iu(9) S_Iu(9)^2; ...
D_L(1) D_L(2) C_D_L(9) S_D_L(9) S_D_L(9)^2; ...
ff(9) sff(9) sff(9)  sff(9) sff(9)^2 ; ...
1e-3*R11(9,2) Rep(9)'*1e-3  Rep(9)'*1e-3  Rep(9)'*1e-3 ...
(Rep(9)'*1e-3)^2; ...
Variance_Sum(9) Variance_Sum(9) Variance_Sum(9) u(9) U(9)]
```

C2 : All measurement calculation made with classical uncertainty are repeated by using Monte Carlo uncertainty calculation.

```
clear all; clc;
%  Radiance: L=(Iu*Is*Cor1*Cor2*Cor3)/(Im*D_Res*D_C*D_L)
Cor1=[1.23 ;1.933e-4]';                 % unitless
Cor2=load('Cor_Uncer_Datas_2.txt');     % unitless 1st column is
                                          wavelength 1.7 5 11
                                          respectivelty with sigma_1
Cor3=load('Cor_Uncer_Datas_3.txt');     % unitless 1st column is
                                          wavelength 1.7 5 11
                                          respectivelty with sigma_1
D_C=[6.14206e-7 ;1.25363e-8]';          % unit is (m^2 sr)
D_Res=load('det_resposivity.txt');      % unir is Amper/Watt 1st
                                          column is wavelength 2nd and
                                          3th value and sigma
D_L=[2.65 ;0.01]';                      % unit is nm
Is=load('I_Trap_11mrad_1st_Der.txt');   % unit is Amper 1st column
                                          is wavelength 2nd and 3th
                                          value and sigma
Im=load('I_Mono_11mrad_1st_Der.txt');   % unit is Amper 1st column
                                          is wavelength 2nd and 3th
                                          value and sigma
Iu=load('SRS12_Amper_11mrad_10data.txt'); % unit is Amper 1st and

% 11mrad 632.8nm
n=1e6;           % random number count
MCor1  = normrnd(Cor1(1),Cor1(2),1,n);
MCor2  = normrnd(Cor2(9,6),Cor2(9,7),1,n);
MCor3  = normrnd(Cor3(9,6),Cor3(9,7),1,n);
```

```
MD_C   = normrnd(D_C(1),D_C(2),1,n);
MD_Res = normrnd(D_Res(9,2),D_Res(9,3),1,n);
MD_L   = normrnd(D_L(1),D_L(2),1,n);
MIs    = normrnd(Is(9,2),Is(9,3),1,n);
MIm    = normrnd(Im(9,2),Im(9,3),1,n);
MIu    = normrnd(Iu(9,1),Iu(9,2),1,n);

% Radiance
L=(MIu.*MIs.*MCor1.*MCor2.*MCor3)./(MIm.*MD_Res.*MD_C.*MD_L );
% Histogram
MCRad=fitdist(L','Normal');
MCRadMu=MCRad.mu;
MCRadSigma=2*MCRad.sigma;
Mu=MCRadMu';
Sigma=MCRadSigma';
Lambda=Cor2(9,1);
format shortg
[Lambda Mu Sigma (100*Sigma)./Mu]
LL=histfit(L,100);
grid on
hold on
title({'Spectral Radiance for 11 mrad FOV' ; 'Histogram Distribution
in the 633nm '},'FontSize',13,'FontName','times')
xlabel('Radiance (W/m^2sr nm)')
ylabel('Count')
legend('Distribution','Gaussian Fit', 'NorthEast','fontSize',8)
size=[2400 1800];
res=300;
hold off
set(gca,'FontName','times');
set(gca,'FontSize',13);
set(gcf,'paperunits','inches','paperposition',[0 0 size/res]);
print('633nm_11mrad_Hist.tiff','-dtiff',['-r' num2str(res)]);
```

CURRICULUM VITAE

MUSTAFA KILIN

Mobile: +90 (555) 342 29 30
Office : +90 (342) 317 22 17
mkilin@gantep.edu.tr
kilin.mustafa@gmail.com

University Avenue 27310
Gaziantep University
Engineering Physics
Engineering Optic and Acoustic
Sehitkamil, Gaziantep
TURKEY

EDUCATION

PhD Physics Engineering (2014-)

Gaziantep University, Turkey

- Thesis: *Investigation of Spectral Radiation Sensitivity for Optical Systems.*
- Supervisor: Prof. Dr. Hayriye TUTUNCULER tutunculer@gantep.edu.tr
- Co-Supervisor: Assoc. Prof. Dr. Ozcan BAZKIR ozcan.bazkir@tubitak.gov.tr

MS Physics Engineering (2011-2013)

Gaziantep University, Turkey

- Thesis: *Investigation of Bose-Einstein Condensation for Different Potentials.*
- Supervisor: Prof. Dr. Hayriye TUTUNCULER tutunculer@gantep.edu.tr

BSPhysics (2005-2009)

Anadolu University, Turkey

- Thesis: *Specialized in Solid State Physics and Characterization.*
- Supervisor: Prof. Dr. Metin KUL mkul@eskisehir.edu.tr

RESEARCH EXPERINCE

Research Project (PhD Study): For my doctoral studies, I worked for 2 years in the NMI (National Metrology Institute) of Turkey to study for radiometric traceability in the optic laboratory. Relative standard uncertainty and Monte Carlo uncertainty calculation realized and some papers published about it.

Research Project (present): Artificial intelligence calculation of the radiometric measurement that is part of the PhD study is interested by me nowadays. I am working on some methods for these calculations.

Research Project (present): High spatial resolution X-ray detection with photonic crystal; I am currently working on this computational project and running a variety of simulation packages to improve the resolution of the scintillator materials with a specific photonic crystal structure.

Optic Laboratory

- Double and Single monochromator wavelength calibration.
- Optical material in the UV-Vis-IR region, reflection transmission and absorption measurements.
- Optical measurement using different laser type.
- Theoretical Laser definition background.
- Material calibration according to reference standards.
- Si, Ga, InGaAs based trap detectors characterization (responsivity, polarization dependence, linearity, quantum efficiency, etc.)
- Optic region metrological traceability measurement and calculation can be realized.
- Optical measurement setup alignment, integrating and data analyzing.

COMPUTER SKILLS

- **Windows** environments and **Office package** (Word, Excel, PowerPoint and Outlook).
- **MatLab** for data analysis, **Monte Carlo** calculations, **Machine-Learning** and applications.
- **ZEMAX Optic Studio** optic design, thin and exact ray tracing.
- **MPB** for computing photonic band structures.
- **Lumerical Solutions** in both time and frequency domain photonic crystal and device applications.

PUBLICATIONS

Proceeding of International Conferences

- M. Kilin, H. Tutunculer "Investigation *of Bose-Einstein Condensation for Different Potential* "Turkish Physics Society (TPS-28), abstract, 2012

- M. Kilin, O. Bazkir "*Reflection Type Trap Detector Characterization and Responsivity in terms of the TUBITAK UME Spectral Responsivity*"Turkish Physics Society (TPS-32), abstract, 2016.

- M. Kilin, O. Bazkir, S. Meric "*Extended Wave Length Accuracy Calibration from 250nm to 2500nm by using Pen-Ray Type Mercury Lamps and the Orders of the Helium Neon Tunable Laser*" Turkish Physics Society (TPS-32), abstract, 2016.

- M. Kilin, H. Tutunculer, S. Meric "*Effective Measurement of the Wavelength Accuracy Calibration by using Monte Carlo Uncertainty Calculation"* Turkish Physics Society (TPS-35), abstract, 2019.

- A. Bingul, H. Mutaf, M. Kilin *"Measurement of the angular velocity of the Earth with the Long Exposure method"* 3rd international congress of professional and technical sciences, full paper, 2018.

Journal Publication

- M. Kilin, H. Tutunculer, S. Meric "*Effective Measurement of the Wavelength Accuracy Calibration by using Monte Carlo Uncertainty Calculation" American Institute of Physics Conference Proceeding, volume 2178,* 10.1063/1.5135406, full paper, 2019

- M. Kilin, H. Tutunculer, O. Bazkir, S. Meric " *Realization of the Radiance Scale Using Transfer Function of the Laser Based Optical System*" International Journal of Optics, HINDAWI, Volume 2020, Article ID 4184360, 10 pages https://doi.org/10.1155/2020/4184360

Journal Papers in Review

- F. Yasar, M. Kilin and Z. Yu, "*Control over scintillation in Tungstate compound scintillators and enhanced spatial detection resolution for X-ray application*",

PROFESSIONAL TRAINING

Conference

- Turkish Physical Society, 28^{th} International Physics Congress 2012.
- PHOTONICS 2015, 17^{th} National Optics, Electro-Optics and Photonics Workshop.
- Turkish Physical Society, 32^{nd} International Physics Congress 2016.
- Turkish Physical Society, 35^{th} International Physics Congress 2019.

Researcher

- National Metrology Laboratory TUBITAK-UME optic laboratory guess researcher to measure PhD working, also radiometry, photometry, spectrometry, detector calibration measurements experience skills (2016-2018)

Overseas Experience

- United State of America, Work and Travel program, Six Flags Great America funfair, 2008.

- Erasmus international researcher education programs, University of Debrecen, Faculty of Engineering, Hungary 2013.